

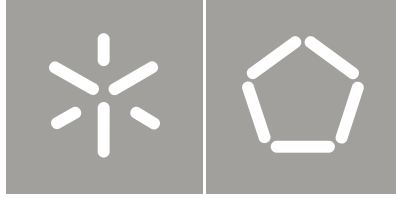


Universidade do Minho
Escola de Engenharia

Joana Barbas The use of on-line characterization technologies
during the manufacture of nanostructured materials

Joana Margarida de Oliveira Barbas

The use of on-line characterization
technologies during the manufacture
of nanostructured materials



Universidade do Minho
Escola de Engenharia

Joana Margarida de Oliveira Barbas

The use of on-line characterization
technologies during the manufacture
of nanostructured materials

Tese de Doutoramento
Ciência e Engenharia de Polímeros e Compósitos

Trabalho efectuado sob a orientação de
Professora Doutora Ana Vera Alves Machado
Professor Doutor José António Covas

ACKNOWLEDGEMENTS

The present thesis is the resulting outcome of a research carried out between 2008 and 2012 in the Department of Polymer Engineering of the University of Minho. It represents a great achievement, both personal and professional, and its completion would not have been possible without the help and support of many people.

First and foremost I wish to thank to my supervisors, Doutora Ana Vera Machado e Professor José António Covas, for the scientific knowledge, guidance, encouragement and support, not only during the course of this research, but along the past 8 years we have been working together. It has been a long sometimes hard journey, but I have enjoyed every step of the way! It has been a pleasure working with you.

I would also like to address a special appreciation message to my colleagues Sacha Mould and Simão Pereira, for the helping hand, support and companionship, making easy to endure the long hours of extrusion runs that this research involved. Thank you!

To all my friends and colleagues of the Department of Polymer Engineering, Ricardo Andrade, Isabel Moura, Manuel Oliveira, Fátima Almeida and Ana Luísa Lima. To Carla Leer-Lake for the kind advices, support, encouragement and for being a role model. To Jorge Jardim Silva for the rheological knowledge you shared and your friendship. Thank you all!

To my longtime friend Liliana Rosa Santos, for never letting me down and always supporting me, even though sometimes I am not the best company you never left me alone. Thank you so much Rosa!

I would also like to acknowledge the important contribution of the technical staff of the Polymer Engineering Department, particularly Mauricio Malheiro, Francisco Mateus and João Paulo Peixoto.

To the University of Minho and the Institute of Polymers and Composites for the financial support granted through the Multihybrids European Project (IP026685-2IP, 6th Framework EC Programm).

Aknowledgements

More importantly, I wish to thank to my parents, for their love and support, for teaching me to never give up and for giving me a much valuable sense of self-confidence and self-worth. To my younger sister and brother, in the hope I had never disappointed them with my absences or divided attention.

Finally I would like to thank to Renato, to whom I dedicate this thesis. You are my role model of determination and resolution. Thank you for the encouragement, support and love. Thank you for being there for me every step of the way!

PUBLICATIONS

International Journals Publications

S.T. Mould, **J.M. Barbas**, A.V. Machado, J.M. Nóbrega, J.A. Covas. “Measuring the rheological properties of polymer melts with on-line rotational rheometry”, *Polymer Testing*, 30 (2011) 602-610

This doctoral thesis is based on the following papers:

J.M. Barbas, A.V. Machado, J.A. Covas. “In-line Near-Infrared spectroscopy for the characterization of dispersion in polymer-clay nanocomposites”; *Polymer Testing* 31 (2012) 527-536 (Chapter 3)

J.M. Barbas, A.V. Machado, J.A. Covas. “In-line Near-Infrared spectroscopy: a tool to monitor the preparation of polymer-clay nanocomposites in extruders”, *article in press*, *Journal of Applied Polymer Science*. DOI: 10.1002/app.38106 (Chapter 4)

J.M. Barbas, A.V. Machado, J.A. Covas. “The evolution for dispersion along the extruder during the manufacture of polymer-organoclay nanocomposites”, submitted to *Macromolecular Materials and Engineering* (Chapter 5)

J.M. Barbas, A.V. Machado, J.A. Covas. “The effect of processing conditions on the evolution of dispersion of different polymer-clay nanocomposites”, under preparation, (Chapter 6)

Publications

International Conferences Proceedings books

Oral Communications

S.T. Mould, **J.M. Barbas**, J.M. Nóbrega, A.V. Machado, J.A. Covas. "Recent Developments on On-Line Rheometry to Monitor the Extrusion Process", Novel Trends in Rheology III – Proceedings of the International Conference (American Institute of Physics) Czech Republic, July 2009

J.M. Nóbrega, S.T. Mould, **J.M. Barbas**, A.V. Machado, J.A. Covas. "Monitoring Nanoclay Dispersion in Polymer Matrix by On-Line Rotational Rheometry", 6th International ECNP Conference, Madrid, Spain, April 2010.

S.T. Mould, **J.M. Barbas**, J.M. Nóbrega, A.V. Machado, J.A. Covas. "On-Line Rheometry to Monitor Nanocomposites Production: From the Lab to the Industrial Scale", 3rd ECNP Young Polymer Scientist Conference, Madrid, Spain, April 2010.

J.M. Barbas, A.V. Machado, J.A. Covas. "Near-Infrared Spectroscopy as On-line Tool for Characterization of Polymer Matrix Nanocomposites" – PPS-27, 27th World Congress of the Polymer Processing Society, Marrakech, Morocco, May 2011

S.T. Mould, S.P. Pereira, **J.M. Barbas**, E. Masarati, J.M. Nóbrega, A.V. Machado, J.A. Covas. "On-line Rheometry: a Tool to Monitor Polymer Nanocomposites Production", Novel Trends in Rheology IV – Proceedings of the International Conference (American Institute of Physics) Czech Republic, July 2011

J.M. Barbas, A.V. Machado, J.A. Covas. "On-line monitoring along the extruder of the dispersion of clay nanocomposites" – PPS-Americas 2012, Regional Congress of the Polymer Processing Society, Niagara Falls, Canada, May 2012

S.T. Mould, **J.M. Barbas**, E. Masarati, J.M. Nóbrega, A.V. Machado, J.A. Covas. "On-line Rheometry: a Tool to Monitor Polymer Nanocomposites Production" – XVIth International Congress on Rheology, Lisboa, Portugal, August 2012

J.M. Barbas, A.V. Machado, J.A. Covas. "The effect of processing conditions on the evolution of the dispersion of Polymer-Clay nanocomposites along the extruder" – PPS-28, 28th World Congress of the Polymer Processing Society, Pattaya, Thailand, December 2012

Posters

A.V. Machado, **J.M. Barbas**, M. van Duin, J.A. Covas. *“Rheological Properties of Thermoplastic”* – AERC 2003, European Rheology Conference, Guimarães, Portugal, September 2003

J.M. Barbas, A.V. Machado, J.A. Covas. *“On-line Characterization of Nanocomposites by Near-Infrared Spectroscopy”* – II Annual Meeting I3N, Fatima, Portugal, February 2010

J.M. Barbas, A.V. Machado, J.A. Covas. *“On-Line Characterization of Nanocomposites Preparation by Near-Infrared Spectroscopy”*, MPA - 4th International Meeting on Developments in Materials, Processes and Applications of Emerging Technologies, Braga, Portugal, July 2010

J.M. Barbas, A.V. Machado, J.A. Covas. *“On-line Characterization of Nanocomposites preparation by Near-Infrared Spectroscopy”* – Semana da Escola de Engenharia, Guimarães, Portugal, October 2010

S.T. Mould, **J.M. Barbas**, S.P. Pereira, A.V. Machado, J.M. Nóbrega, J.A. Covas. *“On-line Rheometry to Monitor Nanocomposites Production”* – III Annual Meeting I3N, Fatima Portugal, February 2011

J.M. Barbas, A.V. Machado, J.A. Covas. *“On-line Near-infrared Spectroscopy applied to Polymer Nanocomposites Characterization”* – III Annual Meeting I3N, Fatima, Portugal, February 2011

J.M. Barbas, A.V. Machado, J.A. Covas. *“Near-Infrared Spectroscopy for On-line Monitoring of Nanoclay Dispersion in Polymer Nanocomposites”* – MATERIAIS 2011, VI International Materials Symposium, Guimarães, Portugal, April 2011

J.M. Barbas, A.V. Machado, J.A. Covas. *“In-line NIR spectroscopy for monitoring the preparation of polymer-clay nanocomposites in extruders”* – IV Annual Meeting I3N, Quiaios Portugal, March 2012

ABSTRACT

The use of on-line characterization technologies during the manufacture of nanostructured materials

Since their potential has become widely recognized, one of the major research lines on polymer-clay nanocomposites has focused on the preparation of well dispersed systems, which involves investigating their compounding (including their structural and morphological characterization) and the determination of their physical and mechanical performances. Currently, there is an understanding that a high degree of dispersion, particularly exfoliation, of the nanoclay is required to improve the overall performance. Although the influencing parameters are known – interfacial adhesion, chemical affinity and operating conditions – the effect of each on the onset and extent of the organoclay dispersion are still subject of debate.

Twin screw extrusion allows for control of the main variables (shear, stress and time), but also, due to the typical modular construction, offers a high degree of freedom in creating the adequate screw design and enables knowledgeable alteration of the barrel. These features offer a solid basis for the development and implementation of apt on-line/in-line monitoring techniques, able to follow up the evolution of dispersion of polymer-clay nanocomposites during processing.

This research included the validation, implementation and application of a methodology based on in-line Near-Infrared (NIR) Spectroscopy for the characterization of the dispersion along the extruder axis. The results showed that the operating conditions have great impact on the dispersion level, but also that degradation may affect the interfacial chemistry of the system, altering the dispersion pathways.

Overall the results obtained confirm that NIR is a valid tool for the on-line characterization of these materials, offering the possibility of assessing in real time the clay dispersion, enabling proper corrective and optimization actions over the material characteristics in a timely manner.

CONTENTS

AKNOWLEDGEMENTS	iii
PUBLICATIONS.....	v
ABSTRACT	ix
CONTENTS	ix
LIST OF FIGURES	xv
LIST OF TABLES.....	xix
1. INTRODUCTION	
1.1. Motivation	1
1.2. Thesis Outline	3
1.3. References.....	4
2. POLYMER-CLAY NANOCOMPOSITES: A BRIEF OVERVIEW	
2.1. Introduction.....	5
2.2. Layered silicates.....	5
2.2.1. Crystal Structure	5
2.2.2. Modification of clay minerals	7
2.3. Polymer - Clay nanocomposites	8
2.3.1. Structure, Morphology and Properties.....	8
2.3.2. Preparation methods.....	11
2.3.3. Characterization.....	12
2.3.4. Dispersion in melt mixing.....	17
2.3.5. On-line and In-line Monitoring.....	21
2.4. Research Objectives	27
2.5. References	28

Contents

3. IN-LINE NEAR-INFRARED SPECTROSCOPY FOR THE CHARACTERIZATION OF DISPERSION IN POLYMER - CLAY NANOCOMPOSITES

3.1. Introduction.....	44
3.2. Experimental	46
3.2.1. Materials and composites	46
3.2.2. In-line set-up	47
3.2.3. Characterization of the Composites	48
3.3. Development of the chemometric model	50
3.3.1. Chemometrics	50
3.3.2. Quality of the model	50
3.3.3. Model Parameters.....	52
3.4. Results and Discussion.....	53
3.4.1. Single parameter models	53
3.4.2. Population Size	57
3.4.3. Multi-parameter models	58
3.4.4. Validity limitations	61
3.5. Real-time prediction.....	63
3.6. Conclusions	65
3.7. References	66

4. IN-LINE NEAR-INFRARED SPECTROSCOPY: A TOOL TO MONITOR THE PREPARATION OF POLYMER - CLAY NANOCOMPOSITES IN EXTRUDERS

4.1. Introduction.....	72
4.2. Experimental	74
4.2.1. Materials and composites	74
4.2.2. Process monitoring set-up.....	75
4.2.3. Characterization of the Composites	77
4.2.4. Chemometrics	79
4.3. Results and discussion	79
4.3.1. Analysis of the NIR spectra.....	79

4.3.2. Determining the model parameters	83
4.3.3. Transmission vs. Reflection On-line measurements.....	87
4.4.4. Real-time monitoring with Diffuse Reflectance	88
4.5. Conclusions	91
4.6. References	93

5. THE EVOLUTION OF DISPERSION ALONG THE EXTRUDER DURING THE MANUFACTURE OF POLYMER-ORGANOCLAY NANOCOMPOSITES

5.1. Introduction.....	98
5.2. Experimental	100
5.2.1. Materials	100
5.2.2. Preparation of the nanocomposites	101
5.2.3. Sample collection and On-line/In-line Monitoring	103
5.2.4. Off-line Characterization of the Composites.....	104
5.3. Results and discussion	106
5.3.1. Evolution of clay dispersion	106
5.3.2. Towards a dispersion model.....	112
5.4. Conclusions	121
5.5. References	122

6. THE EFFECT OF PROCESSING CONDITIONS ON THE EVOLUTION OF DISPERSION OF DIFFERENT POLYMER-CLAY NANOCOMPOSITES

6.1. Introduction.....	128
6.2. Experimental	130
6.2.1. Materials and composites	130
6.2.2. Sample collection and process monitoring.....	131
6.2.3. Off-line Characterization of the Composites.....	135
6.3. Results and discussion	138
6.3.1. Global effects.....	138
6.3.2. Effect of screw speed	140
6.3.3. Effect of the throughput.....	146

Contents

6.3.4. The relation between processing conditions – chemistry – dispersion	150
6.4. Conclusions	153
6.5. References	154

7. CONCLUSIONS AND FUTURE WORK

7.1. Conclusions	159
7.2. Future work.....	161

LIST OF FIGURES

Figure 2. 1. Schematic representation of the crystal structure of MMT [9, 10].	7
Figure 2. 2. Schematics of possible polymer-clay composite structures [27].	9
Figure 2. 3. Illustration of the different states of clay dispersion and corresponding WAXS and TEM results [38].	13
Figure 2. 4. Evolution of melt yield stress as a function of the filling ratio (Q/N) for nanocomposites prepared under different operating condition [29].	14
Figure 2. 5. TEM micrographs showing different states of dispersion of the nanocomposites and respective Young modulus data [13].	17
Figure 2. 6. Mechanism of dispersion of the organoclay particles during melt processing, proposed by Dennis et al [25].	20
Figure 2. 7. Effect of the feed rate on the variation of the interlayer spacing (left) and the melt yield stress (right), along the extruder [31].	21
Figure 2. 8. General view of the on-line rheometer when inserted at a given position along the barrel of a twin screw extruder [100].	23
Figure 2. 9. Linear viscoelastic behaviour of PP/PP-g-MA/D67G nanocomposite at 200 °C, measured on-line in three different positions along the extruder [100].	24
Figure 2. 10. Photograph of the NIR in-line set-up used by Moghaddam et al [123].	25
Figure 3. 1. In-line NIR set-up.	47
Figure 3. 2. (a) Typical batch mixer torque and temperature curves for samples 100/0/0, 95/0/5 and 80/15/5. (b) Examples of NIR spectra for the same materials.	48
Figure 3. 3. Individual calibration models and their validation: (a) Maximum Torque; (b) peak shift at 1050 cm ⁻¹ .	55

List of Figures

Figure 3. 4. Chemometric model using the normalized average of maximum torque, rheology and FT-IR.	60
Figure 3. 5. Spectra measured during mixing for 87.5/7.5/5 w/w/w.	63
Figure 3. 6. Time evolution of torque and (predicted) dispersion: (a) 87.5/7.5/5 at 50 rpm (b) 90/5/5 at 125 and 175 rpm.	64
Figure 4. 1. In-line set-up.	76
Figure 4. 2 Spectra acquired for the 90/5/5 nanocomposite prepared at 3 kg/h and 100 rpm: (a) Transmission (b) Diffuse reflectance.	80
Figure 4. 3. Spectra acquired for the composites prepared with different screw speeds: (a) Transmission (b) Diffuse reflectance.	81
Figure 4. 4. Spectra acquired for the composites prepared with different PP-g-MA content: (a) Transmission (b) Diffuse reflectance.	81
Figure 4. 5. Spectra acquired for the composites prepared with different clay content: (a) Transmission (b) Diffuse reflectance.	82
Figure 4. 6. Linear viscoelastic response against frequency of the nanocomposites prepared with different screw speeds: (a) complex viscosity and (b) storage modulus.	83
Figure 4. 7. FT-IR spectra in the Si-O band region of the nanocomposites prepared with different screw speeds: (a) as measured; (b) 1050 and 1080 cm ⁻¹ fitted peaks.	85
Figure 4. 8. Calibration models: (a) Transmission; (b) Reflection.	88
Figure 4. 9. Linear viscoelastic response against frequency of the PP/PP-g-MA/D67G 90/5/5 w/w/w nanocomposite prepared with different feed rates. (a) complex viscosity; (b) storage modulus.	89
Figure 4. 10. FT-IR spectra in the Si-O band region of the PP/PP-g-MA/D67G 90/5/5 w/w/w nanocomposite prepared with different feed rates: (a) as measured; (b) 1050 and 1080 cm ⁻¹ fitted peaks.	90
Figure 5. 1. Layout of the twin-screw extruder.	101

List of Figures

Figure 5. 2. Complex viscosity (η^*) over frequency at different locations for all screw profiles used: (a) SC 1, (b) SC 2 and (c) SC 3.....	107
Figure 5. 3. Storage modulus (G') over frequency at different locations for all screw profiles used: (a) SC 1, (b) SC 2 and (c) SC 3.....	107
Figure 5. 4. On-line rheometry data along the extruder: (a) storage modulus (G') at 0.158 rad/s; (b) calculated melt yield stress.	109
Figure 5. 5. NIR spectra along the extruder barrel for all screw profiles used: (a) SC 1, (b) SC 2 and (c) SC 3.....	110
Figure 5. 6. NIR real-time predictions of the degree of dispersion for the different screw profiles used.....	111
Figure 5. 7. Off-line FTIR analysis: (a) in-plane peak (1050 cm^{-1}) shift; (b) out-of-plane peak (1080 cm^{-1}) shift.....	116
Figure 5. 8. CIELab color coordinates (a) luminosity and (b) yellowness.....	117
Figure 5. 9. (a) Dynamic TGA derivative curves of the organoclay (D67G), the polymer matrix (PP/PP-g-MA) and the nanocomposite (PP/PP-g-MA/D67G) prepared with SC2. (b) Isothermal TGA curves of the organoclay and the polymer matrix.....	118
Figure 6. 1. Layout of the twin-screw extruder and screw profile.....	131
Figure 6. 2. NIR calibration curve developed at L/D 11 for the nanocomposites prepared under different processing conditions: (a) PP/PP-g-MA/D67G system; (b) PA6/D43B system.....	133
Figure 6. 3. Thermal stability of the organoclays by TGA: (a) derivative curve of the dynamic temperature sweeps of D67G and D43B, (b) isothermal at various temperatures of D67G and (c) isothermal at various temperatures of D43B.	138
Figure 6. 4. Effect of the throughput and screw speed on the final dispersion levels: (a) PP nanocomposites, (b) PA6 nanocomposites.....	139
Figure 6. 5. Effect of the throughput and screw speed on the FT-IR peak shifts: (a) PP nanocomposites, (b) PA6 nanocomposites.....	140

List of Figures

Figure 6. 6. Values of G' at 0.1 rad/s plotted against the extruder location for the effect of screw speed: (a) PP/PP-g-MA/D67G nanocomposites, (b) PA6/D43B nanocomposites.	142
Figure 6. 7. FT-IR peak shifts along the extruder of the prepared with different screw speeds: PP based nanocomposites (a) 1050 cm^{-1} and (b) 1080 cm^{-1} ; PA6 based nanocomposites (c) 1055 cm^{-1} and (d) 1075 cm^{-1}	144
Figure 6. 8. Normalized values for the effect of screw speed: PP based nanocomposites (a) storage modulus and (b) NIR predictions; PA6 based nanocomposites (c) storage modulus and (d) NIR predictions.	146
Figure 6. 9. Values of G' at 0.1 rad/s plotted against the extruder location for the effect of screw speed: (a) PP/PP-g-MA/D67G nanocomposites, (b) PA6/D43B nanocomposites.	148
Figure 6. 10. FT-IR peak shifts along the extruder of the prepared with different throughputs: PP based nanocomposites (a) 1050 cm^{-1} and (b) 1080 cm^{-1} ; PA6 based nanocomposites (c) 1055 cm^{-1} and (d) 1075 cm^{-1}	149
Figure 6. 11. Normalized values for the effect of throughput: PP based nanocomposites (a) storage modulus and (b) NIR predictions; PA6 based nanocomposites (c) storage modulus and (d) NIR predictions.	150

LIST OF TABLES

Table 3. 1. Materials and main characteristics.	46
Table 3. 2. Compositions of the PP/PP-g-MA/C20A nanocomposites.....	46
Table 3. 3. Values of the parameters associated to the selected reference techniques.....	54
Table 3. 4. Quality factors of the individual calibration models and respective validation.....	56
Table 3. 5. Validation of the chemometric models using different validation/calibration population ratios.....	58
Table 3. 6. Calibration and Validation results for the multi-parameter models.....	59
Table 3. 7. Predicted final dispersion level of nanocomposites prepared using different rotor speeds...	62
Table 3. 8. Global 7-parameter model: calibration and validation quality factors.	62
Table 4. 1. Materials used in the work.....	74
Table 4. 2. Composition of the various PP/PP-g-MA/D67G nanocomposites prepared.	75
Table 4. 3. Values of the properties of the 7-parameter model for the range of compounding runs.	86
Table 4. 4. Normalized average values associated to each of the nanocomposites prepared.....	86
Table 4. 5. Calibration and Validation results for the 7-parameter models.	88
Table 4. 6. Final dispersion levels of nanocomposites prepared using different throughputs.	89
Table 4. 7. SME, σ_0 and b for the PP/PP-g-MA/D67G 90/5/5 w/w/w nanocomposite prepared with different feed rates.....	90
Table 5. 1. Materials used in the work.....	100
Table 5. 2. Screw profiles used in the preparation of the PP/PP-g-MA/D67G nanocomposites.	102
Table 5. 3. Process monitoring parameters registered during compounding with the different screw profiles.	103

List of Tables

Table 5. 4. NIR real-time predictions of the degree of dispersion of the nanocomposites prepared using different screw geometries.....	111
Table 5. 5. Scanning transmitted electron microscopy images of the nanocomposites prepared with SC1 and SC2.	114
Table 6. 1. Materials used in the work.....	130
Table 6. 2. Process monitoring parameters registered during compounding with different conditions.	134
Table 6. 3. NIR real-time predictions of the degree of dispersion of the nanocomposites prepared using different screw speeds.....	142
Table 6. 4. NIR real-time predictions of the degree of dispersion of the nanocomposites prepared using different throughputs.	147

1.1. Motivation

Nanomaterials constitute an important subset [1 – 3] within the field of nanotechnology. The creation of nanoscale structures enables control and manipulation over the materials' fundamental characteristics, such as melting temperature, optical and electromagnetic properties, without interfering with its inherent chemical composition [4].

In an era where sustainability and power efficiency are the major driving forces for technological innovation and development, lightweight high performance materials, like polymer nanostructured materials, represent a wise choice in replacement of traditional materials. By 2009, the revenues for nanotechnology and nanomaterials in consumer goods, mainly from electronics, automotive and household care segments, reached US\$1545 million and is expected to be over US\$5000 million by 2015 [5].

The growing availability of nanofillers and their precursors [6 – 7] prompted the development of a new class of composite materials. The reinforcement of polymers with fillers, either organic or inorganic, has become a regular practice in the plastics industry.

Polymer nanocomposites present several advantages over their unfilled counterparts and to conventional micron-scale composites, resulting in low-density materials with enhanced mechanical and physical properties. These materials are composed by discrete elements having at least one dimension at the nanoscale [1 – 3, 6]. Uniform dispersion of these nanosized fillers maximizes the polymer-filler interactions by producing a large interfacial area.

Polymer-clay nanocomposites consist of a polymer/copolymer/blend matrix in which the clay particles are dispersed [6]. In comparison with the unfilled resin, these materials present enhanced mechanical performance, thermal and dimensional stability, higher flame retardancy and better barrier properties. Typically these properties are attained at very low clay loadings (up to 5% weight), therefore density is virtually unaffected, making these materials attractive alternatives in construction, textile, packaging, healthcare, automotive, electronics and aerospace industries [2 – 3,

Chapter 1. Introduction

6, 8 – 9]. The global returns for polymer-clay nanocomposites in the world market were over US\$200 million in 2009 [10].

The challenge of polymer-clay nanocomposites is to prepare the materials with the necessary levels of dispersion. It is known, that the final properties are determined by the morphology, which in turn depends on the chemistry of the polymer-clay interface and also on the processing method adopted and operating conditions [2 – 3, 8 – 9].

There are three main processes for the preparation of polymer-clay nanocomposites: intercalation from solution, in situ intercalative polymerization and melt intercalation [2 – 3, 7 – 9]. The first two are solvent based methods, therefore presenting some disadvantages for large scale production. Melt intercalation is a cost-effective and environmentally sound alternative for the industrial scale production of these materials. It can be performed using conventional plastic compounding and/or processing equipments, providing the mechanical inputs necessary to achieve proper dispersion of clay within the polymer matrix.

The dispersion of the clay by melt mixing comprises the diffusion of the polymer within the galleries (intercalation) and delamination of the individual silicate sheets (exfoliation) [11]. However, the preparation of the nanocomposites through melt compounding is not straightforward, since a large number of variables (mechanical, physical and chemical) influence the dispersion mechanism [9, 11]. There are still difficulties in establishing clear correlations between processing conditions and final dispersion levels. More importantly, there is still some lack of knowledge regarding the dispersion mechanism and its evolution during compounding.

This work focuses on the preparation of polymer-clay nanocomposites by melt intercalation, using conventional compounding equipments, such as the batch mixer and, in a larger scale, a twin-screw extruder. The goal is to implement and use on-line or in-line monitoring techniques to follow up the evolution of the clay dispersion during the preparation of the nanocomposites. Ultimately, this will provide a better understanding of the dispersion mechanism and of the effect of the main processing variables.

1.2. Thesis Outline

This thesis is organized in seven chapters. Chapter 1 presents the motivation and global objectives of this work.

Chapter 2 contains a brief overview on polymer/clay systems structure, morphology and properties, production methods and characterization. It emphasizes the preparation by melt mixing and its effect on clay dispersion, as well as the available on-line monitoring techniques.

Chapter 3 describes the implementation and validation of in-line Near-Infrared spectroscopy (NIR) for monitoring the preparation of polymer-clay nanocomposites in a batch mixer. It includes the development of the chemometric model, using parameters from well-established techniques used for the characterization of the degree of clay dispersion, for assessing in real time conditions the dispersion of the material upon compounding.

Chapter 4 discusses the application of NIR during twin-screw extrusion. Considering the influence of the processing conditions on the clay dispersion during the preparation of Polypropylene matrix nanocomposites in a twin screw extruder, an optimization of the chemometric model is also shown here.

Chapters 5 and 6 present the use of on-line/in-line techniques for monitoring the evolution of clay dispersion along the extruder axis. In Chapter 5, both on-line rheometry and in-line NIR are used to assess the evolution of dispersion along the twin-screw extruder. Chapter 6 uses in-line NIR applied along the extruder axis, to monitor the effect of the processing conditions on the nanocomposites dispersion. In both cases, the on-line/in-line characterization results are complemented with adequate off-line analysis.

Finally, Chapter 7 presents the overall conclusions of this work, considering its initial objectives. Ideas for prospective work are also suggested here.

1.3. References

1. R.K. Gupta, E. Kennel, K. Kim. Polymer Nanocomposites Handbook. USA: CRC Press, (2010).
2. M. Alexandre, P. Dubois. Polymer-layered silicate nanocomposites: preparation, properties and uses of a new class of materials. *Materials Science and Engineering*. 28, p.1-63, (2000).
3. D.R. Paul, L.M. Robeson. Polymer nanotechnology: Nanocomposites. *Polymer*. 49, p. 3187-3204, (2008).
4. J.H. Koo. Polymer Nanocomposites: Processing, Characterization and Applications. USA: McGraw-Hill, (2006).
5. The World market for nanotechnology and nanomaterials in consumer products, 2010 – 2015; Future Markets Inc. (2010); <http://www.researchandmarkets.com/reports/1230584>
6. L.A. Utracki. Clay-Containing Polymer Nanocomposites - vol.1. UK : Rapra Technology Ltd., (2004).
7. L.B. Paiva, A.R. Morales, F.R. Valenzuela Díaz. Organoclays: Properties, preparation and applications. *Applied Clay Science*. 42, p. 8-24, (2008).
8. S.S. Ray, M. Okamoto. Polymer/layered silicate nanocomposites: a review from preparation to processing. *Progress in Polymer Science*. 28, p.1539-1641, (2003).
9. S. Pavlidou, C.D. Papaspyrides. A review on polymer-layered silicate nanocomposites. *Progress in Polymer Science*. 33, p. 1119-1198, (2008).
10. The World market for nanocomposites (metal nanoparticles, nanotubes, nanoclay, nanofibers, grapheme, fullerenes and POSS); Future Markets Inc. (2010); <http://www.researchandmarkets.com/reports/1382564>
11. M. Bousmina. Study of the intercalation and exfoliation processes in polymer nanocomposites. *Macromolecules* 39, p. 4259-4263, (2006).

POLYMER-CLAY NANOCOMPOSITES: A BRIEF OVERVIEW

2

2.1. Introduction

Within the scope of this thesis, thermoplastic polymers reinforced with layered silicates are the subject of interest. Layered silicates are composed of anisometric platelets, for which only one dimension is on the nanometer scale. Each individual particle, in the form of sheets or platelets, has one to a few nanometers thick and hundreds to thousands nanometers long and wide. This type of filler is preferred for a highly structured material with improved physical and mechanical performance

This Chapter presents a brief overview on polymer-clay nanocomposites. It starts with the description of the chosen clay, montmorillonite (MMT), its crystal structure and characteristics. This section also includes information about the polymer-clay nanocomposites structure, morphology and general properties, preparation methods and characterization techniques. Since the objective of the thesis is the implementation and use of on-line/in-line techniques for monitoring the preparation of polymer-clay nanocomposites by melt compounding, a more detailed description about polymer melt-intercalation and the available on-line monitoring techniques is provided here.

2.2. Layered silicates

2.2.1. Crystal Structure

Clay mineral is a general term often applied to phyllosilicates featuring a layered structure, with silicate fractions of either a hydrous magnesium or aluminum. Layered silicates crystallographic structures include two types of sheets, tetrahedral and octahedral [1]. Depending on the arrangement of the sheets, clays can be classified into 2 groups: (i) 1:1 phyllosilicates, meaning a structure composed by one tetrahedral sheet for every octahedral sheet; (ii) 2:1 phyllosilicates,

Chapter 2. Polymer-clay nanocomposites: a brief overview

presenting a “sandwich” type of structure with a tetrahedral-octahedral-tetrahedral organization. Montmorillonite belongs to the 2:1 phyllosilicates group and is the most common layered silicate used for polymer reinforcement [1 – 3].

The crystal lattice consists of two tetrahedral layers with a central octahedral sheet. In the tetrahedral sheets each silicon (Si) atom is surrounded by four oxygen (O^{2-}) atoms and the tetrahedrally coordinated Si cations (Si^{4+}) are linked to one another via covalent bonding through the shared oxygens. These shared oxygens form the basal plane and the remaining apical oxygens are shared by another layer of cations. The central octahedral sheets have either aluminum (Al^{3+}) or magnesium (Mg^{2+}) cations that are coordinated with six O^{2-} or hydroxyl groups (OH); these units form a covalent bond with the sheet structure as well [1 – 5]. On their turn, tetrahedral and octahedral sheets are also covalently linked through the apical tetrahedral oxygens. Figure 2. 1 depicts the lattice structure of a 2:1 phyllosilicate.

The layer thickness varies from 1 – 2 nm and the lateral dimensions may vary from 30 nm to several microns, hence each platelet has a very large aspect ratio ranging between 100 and 1000 [1 – 3, 5 – 8]. Typically, several hundreds of layers are displaced in stacks, forming large agglomerates or tactoids with about 10 to 40 μm in size, separated by regular van der Waals gap, called interlayer or gallery. Smectites have low surface charges, as such isomorphic substitution within the layers is easier and cations interchange is common, with Al^{3+} and Mg^{2+} often being replaced by calcium II (Ca^{2+}), iron II (Fe^{2+}), sodium (Na^+), or even lithium (Li^+) and potassium (K^+). This interchange generates negative charges that are counterbalanced by alkaline earth cations situated in the interlayer. The layer charges are negative ranging from 0.5 – 1, for the MMT specific case is about 0.67 per unit cell [1 – 3, 5].

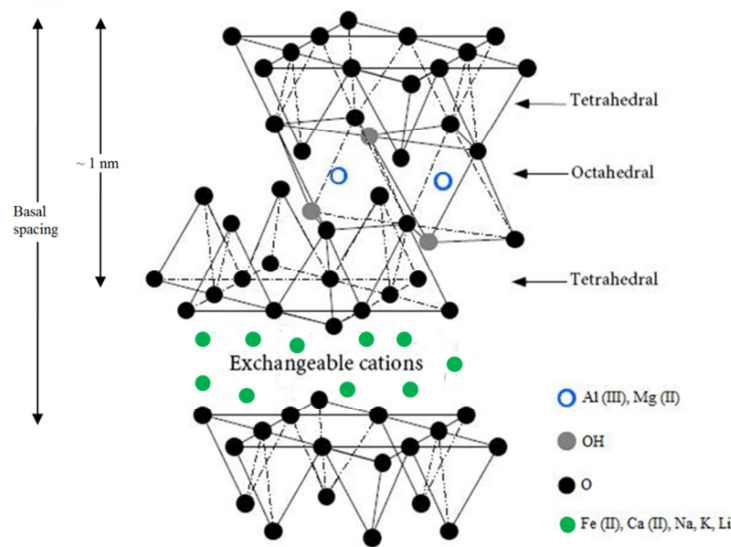


Figure 2. 1. Schematic representation of the crystal structure of MMT [9, 10].

2.2.2. Modification of clay minerals

Because, naturally occurring silicates are hydrophilic they are compatible with polymers like polyethylene oxide and polyvinyl alcohol, but they interact poorly with organic polymers, making proper dispersion difficult to achieve [3, 11 – 14]. As such chemical modification is often applied, to render a more organophilic behavior.

The ability to organically modify these clays depends on their cation exchange capacity (CEC). MMT is considered to have a moderate CEC, ranging from 60 – 150 meq/100 g [1, 3, 9 – 10]. Thus, to a certain extent, the affinity between the clay and the polymer (dependent on the type of interlayer cation) can be enhanced by optimizing the clay surface chemistry for a given polymer matrix.

Ion exchange reactions with cationic surfactants, like alkylammonium, are common and facilitate the clay intercalation by many engineering polymers [14]. Basically, these organic modifiers lower the surface energy of the inorganic particles, improve the wetting characteristics, and generate a more favorable chemical environment in the interlayer spacing for the intercalation of the polymer molecules [6, 14]. They also provide functional sites in the layer surface that can directly react with the polymer or even initiate polymerization of monomers. Hence, the strength of the generated interface between the clay sheets and the polymer is improved [6, 9, 10 – 11, 14 – 18].

Chapter 2. Polymer-clay nanocomposites: a brief overview

Because the stacked layers are held together by electrostatic forces, they cannot be broken into individual platelets just by applying mechanical shear. Thus, the organic modification enables this separation due to the increase of the basal spacing, which can increase from 1 nm to 3 nm or even higher [6, 9 – 10, 14 – 15]. It then becomes easier for polymer chains to diffuse between the layers and eventually separate them [9 – 11, 13 – 18].

Along these past decades several studies have focused on this matter and have shown that for high polarity matrices like polyamides, the best dispersion degree (exfoliation) is achieved with organoclays modified with one long alkyl tail [17 – 20]. Whereas for nonpolar polymers, like polyolefins, the affinity with the silicate surface is inferior and more alkyl tails are preferred, since these block the unfavorable silicate/polyolefin interaction and increase the alkyl/polyolefin contacts [11, 21 – 23].

2.3. Polymer - Clay nanocomposites

2.3.1. Structure, Morphology and Properties

The simple mixing of a polymer and a silicate does not necessarily results in a nanocomposite. Depending on the interaction between the polymer and the clay surface, as well as on the thermomechanical conditions, the separation of the clay stacks into discrete uniformly dispersed particles may not be attainable [2 – 3, 12, 16, 24 – 27]. Figure 2. 2 shows a schematic representation of the possible polymer-clay composite structures.

Conventional immiscible composites result from the inability of the polymer to intercalate into the interlayer spacing. In this case the clay remains in its agglomerate state, comprising a micron size dispersed phase. The properties of such materials are comparable to that of traditional microcomposites. The most beneficial structures are those that maximize the polymer-clay interactions by producing a large interfacial area, resulting in the uniform dispersion of nano size particles of filler [27 – 28]. These structures include intercalated nanocomposites and exfoliated nanocomposites. Intercalation is used to describe the morphology where a single polymer chain (sometimes more) enters the interlayer, resulting in a multilayer ordered structure. The intercalation

Chapter 2. Polymer-clay nanocomposites: a brief overview

of the polymer chains results in the increase of the interlayer spacing, but causing less than 2 – 4 nm separation between the platelets [2 – 3, 25]. The exfoliated structure is characterized by the complete delamination of the clay platelets, comprising individual clay sheets dispersed within the polymer matrix. In such case, the platelets separation exceeds the 8 – 10 nm [2 – 3, 12, 25]. It should be noted, that the majority of polymer-clay nanocomposites, particularly those prepared by melt mixing, have an intermediate morphology, consisting of intercalated clay tactoids and some exfoliated platelets [3, 13, 25, 29 – 31].

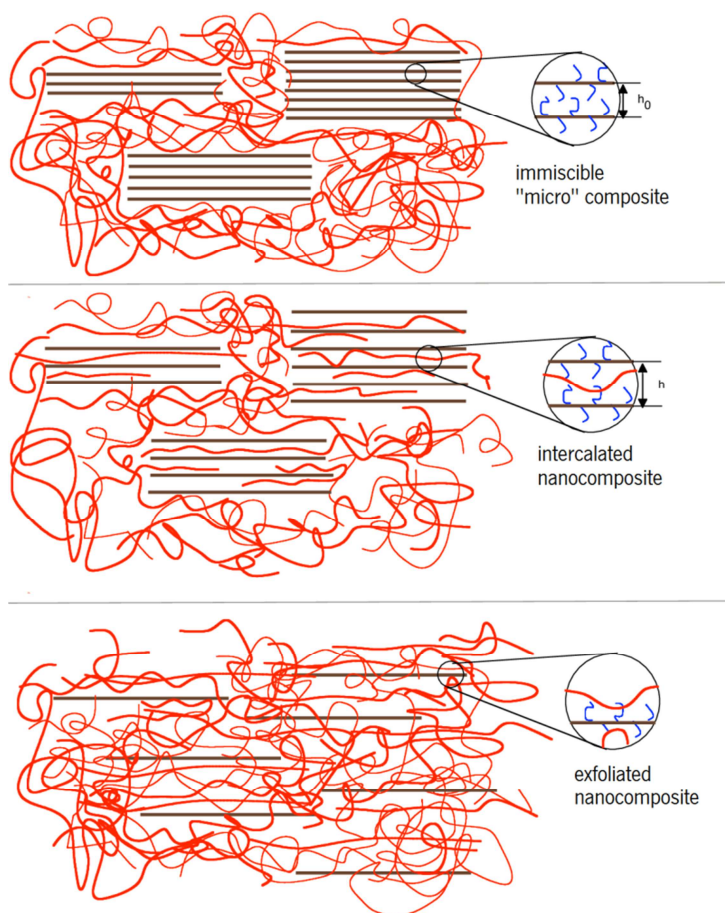


Figure 2. 2. Schematics of possible polymer-clay composite structures [27]

Polymer-clay nanocomposites are sought because of their improved properties, which are highly dependent of the developed structure. High dispersion levels are required in order to maximize the polymer-clay interactions, resulting in materials with enhanced mechanical properties, low permeability, improved flame retardant behaviour and thermal stability, and catalytic effect over the

Chapter 2. Polymer-clay nanocomposites: a brief overview

biodegradability of biodegradable polymers, while keeping the optical transparency, low density and processability [3, 9 – 10, 26, 32 – 33].

The tensile properties, namely the Young's Modulus and elongation at break, can be strongly improved when highly dispersed nanocomposites are formed. For example, Hasegawa *et al* [34] reported an 86% increase in the tensile modulus of the nanocomposite with 5 wt.% of clay loading, relative to the PP-g-MA matrix. However, the mechanism by which the clay particles exert mechanical reinforcement is still disputed [7, 9 – 10, 13, 22, 35 – 37]. Bousmina [13] showed that the nanocomposites yielding better dispersion do not necessarily exhibit better mechanical performance. The author explains that to play their role as rigid fillers, some level of stacking is preferred. Completing that stacks of 10 to 20 layers (approximately 10 to 20 nm thick) are less flexible and bend less, imparting better reinforcement to the flexible polymeric matrix.

Flame retardant materials are increasingly required for applications in automotive, construction and electronics [3, 9 – 10, 32, 38]. This characteristic is thus associated with the majority of applications of these materials. Curiously, the mechanism by which a polymer reinforced with clay becomes flame retardant is related to the higher thermal stability and the enhanced barrier properties. The clay acts as insulator and as mass transport barrier to the volatile products resultant of thermal decomposition, improving the thermal stability [9 – 10, 32]. The principle for improving barrier properties is based on tortuous paths [9] formed by the large number of highly anisometric particles dispersed within the polymer, making harder for gases like O₂ and CO₂ to diffuse. This characteristic is extremely useful for the applications in the packaging industry [3, 9 – 10, 38].

The improvement of the biodegradability of biodegradable polymers (like PCL and PLA) is not a recent discovery, but yields the prospective evolutionary steps of polymer-clay nanocomposites [9 – 10, 33, 39 – 40]. Ray *et al* [41 – 42] used PLA-based nanocomposites and showed a significantly improvement of the biodegradability of the nanocomposites relative to the PLA matrix. However, as for plenty other aspects, some authors [43 – 44] present contradictory results concerning the effect of clay dispersion on polymer biodegradability. Lee *et al* [43] found that the increasing intercalation levels caused lowering of the biodegradability under composting, assuming that the highly dispersed particles formed a more tortuous path that hinders the microorganisms penetration and diffusion. Maiti *et al* [44] found similar results and related this with the improvement of barrier properties.

2.3.2. Preparation methods

Polymer-clay nanocomposites are obtained by the intercalation of the polymer inside the gallery space between the silicate layers, eventually leading to delamination of individual platelets, uniformly dispersed within the host resin. In order to attain the desired properties, it is necessary to control the polymer-filler and filler-filler interactions, as well as several other thermodynamic and thermomechanic factors that may influence the clay dispersion. The most controllable variables are related to processing conditions and the interfacial chemistry.

There are several routes for the manufacture of polymer-clay nanocomposites, which can be included in three main processes [2 – 3, 9 – 10, 12, 33]:

- i. Intercalation of polymer (or prepolymer) from solution: It is a solvent based method, in which the polymer solution replaces an appropriate previously intercalated solvent. When using adequate organic solvents the clay stacks can be easily dispersed. The polymer is adsorbed onto the layer surfaces, and by evaporation of the solvent, the clay platelets return to the equilibrium state, fixing the polymer chains inside the galleries. Methodologies based on this process are limited to polymers soluble in organic solvents. Moreover, large scale production using this technique presents high costs and serious environmental and health hazards.
- ii. In-situ intercalative polymerization: This was the first method used to prepare nylon 6-clay nanocomposites. The method includes the swelling of the modified clay by a liquid monomer or a monomer solution. Polymerization is triggered by heat or radiation, aided by the diffusion of a proper initiator or catalyst, which was previously fixed in the interlayer spacing by cationic exchange. Once more, this method presents some disadvantages of applicability in industrial scale production.
- iii. Melt intercalation: This method involves the direct mixing of the clay with the polymer matrix in the molten state. Under the right conditions, the polymer melt can diffuse within the clay layers forming the nanocomposite. Melt intercalation can be carried out in conventional polymer compounding and/or processing equipment, representing a cost effective and environmentally sound way for the industrial scale production of polymer nanocomposites.

2.3.3. Characterization

Transmission Electron Microscopy (TEM) and X-ray diffraction (XRD) are the most commonly used techniques [2, 21, 38, 45 – 47] for the characterization of polymer-clay nanocomposites. TEM analysis provides a direct view of clay dispersion, enabling the determination of agglomerates/particle size and number of stacks/platelets per area. However, TEM analyses only very small areas, requires time consuming sample preparation and tedious data treatment [2, 38, 45]. XRD presents a clear region of interest at low angles, due to the clay typical Bragg's diffraction peak, from which the clay spacing and the stacks height may be estimated. However, XRD fails to provide information on the spatial distribution of the clays within the host resin, and is prone to interferences [2, 21, 38, 45]. Many factors, such as clay loading, orientation and crystallinity, influence the XRD peaks of polymer-clay nanocomposites. Some recent studies have focused on developing a quantitative analysis of the clay dispersion, by combining TEM and XRD techniques [46 – 47]; this appears to work well, given that one technique is able to fill the information gap of the other. It is reasonable to say that the results are good and within the nanoscale range, but also exceedingly localized. In order to perceive the overall state of clay dispersion a very extent and exhaustive study would be required, making these techniques extremely time consuming and expensive [2, 38, 45]. Figure 2. 3 shows TEM and X-ray results of the different states of dispersion of the organoclays in the polymer matrix [38].

Chapter 2. Polymer-clay nanocomposites: a brief overview

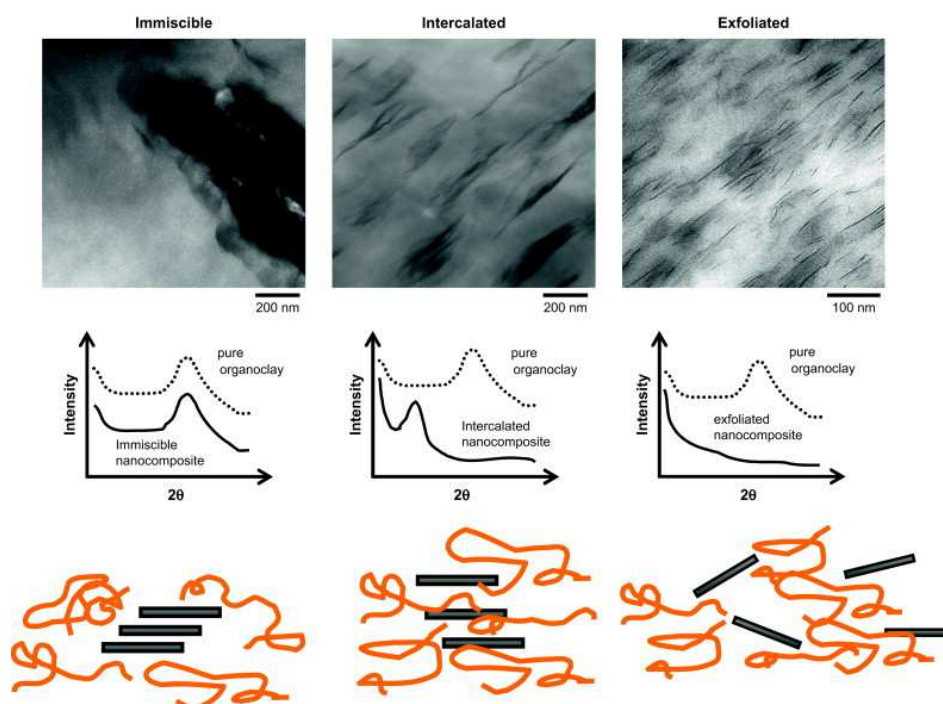


Figure 2. 3. Illustration of the different states of clay dispersion and corresponding WAXS and TEM results [38].

Rheology is amongst the most mentioned analytical tools for the characterization of nanocomposites [47 – 52]. It is known that melt rheological properties of filled polymers are sensitive to the structure, particle size and shape, as well as interfacial characteristics, thus providing valid means to assess the state of dispersion of the nanocomposites. Several authors have successfully related the rheological response with the state of dispersion [29, 31, 47, 49 – 50, 53 – 54] while others used it for distribution and structural effects [10, 47, 50 – 53, 55 – 57]. However, if the rheological behavior of nanocomposites offers a practical qualitative insight on the filler dispersion, a special care is required when performing a quantitative assessment by these means. Quantitative analysis of filler dispersion by rheological measurements is limited in the literature, mainly due to the difficulties to model the variation of the linear viscoelastic properties that depend on the filler concentration and exfoliation state [52, 55]. In recent studies, Lertwimolnun and Vergnes [29, 31, 53] defined the use of a modified Carreau-Yasuda model with yield stress (σ_0) to describe the frequency dependence of the absolute complex viscosity. It is of general assumption that the melt yield stress is associated with transition from liquid-like to solid-like behavior, and is attributed to the formation of a percolated network structure of intercalated tactoids and exfoliated platelets [48, 52,

Chapter 2. Polymer-clay nanocomposites: a brief overview

55 – 56, 58]. Lertwimolnun and Vergnes related the melt yield stress to the level of exfoliation in the polypropylene (PP) based nanocomposites, as shown in Figure 2. 4. Accordingly, they were able to quantitatively study the effects of several extrusion operating-conditions and material characteristics on the nanocomposite dispersion. Other studies used a power law expression to explain the complex viscosity (η^*) and storage modulus (G') behavior at low frequency [47, 49 – 50, 54]. In both cases, the power law exponent (b) was correlated to the state of clay dispersion. However, the same dependence was found both for high clay loading in a poorly dispersed composite and for good clay dispersion at lower clay concentration [47, 50]. Also, the storage and loss moduli values (G' and G'') may provide a good perception of dispersion, the increase of their values having been related to a finer dispersion [53], while the formation of a plateau at low frequencies has been attributed to the deformation and recovery of the dispersed particles [51 – 52, 56 – 57].

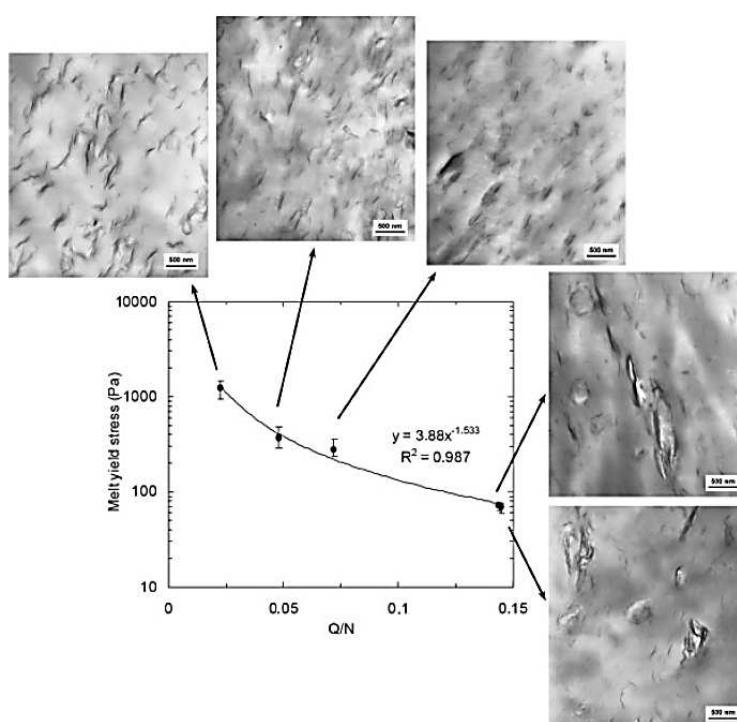


Figure 2. 4. Evolution of melt yield stress as a function of the filling ratio (Q/N) for nanocomposites prepared under different operating condition [29].

Several spectroscopy techniques, like nuclear magnetic resonance (NMR), have also been used to characterize the morphology, surface chemistry and dynamics of exfoliated polymer nanocomposites [59 – 62]. Vander Hart *et al* [59 – 62], use solid state ^1H -NMR to evaluate the degradation of the organic modifier of the clay, through the resonance potions. Also, considering the paramagnetic spin

Chapter 2. Polymer-clay nanocomposites: a brief overview

effects of the metallic cations present in the clay chemical composition, the authors use the relaxation spin times (T_1^H), measured by ^{13}C -NMR, to evaluate the clay dispersion. In principle, if the clay is poorly dispersed, the greater is the average distance between each polymer-clay interface and the weaker is the average paramagnetic contribution to T_1^H .

Fourier transformed infra-red spectroscopy (FT-IR) is also used to gather information about the dispersion of polymer-clay nanocomposites [4, 63 – 66]. For some authors FT-IR analysis is more efficient than XRD, as it can overcome the maximum limit of interlayer distance (8 nm) detected. It also is less time consuming than TEM [4, 64]. Due to its structure (Figure 2. 1) layered-silicates present a complex FT-IR spectrum, but also due to its Si-O bonds, with a pronounced band between 1300 and 900 cm^{-1} , the clay layers are easily differentiated of the polymer spectrum. The applicability of FT-IR is based on the principle that the clay band can be decomposed into at least four peaks, three of those related to the Si-O in-plane vibrations (or bonds with basal oxygen) and one peak for the Si-O out-of-plane vibration (with apical oxygen or hydroxyl group). This is accomplished by fitting this spectral region with a Pearson VII expression, forcing a 75% Gaussian peak shape [63 – 65]. It is established [4, 5, 63, 65 – 68] that the in-plane vibration peaks appear at about 1120, 1050 and 1020 cm^{-1} and the out-of-plane vibration peak appears at about 1075 cm^{-1} . However, because of the trichroic behavior of the clay, preferential orientation of the particles may induce misleading conclusions in terms of intercalation/exfoliation quality. To overcome this, the use of a polarizing lens [63, 66], enables the measurement of the spectra with different dipole moments, necessary for the subsequent calculation of the structural factor (SF) spectrum, which is equivalent to the spectrum of the nanocomposite with no preferential orientation of the clay in the polymer matrix [63, 66]. From this analysis it is expected that the area, or height, of the in-plane peaks ratio (1050 cm^{-1} /1020 cm^{-1}) increases with swelling of the interlayer spacing (intercalation), whilst the intensity of the peak at 1075 cm^{-1} increases as the individual clay layers become more spaced out (exfoliation). Also, when the obtained structure is ordered and intercalated, the peak at 1050 cm^{-1} will show a negative shift towards lower wavenumbers becoming 1040 cm^{-1} , whilst the peak at 1075 cm^{-1} will show a positive shift towards higher wavenumbers in case of highly intercalated or partially exfoliated structures [63 – 64, 66].

Measuring the mechanical properties is a direct way to determine the reinforcement effect of the nanosilicate [2, 9, 13, 35, 37 – 38]. Yet again, the exact relation between improvement of

Chapter 2. Polymer-clay nanocomposites: a brief overview

mechanical properties and clay dispersion is much disputed. The nanoclays reinforcement effect depends on the level of adhesion between filler and matrix, the nanoparticles aspect ratio (individual layers, stacked layers or tactoids) and also the nucleating effect of the clays that can greatly change the crystallinity of the polymer matrices. Early studies by the Toyota group [34] presented DMA results of different nanocomposites and showed a direct dependence between the reinforcement effect and the higher clay dispersion. Similar results were found by others [20, 25, 69], particularly for nanocomposites prepared with high polarity polymer matrices. The effect of using Maleic Anhydride (MA) as compatibilizer has also been studied [35, 37]. When using non-polar matrices, like polyethylene and polypropylene, the use of a maleated compatibilizer is often required to increase the adhesion between the clay layers and the matrix, thus maximizing the dispersion potential. However, the results show that beyond a critical concentration, the content of MA is damaging, as the clay reinforcement effect is not able to outdo the reduced mechanical properties of the highly modified matrix. The effect of MA grafting is well known to result in the loss of viscoelastic properties as well as mechanical performance [70, 71]. As it was mentioned before, Bousmina [13] applied different shearing conditions to the same polymer-clay system, the author obtained nanocomposites with different states dispersion (as confirmed by TEM) yet the mechanical results showed that the fully exfoliated sample presents an intermediate value of Young's modulus. Figure 2. 5 shows the TEM micrographs and respective Young modulus results. The author related this to the flexibility of the individual clay sheets and polymer matrix, stating that to increase the modulus the clay particles should play their role as rigid fillers, and for that it is better to have some dispersed stacks rather than individual clay lamellae.

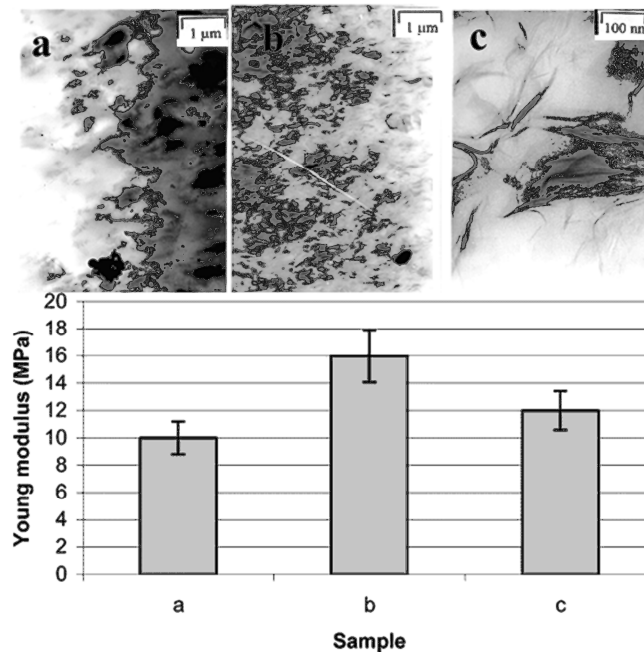


Figure 2. 5. TEM micrographs showing different states of dispersion of the nanocomposites and respective Young modulus data [13].

2.3.4. Dispersion in melt mixing

Since Vaia *et al* [72] demonstrated that polymer-clay nanocomposites can be obtained by direct polymer melt intercalation, the attention turned from in-situ intercalation to melt intercalation. As such, it is currently well established that melt compounding, is an industrially viable mean of preparing polymer-clay nanocomposites [25, 30, 72]. This approach can be implemented using conventional polymer processing techniques such as extrusion, enabling the reduction of the time needed for the nanocomposite structure development, by breaking the clay particles and increasing sample uniformity [25, 30, 72].

With this preparation method, usually the polymer is melted and compounded with previously intercalated (i.e. modified) clay using an extruder, a batch mixer, etc, [2 – 3, 9 – 10, 38]. During melt mixing, proper dispersion of the clay particles is achieved if the cohesive forces between the clay layers are exceeded by the hydrodynamic stresses applied by the polymer melt [3, 13]. Hence, for a successful melt intercalation to take place, at least three base conditions must be verified: (i) there must be an enthalpic driving force for the polymer; (ii) the interlayer space should be at least of the same order of magnitude as the diameter of the polymer macromolecular coil; (iii) sufficient

Chapter 2. Polymer-clay nanocomposites: a brief overview

residence time must be provided for the diffusion process. During melt compounding there are plenty parameters (screw speed, feed rate, temperature, screw profile) that can disturb this process, influencing the validity of these base conditions [2 – 3, 9, 13, 25, 30].

Along the past decade, researchers explored the effects of the matrix viscosity/molecular weight [73 – 75], the chemical affinity of the polymer-clay interface [13, 35, 37, 55, 75 – 77], the type of mixer and mixing protocols [25, 30, 78 – 79] and the effects of screw speed and throughput [25, 29, 31, 36, 53]. It is accepted that the dispersion mechanism combines the process of diffusion of the polymer chains within the clay interlayer spacing (intercalation) and proper mechanical effort to delaminate the individual platelets (exfoliation). Despite a few discrepancies, the main conclusions include the following [13, 25, 78]:

- Intercalation is practically independent of the processing conditions, but time is a critical parameter to enable polymer melt diffusion with the layer spacing;
- Exfoliation is extremely dependent on the chemistry, as well as on the mechanics and physics of the melt mixing process.
- A balance between time for diffusion and shear for exfoliation is required.
- If the conditions favour higher mobility of the polymer chains and if proper chemical affinity exists, exfoliation could happen even at a low shear rates.

For a polypropylene/polypropylene grafted with maleic anhydride/Cloisite 20A (PP/PP-g-MA/C20A) system, Lertwimolnun and Vergnes [29] established a correlation between the exfoliation levels, determined by the melt yield stress and the processing conditions (see Figure 2. 4), stating that higher exfoliation is achieved with for low Q/N ratios, meaning higher screw speeds and lower feed rates.

Dennis *et al*/[25] proposed a mechanism that includes a diffusion controlled route, in which occurs a shear controlled breakage of the organoclay particles, sequential intercalation of the polymer, and the peeling off of clay layers, one by one, from the top and bottom of each clay stack [3, 25]. Figure 2. 6 exhibits the schematics of the proposed mechanism.

Figure 2. 6(a) represents the mechanism based on the relationship between the polymer-clay affinity and the operating conditions used during melt compounding. The first pathway is chemistry

dependent, in this case the compatibility between the clay surface and the matrix is high and well exfoliated nanocomposites can be prepared in virtually any set of processing conditions [25]. Identical interpretations have been reported for most cases studying polyamide based nanocomposites [17 – 18, 20, 25, 30, 38, 73 – 74]. The second pathway proposed by Dennis *et al* [25], considers the effect of marginally compatible polymer-clay systems, this being the case of most polyolefin based systems [7, 11, 21 – 22, 29, 31, 34 – 37, 53, 55, 76, 78]. In this situation both chemical affinity and processing conditions can be optimized in order to obtain improved clay dispersion. The third pathway is that where there are no compatibility between the clay and the matrix, and although processing conditions can be adjusted, it is difficult to achieve a nanoscale dispersed phase.

Figure 2. 6(b) shows the possible mechanism for delamination of the clay particles under action of shear forces. Although the authors [25] claim that shearing is not the whole solution for delamination, they state that increasing shear intensity leads to improved exfoliation. This mechanism includes the break-up of the agglomerates into stacks, by sliding the platelets apart (which requires high shear intensity), followed by diffusion of the polymer chains in the clay galleries (driven by chemical affinity) causing the peeling of the platelets, starting from the edges.

More recently, Bousmina [13] showed that the diffusion of the polymeric chains inside the clay galleries (intercalation) is best obtained under mild shearing conditions (or in a medium to low viscosity matrix) applied during sufficient residence time, whereas extensive exfoliation requires a high level of shearing/deformation.

The majority of these studies are based on small-scale experiments [13, 74, 76] and on characterization of the final nanocomposites collected at the end of a compounding cycle [53], or at the extruder die exit [25, 30]. Despite the well-established global correlations between processing conditions and final dispersion levels, the role of the process parameters on the onset and kinetics of these steps has been the subject of debate. Logically, the evolution of clay dispersion along an extruder, where a complex non-isothermal 3D flow develops, seems less well understood.

Chapter 2. Polymer-clay nanocomposites: a brief overview

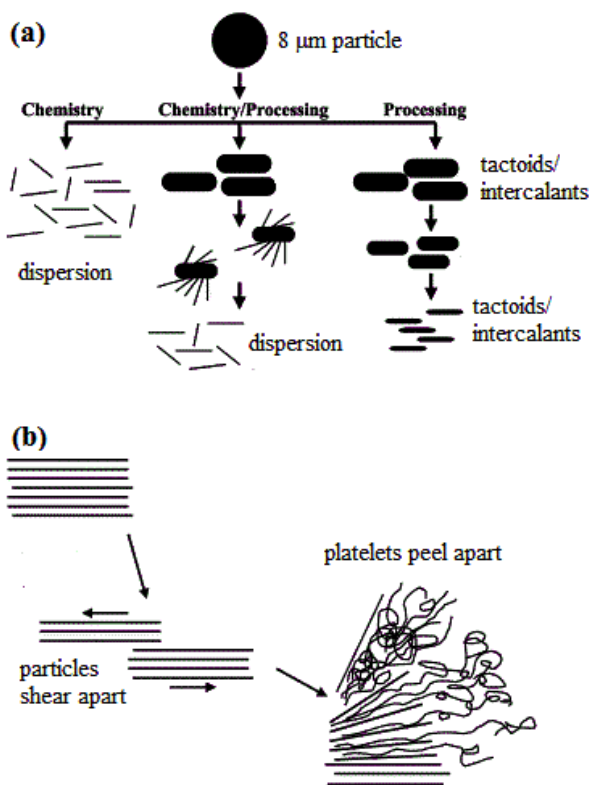


Figure 2. 6. Mechanism of dispersion of the organoclay particles during melt processing, proposed by Dennis et al [25]:

(a) three possible pathways involving the combination of chemistry and processing conditions;

(b) break-up of the agglomerated under action of shear, and peeling of the platelets.

Lertwimolnun and Vergnes [29, 31] characterized post-mortem samples collected from various locations along a co-rotating twin screw extruder (TSE). Based upon previously proposed correlations between the rheological response and dispersion of nanocomposites, they concluded that both intercalation and exfoliation can reach relatively high levels immediately after melting. They also observed that less restrictive screw profiles yielded better dispersion levels. Furthermore, depending on the combination of screw profile and operating conditions, dispersion could develop, remain constant, or apparently revert along the screw axis. Figure 2. 7 shows the results obtained by Lertwimolnun and Vergnes [31] for the effect of feed rate, along the extruder. The figure presents the variation of the interlayer spacing (d_{001}) determined by XRD (left), which is associated with intercalation, and of the melt yield stress (right) that is related to exfoliation. Here the feed rate appears to have a small impact of the intercalation levels, whereas for the exfoliation a significant increase is seen for the lower feed rate. All conditions show evidences of reversion of the exfoliation levels close to the die exit.

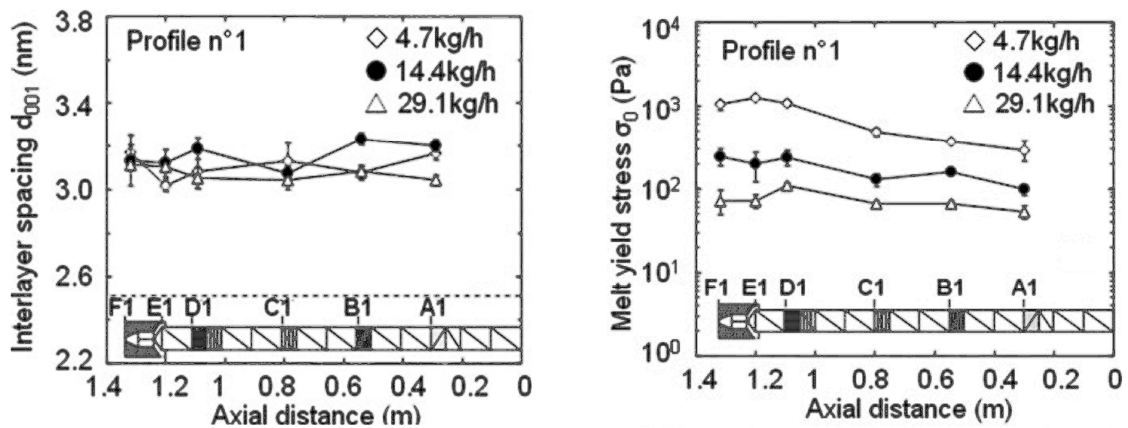


Figure 2. 7. Effect of the feed rate on the variation of the interlayer spacing (left) and the melt yield stress (right), along the extruder [31].

2.3.5. On-line and In-line Monitoring

During industrial extrusion and compounding only a few process parameters are continuously monitored (typically temperature, pressure and motor torque), which are unable to provide useful information about the material characteristics during processing. Thus, the possibility of assessing in real time the nanocomposite dispersion during processing remains an important scientific and technological target. Most of the techniques described in the previous section are exceedingly difficult, or even, impossible to implement as process monitoring tools. For example, the case of XRD, although feasible [80], requires extreme modifications to the processing equipment and sometimes the use of synchrotron radiation [81 – 87].

Of the aforementioned techniques, rheology appears an alternative. Since the viscoelastic behaviour of a polymer-clay nanocomposite is sensitive to composition, morphology, degree of mixing, temperature, etc, the data measured in real time can be used to assist the definition of material recipes, the optimization of operating conditions and/or screw design, as well as for quality control and, ultimately, process control. In fact, over the past two decades, academic groups [88 – 94] and rheometer manufacturers [95 – 98] have been attempting to develop reliable, precise, simple to operate and economically attractive in-line and on-line equipments. In-line fixtures are preferred, as they avoid melt by-passes [88, 90 – 93, 99]. Various constructions with different automation levels are available, but the majority of the devices are implemented in instrumented dies and it seems

Chapter 2. Polymer-clay nanocomposites: a brief overview

difficult to envision their application along the extruder axis. Most commercial solutions use capillary or slit rheometers to provide on-line measurements [95 – 97], comprising the continuous deviation of the melt from the main flow to the rheometer, at constant rate, as set by means of a gear pump. Although these devices are usually inserted between the extruder and the die, it is conceptually acceptable to fix them upstream. In this regard, the Piezo Axial Vibrator is particularly attractive, since its feed port has the geometry of a standard melt pressure transducer (standard 1/2 UNF thread) [98]. This apparatus generates an axial oscillation on the material sample and uses piezo elements to record the rheological moduli. However, it still requires improvements in robustness, handling and signal noise.

On-line solutions seem easier to adapt to different equipments, easier to operate, and provide simpler means of varying the shear rate/frequency and offer good temperature control. However, it is also important to ensure that these devices: i) minimize the time-lag between sample collection and measurement, ii) prevent material morphology changes both during sampling and measurement, iii) enable measurements along the axis of the extruder (under normal conditions, the morphology or chemical reaction of a given polymer system will have achieved steady-state or been completed well upstream of the die) and iv) are capable of performing measurements at temperatures different from the processing temperature (or even carry out temperature sweeps). Covas *et al.* [89] developed an on-line capillary rheometer capable of collecting quickly, but under adequate conditions, material samples from within an extruder, that could be fixed at different axial locations of the machine. The device was successfully used to study the viscosity evolution of various polymer systems along the screw, thus contributing to understand the corresponding mixing and/or chemical mechanisms. Later, an on-line rotational rheometer, capable of working either in steady shear or oscillatory mode, was developed [94]. The authors were able to demonstrate its usefulness by measuring the evolution of the rheological moduli (G' and G'') of a non-compatibilized and equivalent compatibilized polymer blend. They also showed how off-line measurements of samples collected from the extruder can produce misleading results, due to the changes in their characteristics that are induced by the several thermal cycles that they are subjected to during sample collection and preparation. Despite the encouraging results, the reproducibility of the device was somewhat operator dependent, owing to its mostly manual operation. Recently, an updated and fully automated version of the prototype on-line oscillatory rheometer has been presented [100].

Chapter 2. Polymer-clay nanocomposites: a brief overview

Figure 2. 8 provides a general view of the on-line rheometer when inserted at a given position along the barrel of a modular twin screw extruder. The system comprises a linear motor (A) to control the position of the lower plate, a rotational motor (B) to open/close the rotary valve (C) through which the melt is withdrawn from the extruder, a linear actuator (D) to move the cleaning ring and a commercial rotational rheometer head (E, Anton Paar DSR301). A more detailed description of the system set-up and operating sequences can be found elsewhere [94, 100]. The temperature inside the rheometer chamber is controlled by means of a thermocouple embedded in the lower plate, working independently of the extruder, enabling to perform measurements at temperatures different from the process settings, or even perform temperature ramps.

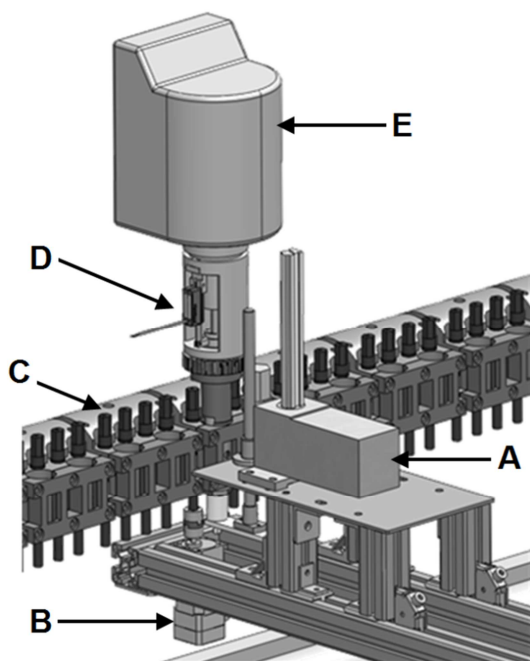


Figure 2. 8. General view of the on-line rheometer when inserted at a given position along the barrel of a twin screw extruder [100].

As seen in the figure if enough modified barrel elements are available, rheological measurements at small axial increments (typically $1D$, D being the screw diameter) are possible, i.e., a detailed evolution of the rheological response of a given material can be obtained. It is also worth mentioning that, in practice, these modified barrel elements can also accommodate other available on-line devices, namely an on-line Capillary Rheometer [89] and an on-line optical sensor for the measurement of Residence Time Distribution (RTD) [101].

Chapter 2. Polymer-clay nanocomposites: a brief overview

Recently, the on-line prototype rheometer has been successfully applied in the rheological characterization of a polypropylene/polypropylene grafted with maleic anhydride/Dellite 67G (PP/PP-g-MA/D67G) nanocomposite along the axis of a twin-screw extruder [100]. Figure 2. 9 shows the G' and G'' curves obtained in small amplitude oscillatory shear (SAOS) mode in three different locations along the extruder.

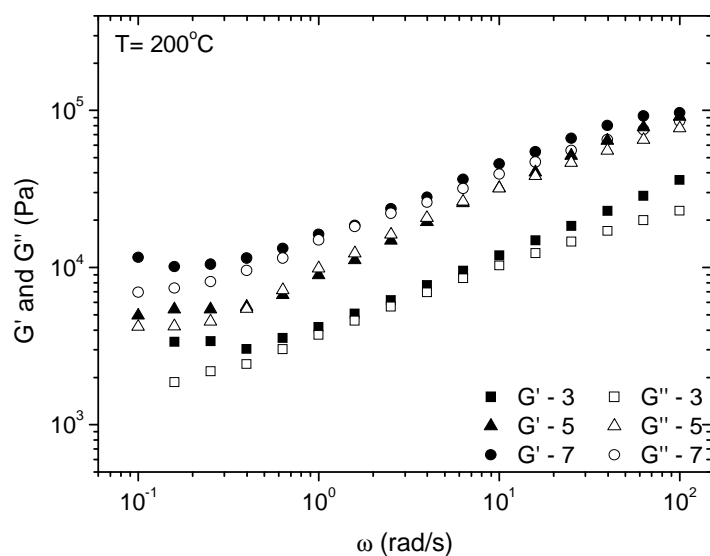


Figure 2. 9. Linear viscoelastic behaviour of PP/PP-g-MA/D67G nanocomposite at 200 °C, measured on-line in three different positions along the extruder [100].

Several spectroscopic techniques have also been successfully applied to monitor polymer processes [102 – 105]. Besides the conventional spectroscopic techniques like Raman [106 – 110], ultra violet-visible (UV-vis) and fluorescence [108 – 111] and attenuated total reflectance Infrared (ATR-IR) [106 – 107, 112 – 113], ultrasound [102, 106, 114] and dielectric probing [115 – 116] are also used for in-line monitoring. Process monitoring spectroscopy has found a development boost over the last 2 decades, mainly due to the advances in fiber-optic probes, sensors technology and equipment construction [104 – 106, 117 – 118]. However, its use for process monitoring has downsides, which have been overcome with the use of near-Infrared spectroscopy (NIR) [104 – 106, 117 – 118]. In-line monitoring using NIR is performed mostly in transmission mode, with a flow-cell fixture attached to modified extruder dies [104, 106, 108 – 110, 119 – 122] or at the injection machine nozzle [118, 123].

Chapter 2. Polymer-clay nanocomposites: a brief overview

In polymer industry, the use of NIR as a process monitoring tool is already well established, mainly for polymerization, co-polymerization and also depolymerization control [121 – 122, 124 – 129], control of particle size [121, 130 – 131] and diverse polymer process monitoring [104, 106, 109, 118, 120, 124]. For clay minerals the use of NIR is also common, mainly for the study of its chemical modification and adsorption mechanisms [132 – 135] and structural elements analysis [136 – 138]. There are also some studies on the relationship between medium Infrared (mIR) and NIR spectra, mainly in the OH group region [5, 68, 139].

The use of in-line NIR for characterization of polymer matrix nanocomposites is still limited. There are only few studies on the monitoring of melt processing of nanocomposites [123, 140] and reinforcement effect of the clay [141]. Moghaddam *et al* [123] used NIR spectroscopy in applied to polyurethane nanocomposites processing. For this study the NIR probe was connected to a laboratory scale extruder (Thermo-Haake Minilab Rheomex), as show in Figure 2. 10 to monitor the molecular structural changes. The NIR spectra were used to analyze the effect of temperature and particle size during melt-processing, and the small changes perceived indicate a decrease of urethane typical bonds during processing. The chemometric analysis of the measured spectra detected two phenomena occurring during processing; the first related to the softening of the hard segment during the initial 4 to 6 minutes, and the second occurring during the remainder of the processing cycle related to the degradation of TPU [123].



Figure 2. 10. Photograph of the NIR in-line set-up used by Moghaddam *et al* [123].

Chapter 2. Polymer-clay nanocomposites: a brief overview

Witshnigg *et al.* [140] interfaced the NIR probe between a laboratory extruder and the die and studied the effect of screw speed and screw geometry on the final properties of the prepared nanocomposites. The authors developed single parameter chemometric models based on the Young's Modulus, interlayer distance and drawing force. The results are mainly focused on the reinforcement effects of the clay. Some of the models showed a good relation between the measured values and the calculated NIR data, although the confidence of the calibration lines seemed insufficient to perform a quantitative analysis.

Another study was published by Laske *et al.* [141], using off-line NIR as a determination method for the reinforcement of polymer nanocomposites. The nanocomposites were processed at different conditions; the extrudates were granulated and used for the melt strength measurements. The NIR spectra were measured off-line from 0.8 mm thick plates in transmission mode. The results showed a direct correlation between the reinforcement levels determined by melt extensional measurements and the data obtained from off-line NIR spectra, showing that NIR spectroscopy can be applied as qualitative and quantitative method for monitoring the nanocomposite quality. Although they used both techniques off-line, they refer that both may be used as in-line techniques as long as the appropriate probes are selected for NIR and a by-pass die system is applied to enable Rheotens use [141].

2.4. Research Objectives

When preparing polymer-clay nanocomposites prepared by melt intercalation the global effects of the processing conditions in the dispersion levels of the resulting material are well established. However, the effect of the operating conditions, particularly during twin screw extrusion, on the mechanism of dispersion appears to be less understood.

Twin screw extrusion allows for control of the main variables (shear, stress and time), but also, due to the typical modular construction, offers a high degree of freedom in creating the adequate screw design and enables knowledgeable alteration of the barrel. These features offer a solid basis for the development and implementation of apt on-line/in-line monitoring techniques, able to follow up the evolution of dispersion of polymer-clay nanocomposites during processing.

The present research aims at applying on-line/in-line characterization techniques during the manufacture of polymer-clay nanocomposites by extrusion processes. Ultimately, the gathered information will provide further information on the critical processing parameters and a better understanding of their effect on the mechanism of dispersion

The main objectives include:

- i. to implement in-line NIR spectroscopy for monitoring the preparation of polymer-clay nanocomposites by melt mixing;
- ii. to establish a methodology, based on in-line NIR and chemometrics, enabling to follow-up the dispersion evolution along the twin screw extruder axis;
- iii. to establish a correlation between the processing conditions and the dispersion of polymer-clay nanocomposites.

2.5. References

1. S. M. Auerbach, K. A. Carrado, P. K. Dutta (Eds). Handbook of Layered Materials. NY - Basel : Marcel Dekker, Inc., (2004).
2. M. Alexandre, P. Dubois. Polymer-layered silicate nanocomposites: preparation, properties and uses of a new class of materials. *Materials Science and Engineering*. 28, p.1-63, (2000).
3. L.A. Utracki. Clay-Containing Polymer Nanocomposites - vol.1. UK : Rapra Technology Ltd., (2004).
4. L. Yan, C.B. Roth, P.F. Low. Changes in Si-O vibrations of smectite layers accompanying the sorption of interlayer water. *Langmuir*. 12, p. 4421-4429, (1996).
5. J. Madejová. FT-IR techniques in clay minerals. *Vibrational Spectroscopy*. 31, p. 1-10, (2003).
6. T. Mandalia, F. Bergaya. Organo clay mineral - melted polyolefin nanocomposites effect of surfactant/CEC ratio. *Journal of Physics and Chemistry of Solids*. 67, p. 836-845, (2006).
7. Y. Dong, D. Bhattacharyya. Effects of clay type, clay/compatibiliser content and matrix viscosity on the mechanical properties of polypropylene/organoclay nanocomposites. *Composites: Part A*. 39, p.1177-1191, (2008).
8. R. Zouari, T. Domenech, B. Vergnes, E. Peuvrel-Disdier. Time evolution of the structure of organoclay/polypropylene nanocomposites and application of the time-temperature superposition principle. *Journal of Rheology*. 56, p.725-742, (2012).
9. S. Pavlidou, C.D. Papaspyrides. A review on polymer-layered silicate nanocomposites. *Progress in Polymer Science*. 33, p. 1119-1198, (2008).
10. S.S. Ray, M. Okamoto. Polymer/layered silicate nanocomposites: a review from preparation to processing. *Progress in Polymer Science*. 28, p.1539-1641, (2003).
11. E. Passaglia, M. Bertoldo, S. Coiai, S. Augier, S. Savi, F. Ciardelli. Nanostructured polyolefins-clay composites: role of the molecular interaction at the interfaces. *Polymers for Advanced Technologies*. 19, p. 560-568, (2008).
12. R. K. Gupta, E. Kennel, K. Kim. *Polymer Nanocomposites Handbook*. USA : CRC Press, (2010).

Chapter 2. Polymer-clay nanocomposites: a brief overview

13. M. Bousmina. Study of the intercalation and exfoliation processes in polymer nanocomposites. *Macromolecules*. 39, p. 4259-4263, (2006).
14. L.B. Paiva, A.R. Morales, F.R. Valenzuela Díaz. Organoclays: Properties, preparation and applications. *Applied Clay Science*. 42, p. 8-24, (2008).
15. S-S. Lee, M.H. Hur, H. Yang, S. Lim, J. Kim. Effect of interfacial attraction on intercalation in polymer/clay nanocomposites. *Journal of Applied Polymer Science*. 101, p. 2749-2753, (2006).
16. R. Krishnamoorti, R.A. Vaia, E.P. Giannelis. Structure and dynamics of polymer-layered silicate nanocomposites. *Chemistry of Materials*. 8, p. 1728-1734, (1996).
17. T.D. Fornes, D.L. Hunter, D.R. Paul. Nylon-6 nanocomposites from alkylammonium-modified clay: the role of alkyl tails on exfoliation. *Macromolecules*. 37, p. 1793-1798, (2004).
18. T.D. Fornes, P.J. Yoon, D.L. Hunter, H. Keskkula, D.R. Paul. Effect of organoclay structure on nylon-6 nanocomposites morphology and properties. *Polymer*. 43, p. 5915-5933, (2002).
19. T.D. Fornes, D.L. Hunter, D.R. Paul. Effect of sodium montmorillonite source on nylon-6/clay nanocomposites. *Polymer*. 45, p. 2321-2331, (2004).
20. Y. Yoo, D.R. Paul. Effect of organoclay structure on morphology and properties of nanocomposites based on an amorphous polyamide. *Polymer*. 49, p.3795-3804, (2008).
21. B.N. Jang, D. Wang, C.A. Wilkie. Relationship between the solubility parameter of polymers and the clay dispersion in Polymer/clay nanocomposites and the role of the surfactant. *Macromolecules*. 38, p. 6533-6543, (2005).
22. D.H. Kim, P.D. Fasulo, W.R. Rodgers, D.R. Paul. Structure and properties of polypropylene-based nanocomposites: effect of PP-g-MA to organoclay ratio. *Polymer*. 48, p. 5308-5323, (2007).
23. R.K. Shah, D L. Hunter, D.R. Paul. Nanocomposites from poly(ethylene-co-methacrylic acid) ionomers: effect of surfactant structure on morphology and properties. *Polymer*. 46, p. 2646-2662, (2005).
24. E.P. Giannelis. Polymer layered silicates nanocomposites. *Advanced Materials*. 8, p. 29-35, (1996).

Chapter 2. Polymer-clay nanocomposites: a brief overview

25. H.R. Dennis, D.L. Hunter, D. Chang, S. Kim, J.L. White. J.W. Cho, D.R. Paul. Effect of melt processing conditions on the extent of exfoliation in organoclay-based nanocomposites. *Polymer*. 42, p. 9513-9522, (2001).
26. M.J. Solomon, A. Somwangthanaroj. *Intercalated Polypropylene Nanocomposites*. Dekker Encyclopedia of Nanoscience and Nanotechnology. NY: (2004), p. 1483-1490.
27. R. Krishnamoorti, J. Ren, A.S. Silva. Shear response of layered silicate nanocomposites. *Journal of Chemical Physics*. 114, p. 4968-4973, (2001).
28. J.H. Koo. *Polymer Nanocomposites: Processing, Characterization and Applications*. USA : McGraw-Hill, (2006).
29. W. Lertwimolnun, B. Vergnes. Effect of processing conditions on the formation of polypropylene/organoclay nanocomposites in a twin-screw extruder. *Polymer Engineering and Science*. 46, p. 314-323, (2006).
30. J.W. Cho, D.R. Paul. Nylon 6 nanocomposites by melt compounding. *Polymer*. 42, p. 1083-1094, (2001).
31. W. Lertwimolnun, B. Vergnes. Influence of screw profile and extrusion conditions on the microstructure of polypropylene/organoclay nanocomposites. *Polymer Engineering and Science*. 47, p. 2100-2109, (2007).
32. L.A. Utracki. *Clay-Containing Polymer Nanocomposites - vol.2*. UK : Rapra Technology Ltd., (2004).
33. Hussain, M. Hojjati, M. Okamoto, R.E. Gorga. Polymer-matrix nanocomposites, processing, manufacturing and application: an overview. *Journal of Composite Materials*. 40, p. 1511-1575, (2006).
34. N. Hasegawa, H. Okamoto, M. Kato, A. Usuki. Preparation and mechanical properties of polypropylene-clay hybrids based on modified polypropylene and organophilic clay. *Journal of Applied Polymer Science*. 78, p. 1918-1922, (2000).
35. M.W. Spencer, L. Cui, Y. Yoo, D.R. Paul. Morphology and properties of nanocomposites based on HDPE/HDPE-g-MA blends. *Polymer*. 51, p. 1056-1070, (2010).

36. P. Peltola, E. Valipakka, J. Vourinen, S. Syrjala e Hanhi., K. Effect of rotational speed of twin screw extruder on the microstructure and rheological and mechanical properties of nanoclay-reinforced polypropylene nanocomposites. *Polymer Engineering and Science* 46 (2006) 995-1000. 46, p. 995-1000, (2006).
37. M. Modesti, A. Lorenzetti, D. Bon, S. Besco. Effect of processing conditions on morphology and mechanical properties of compatibilized polypropylene nanocomposites. *Polymer* . 46, p. 10237-10245, (2005).
38. D.R. Paul, L.M. Robeson. *Polymer nanotechnology: Nanocomposites*. *Polymer*. 49, p. 3187-3204, (2008).
39. M. Okamoto. Recent advances in polymer/layered silicate nanocomposites: an overview from science to technology. *Materials Science and Technology*. 22, p. 756-778, (2006).
40. S.S. Ray, M. Bousmina. Biodegradable polymers and their layered silicate nanocomposites: in greening the 21st century materials world. *Progress in Material Science*. 50, p. 962-1079, (2005).
41. S.S. Ray, K. Yamada, M. Okamoto, K. Ueda. New polylactide/layered silicate nanocomposites. 2. Concurrent improvements of material properties, biodegradability and melt rheology. *Polymer*. 44, p. 857-866, (2003).
42. S.S. Ray, K. Yamada, M. Okamoto, A. Ogami, K. Ueda. New poly-lactide/layered silicate nanocomposites. 3. High performance biodegradable materials. *Chemistry of Materials*. 15, p. 1456-1465, (2003).
43. S.R. Lee, H.M. Park, H. Lim, T. Kang, X. Li, W.J. Cho, C.S. Ha. Microstructure, tensile poperties and biodegradability of aliphatic polyester/clay nanocomposites. *Polymer*. 43, p. 2495-2500, (2002).
44. P. Maiti, C.A. Batt, E.P. Giannelis. Renewable plastics: synthesis and properties of PHB nanocomposites. *Journal of Macomolecular Science Reviews*. 88, p. 58-59, (2003).
45. A.B. Morgan, J.W. Gilman. Characterization of polymer-layered nanocomposites by Transmission Electron Microscopy and X-Ray Diffraction: a comparative study. *Journal of Applied Polymer Science*. 87, p. 1329-1338, (2003).

Chapter 2. Polymer-clay nanocomposites: a brief overview

46. J. Bandyopadhyay, S.S. Ray. The quantitative analysis of nano-clay dispersion in polymer nanocomposites by small angle X-ray scattering combined with electron microscopy. *Polymer*. 51, p. 1437-1449, (2010).
47. A. Vermogen, K. Masenelli-Varlot, R. Séguela, J. Duchet-Rumeau, S. Boucard, P. Prele. Evaluation of the structure and dispersion in polymer-layered silicate nanocomposites. *Macromolecules*. 38, p. 9661-9669, (2005).
48. J. Ren, B.F. Casanueva, C.A. Mitchell, R. Krishnamoorti. Disorientation kinetics of aligned polymer layered silicate nanocomposites. *Macromolecules*. 36, p. 4188-4194, (2003) .
49. R. Wagener, T. Reisinger. A rheological method to compare the degree of exfoliation of nanocomposites. *Polymer*. 44, p. 7513-7518, (2003).
50. A. Durmus, A. Kasgoz, C.W. Macosko. Linear low density polyethylene (LLDPE)/clay nanocomposites. Part I: Structural characterization and quantifying clay dispersion by melt rheology. *Polymer*. 48, p. 4492-4502, (2007).
51. M.J. Solomon, A.S. Almusallam, K.F. Seefeldt, A. Somwangthanaroj, P. Varadan. Rheology of Polypropylene/Clay hybrid materials. *Macromolecules*. 34, p. 1864-1872, (2001).
52. P. Cassagnau. Melt-rheology of organoclay and fumed silica nanocomposites. *Polymer*. 49, p. 2183-2196, (2008).
53. W. Lertwimolnun, B. Vergnes. Influence of compatibilizer and processing conditions on the dispersion of nanoclay in a polymer matrix. *Polymer*. 46, p. 3462-3471, (2005).
54. J.Vermant, S. Ceccia, M.K. Dolgovskij, P.L. Maffettone, C.W. Macosko. Quantifying dispersion of layered nanocomposites via melt rheology. *Journal of Rheology*. 51, p. 429-450, (2007).
55. L. Xu, H. Nakajima, E. Manias, R. Krishnamoorti. Tailored nanocomposites of Polypropylene with layered silicates. *Macromolecules*. 42, p. 3795-3803, (2009).
56. S. Tanoue, L.A. Utracki, A. Garcia-Rejon, P. Sammut, M.T. Ton-That, I. Pesneau, M.R.Kamal, J. Lyngaae-Jorgensen. Melt compounding of different grades of Polystyrene with Organoclay. Part 2: Rheological properties. *Polymer Engineering and Science*. 44, p. 1061-1076, (2004).

57. J. Ren, A.S. Silva, R. Krishnamoorti. Linear viscoelasticity of disordered polystyrene-polyisoprene block copolymer based layered-silicate nanocomposites. *Macromolecules*. 33, p. 3739-3746, 2000.
58. J. Ren, R. Krishnamoorti. Nonlinear viscoelastic properties of layered-silicate-based intercalated nanocomposites. *Macromolecules*. 36, p. 4443-4451, (2003).
59. D.L. VanderHart, A. Asano, J.W. Gilman. NMR measurements related to clay-dispersion quality and organic modifier stability in nylon-6/clay nanocomposites. *Macromolecules*. 34, p. 3819-3822, (2001).
60. D.L. VanderHart, A. Asano, J.W. Gilman. Solid state NMR investigation of paramagnetic nylon-6 clay nanocomposites. 1. Crystallinity, morphology and the direct influence of Fe³⁺ on nuclear spins. *Chemistry of Materials*. 13, p. 3781-3795, (2001).
61. D.L. VanderHart, A. Asano, J.W. Gilman. Solid state NMR investigation of paramagnetic nylon-6 clay nanocomposites. 2. Measurement of clay dispersion, crystal stratification and stability of organic modifiers. *Chemistry of Materials*. 13, p. 3796-3809, (2001).
62. S. Bourbigot, D.L. VanderHart, J.W. Gilman, W.H. Awad, R.D. Davis, A.B. Morgan, C.A. Wilkie. Investigation of nanodispersion in polystyrene-montmorillonite nanocomposites by solid-state NMR. *Journal of Polymer Science Part B*. 41, p. 3188-3213, (2003).
63. L.S. Loo, K.K. Gleason. Fourier transform infrared investigation of the deformation behavior of montmorillonite in nylon-6/nanoclay nanocomposite. *Macromolecules*. 36, p. 2587-2590, (2003).
64. K.C. Cole. Use of Infrared spectroscopy to characterize clay intercalation and exfoliation in polymer nanocomposites. *Macromolecules*. 41, p. 834-843, (2008).
65. K.C. Cole, F. Perrin-Sarazin, G. Dorval-Douville. Infrared spectroscopic characterization of polymer and clay platelet orientation in blown films based on polypropylene-clay nanocomposite. *Macromolecular Symposium*. 230, p. 1-10, (2005).
66. W. L. IJdo, S. Kemnetz, D. Benderly. An infrared method to assess organoclay delamination and orientation in organoclay polymer nanocomposites. *Polymer Engineering and Science*. 46, p. 1031-1039, (2006), Vol. 46.

Chapter 2. Polymer-clay nanocomposites: a brief overview

67. C.T. Johnston, G.S. Premachandra. Polarized ATR-FTIR study of smectite in aqueous suspension. *Langmuir*. 17, p. 3712-3718, (2001).
68. J. Bishop, J. Madejová, P. Komadel, H. Fröschl. The influence of structural Fe, Al and Mg on the infrared OH bands in spectra of dioctahedral smectites. *Clay Minerals*. 37, p. 607-616, (2002).
69. H.E. Miltner, N. Watzeels, C. Block, N.A. Gotzen, G. Van Assche, K. Borghs, K. Van Durme, B. Van Mele, B. Bogdanov, H. Rahier. Qualitative assessment of nanofiller dispersion in poly(ϵ -caprolactone) nanocomposites by mechanical testing, dynamic rheometry and advanced thermal analysis. *European Polymer Journal*. 46, p. 984-996, (2010).
70. M. Xanthos (Ed.). *Reactive Extrusion*. Germany : Hanser Publishers, (1992).
71. S. Al-Malaika (Ed.). *Reactive modifiers for polymers*. UK : Chapman & Hall, (1997).
72. R.A. Vaia, H. Ishii, E.P. Giannelis. Synthesis and properties of two-dimensional nanostructures by direct intercalation of polymer melts in layered-silicates. *Chemistry of Materials*. 5, p. 1694-1696, (1993).
73. T.D. Fornes, P.J. Yoon, H. Keskkula, D.R. Paul. Nylon 6 nanocomposites: the effect of matrix molecular weight. *Polymer*. 42, p. 9929-9940, (2001).
74. S.W. Kim, W.H. Jo, M.S. Lee, M.B. Ko, J.Y. Jho. Effects of shear on melt exfoliation of clay in preparation of Nylon 6/Organoclay nanocomposites. *Polymer Journal* . 34, p. 103-111, (2002).
75. S. Tanoue, L.A. Utracki, A. Garcia-Rejon, J. Tibouet, K.C. Cole, M.R. Kamal. Melt compounding of diferente grades of Polystyrene with Organoclay. Part 1: Compounding and Characterization. *Polymer Engineering and Science* . 44, p. 1046-1060, (2004).
76. G. Galgali, C. Ramesh, A. Lele. A rheological study on the kinetics of hybrid formation in polypropylene nanocomposites. *Macromolecules* . 34, p. 852-858, (2001).
77. K. Chrissopoulou, S.H. Anastasiadis. Polyolefin/layered silicate nanocomposites with functional compatibilizers. *European Polymer Journal*. 47, p.600-613, (2011).

Chapter 2. Polymer-clay nanocomposites: a brief overview

78. M.A. Treece, W. Zhang, R.D. Moffit, J.P. Oberhauser. Twin-screw extrusion of Polypropylene-Clay nanocomposites: Influence of masterbatch processing, screw rotation mode and sequence . *Polymer Engineering and Science* . 47, p. 898-911, (2007).
79. P. Médéric, J. Ville, J. Huitric, M. Moan, T. Aubry. Effect of processing procedures and conditions on structural, morphological and rheological properties of Polyethylene/Polyamide/Nanoclay blends. *Polymer Engineering and Science*. 51, p. 969-978, (2011).
80. B.H. Hsiao, R. Barton Jr., J. Quintana. Simple on-line X-ray setup to monitor structure changes during fiber processing. *Journal of Applied Polymer Science*. 62, p. 2061-2068, (1996).
81. B. Chu, B.S. Hsiao. Small-angle X-ray scattering of polymers. *Chemical Reviews*. 101, p. 1727-1761, (2001).
82. E.L. Heeley, T. Gough, W. Bras, A.J. Gleeson, P.D. Coates, A.J. Ryan. Polymer processing: using synchrotron radiation to follow structure development in commercial and novel polymer materials. *Nuclear Instruments and Methods in Physics Research B* . 238, p. 21-27, (2005).
83. R. Kolb, S. Seifert, N. Striebeck, H.G. Zachman. Simultaneous measurements of small- and wide-angle X-ray scattering during low speed spinning of polypropylene using synchrotron radiation. *Polymer*. 41, p. 1497-1505, (2000).
84. A. Nogales, B.S. Hsiao, R.H. Somani, S. Srinivas, A.H. Tsou, F.J. Balta-Calleja, T.A. Ezquerro. Shear induced crystallization of isotactic polypropylene with different molecular weight distributions: in-situ small- and wide-angle X-ray scattering studies. *Polymer*. 42, p. 5247-5256, (2001).
85. S. Ran, C. Burger, I. Sics, K. Yoon, D. Fang, K. Kim, C. Avila-Orta, J. Keum, B. Chu, B. S. Hsiao, D. Cookson, D. Shultz, M. Lee, J. Viccaro, Y. Ohta. In situ synchrotron SAXS/WAXD studies during melt spin of modified carbon nanofiber and isotactic polypropylene nanocomposite. *Colloid and Polymer Science*. 282, p. 802-809, (2004).
86. T. Yamaguchi, K. Komoriyama, Y. Ohkoshi, H. Urakawa, Y. Gotoh, N. Terasawa, M. Nagura, K. Kajiwara. Online wide-angle X-ray diffraction/small-angle X-ray scattering measurements for

Chapter 2. Polymer-clay nanocomposites: a brief overview

- the CO₂-laser-heated drawing of poly(ethylene terephthalate) fiber. *Journal of Polymer Science Part B: Polymer Physics*. 43, p. 1090-1099, (2005).
87. M.S. Ellison, P.E. Lopes, W.T. Pennington. In-situ X-ray characterization of fiber structure during melt spinning. *Journal of Engineered Fibers and Fabrics*. 3, p. 10-21, (2008).
 88. M. Dealy, T.O. Broadhead. [autor do livro] A.A. Collyer (Ed.). *Techniques in Rheological Measurement*. London: Chapman & Hall, (1993).
 89. J.A. Covas, J.M. Nóbrega, J.M. Maia. Rheological measurements along an extruder with an on-line capillary rheometer. *Polymer Testing*. 19, p. 165-176, (2000).
 90. N. Dogan, M.J. McCarthy, R.L. Powell. Measurement of polymer melt rheology using ultrasonic-based in-line rheometry. *Measurement Science and Technology*. 16, p. 1684-1690, (2005).
 91. J. Wiklund, I. Shahram, M. Stading. Methodology for in-line rheology by ultrasound Doppler velocity profiling and pressure difference techniques. *Chemical Engineering Science*. 62, p. 4277-4293, (2007).
 92. R.S. Smith, J.A. Glasscock. Measurements of the rheological properties of standard reference material 2490 using an in-line micro-Fourier rheometer. *Korea-Australia Rheology Journal*. 16, p. 169-173, (2004).
 93. D.G. Baird, T.W. Chan, C. McGrady, S.M. Mazahir. Evaluation of the use of a semi-hyperbolic die for measuring elongational viscosity of polymer melts. *Applied Rheology*. 20, p. 34900-34912, (2010).
 94. J.A. Covas, J.M. Maia, A.V. Machado, P. Costa,. On-line rotational rheometry for extrusion and compounding operations. *Journal of Non-Newtonian Fluid Mechanics*. 148, p. 88-96, (2008).
 95. HAAKE ProFlow. (2006).
http://www.thermo.com/eThermo/CMA/PDFs/Product/ProductPDF_18544.pdf.
 96. Göttfert process rheometers. <http://www.goettfert.com>.
 97. Online Rheometer (Viscosensor). <http://www.dynisco.com>.

Chapter 2. Polymer-clay nanocomposites: a brief overview

98. V. Zschuppe, T. Geilen, J.M. Maia, J.A. Covas, H.M. Petri. Rheology Application Note LR-57. s.l. : Thermo Electron Corporation, (2006).
99. D.M. Kaylon, H.S. Gokturk. Adjustable gap rheometer. US Patent No 5, 277, 058 Hoboken, New Jersey , (1994).
100. S. Mould, J.M. Barbas, A.V. Machado, J.M. Nóbrega, J.A. Covas. Measuring the rheological properties of polymer melts with on-line rotational rheometry. *Polymer Testing*. 30, p. 602-610, (2011).
101. O.S. Carneiro, A. Poulesquen, J.A. Covas, B. Vergnes. Visualization and analysis of the flow along the kneading block of a twin-screw extruder. *International Polymer Processing*. 4, p. 301-308, (2002).
102. I. Alig, B. Steinhoff, D. Lellinger. Monitoring of polymer melt processing. *Measurement Science and Technology*. 21, p. 1-19, (2010).
103. D. Fischer, J. Müller, S. Kummer, B. Kretzschmar. Real time monitoring of morphologic and mechanical properties of polymer nanocomposites during extrusion by near infrared and ultrasonic spectroscopy. *Macromolecular Symposia*. 35, p. 10-17, (2011).
104. G. George, N. Hynard, G. Cash, L. Rintoul, M. O'Shea. Spectroscopic probes for real-time monitoring of polymer modification and degradation reactions. *Comptes Rendus Chimie*. 9, p. 1433-1443, (2006).
105. P.D. Coates, S.E. Barnes, M.G. Sibley, E.C. Brown, H.G. Edwards, I.J. Scowen. In-process vibrational spectroscopy and ultrasound measurements in polymer melt extrusion. *Polymer*. 44, p. 5937-5949, (2003).
106. I. Alig, D. Fischer, D. Lellinger, B. Steinhoff. Combination of NIR, Raman, Ultrasonic and Dielectric spectroscopy for in-line monitoring of the extrusion process. *Macromolecular Symposia* . 230, p.51-58, (2005).
107. S.E. Barnes, M.G. Sibley, H.G. Edwards, P.D. Coates. Process monitoring of polymer melts using in-line spectroscopy. *Transactions of the Institute of Measurement and Control*. 29, p.453-465, (2007).

Chapter 2. Polymer-clay nanocomposites: a brief overview

108. Y. Wang, B. Steinhoff, C. Brinkmann, I. Alig. In-line monitoring of the thermal degradation of poly (L-lactic acid) during melt extrusion by UV-vis spectroscopy. *Polymer*. 49, p. 1257-1265, (2008).
109. D. Fischer, K. Sahre, M. Abdelrhim, B. Voit, V.B. Sahdu, J. Pionteck, H. Komber, J. Hutschenreuter. Process monitoring of polymers by ATR-IR, NIR and Raman spectroscopy and ultrasonic measurements. *Comptes Rendus Chimie*. 9, p.1419-1424, (2006).
110. M.P. Villanueva, L. Cabedo, E. Giménez, J.M. Lagarón, P.D. Coates, A.L. Kelly. Study of the dispersion of nanoclays in a LDPE matrix using microscopy and in-process ultrasonic monitoring. *Polymer Testing*. 28, p. 277-287, (2009).
111. Y-H. Lee, A.J. Bur, S.C. Roth, P.R. Start, R.H. Harris. Monitoring the relaxation behavior of nylon/clay nanocomposites in the melt with an online dielectric sensor. *Polymers for Advanced Technologies*. 16, p. 249-256, (2005).
112. A.J. Bur, Y-H. Lee, S.C. Roth, P.R. Start. Measuring the extent of exfoliation in polymer/clay nanocomposites using real-time process monitoring methods. *Polymer*. 46, p. 10908-10918, (2005).
113. T.R. Rodd. Fiber-optic probes for near-infrared spectrometry. [autor do livro] P.R. Griffiths (Eds.) J.M. Chalmers. *Handbook of Vibration Spectroscopy, vol.2 – Sampling Techniques*. John Willey & Sons Ltd, (2002).
114. J.D. Tate, P. Chauvel, R.D. Guenard, R. Harner. Process monitoring by mid- and near-infrared Fourier transform spectroscopy. [autor do livro] P.R. Griffiths (Eds.) J.M. Chalmers. *Handbook of Vibration Spectroscopy, vol.4 – Applications in Industry, Materials and the Physical Sciences*. John Willey & Sons Ltd, (2002).
115. T. Rohe, W. Becker, S. Kölle, N. Eisenreich, P. Eyerer. Near infrared (NIR) spectroscopy for in-line monitoring of polymer extrusion processes. *Talanta*. 50, p. 283-290, (1999).
116. T. Nagata, M. Oshima, M. Tanigaki. In-line monitoring of polyethylene density using near infrared (NIR) spectroscopy. *Polymer Engineering and Science*. 40, p. 1107-1113, (2000).

117. C. Barrès, V. Bounor-Legaré, F. Melis, A. Michel. In-line near infrared monitoring of esterification of a molten ethylene–vinyl alcohol copolymer in a twin screw extruder. *Polymer Engineering and Science*. 46, p. 1613-1624, (2006).
118. O.R. Ghita, D.C. Baker, K.E. Evans. An in-line near-infrared process control tool for monitoring the effects of speed, temperature, and polymer colour in injection moulding. *Polymer Testing*. 27, p.459-469, (2008).
119. A. Cherfi, G. Fevotte, C. Novat. Robust on-line measurement of conversion and molecular weight using NIR spectroscopy during solution polymerization. *Journal of Applied Polymer Science*. 85, p. 2510-2520, (2002).
120. N.S. Othman, G. Fevotte, D. Peycelon, J-B. Egraz, J-M. Suau. Control of polymer molecular weight using near infrared spectroscopy. *AIChE Journal*. 50, p. 654-664, (2004).
121. M.M. Reis, P.H. Araújo, C. Sayer, R. Giudici. Spectroscopic on-line monitoring of reactions in dispersed medium: Chemometric challenges. *Analytica Chimica Acta*. 595, p. 257-265, (2007).
122. L.A. Rodriguez-Guadarrama. Application of online near infrared spectroscopy to study the kinetics of anionic polymerization of butadiene. *European Polymer Journal*. 43, p. 928-937, (2007).
123. L. Moghaddam, D.J. Martin, P.J. Halley, P.M. Fredericks. Vibrational spectroscopic studies of laboratory scale polymer melt processing: Application to a thermoplastic polyurethane nanocomposite. *Vibrational Spectroscopy*. 51, p. 86-92, (2009).
124. G. Lachenal. Characterization of poly(ethylene terephthalate) using near and far FTIR spectroscopy. *International Journal of Polymer Analysis and Characterization*. 3, p.145-158, (1997).
125. R.A. Heikka, K.T. Immonen, P.O. Minkkinen, E.Y.O. Paatero, T.O. Salmi. Determination of acid value, hydroxyl value and water content in reactions between dicarboxylic acids and diols using near-infrared spectroscopy and non-linear partial least squares regression. *Analytica Chimica Acta*. 349, p. 287-294, (1997).

Chapter 2. Polymer-clay nanocomposites: a brief overview

126. T. Amari, Y. Ozaki. Generalized two-dimensional Attenuated Total Reflection/Infrared and Near-Infrared correlation spectroscopy studies of real-time monitoring of the initial oligomerization of bis(hydroxyethyl terephthalate). *Macromolecules*. 35, p. 8020-828, (2002).
127. A. Tuchbreiter, B. Kappler, R. Stockmann, R Mülhaupt, J. Honerkamp. Near-infrared reflection spectroscopy: a versatile tool for rapid characterization of olefin copolymers and high throughput experiments. *Macromolecular Materials and Engineering*. 288, p. 29-34, (2003).
128. E. Marengo, M. Bobba, E. Robotti, M. Lenti. Hydroxyl and acid number prediction in polyester resins by near infrared spectroscopy and artificial neural networks. *Analytica Chimica Acta*. 511, p. 313-322, (2004).
129. M. Blanco, J. Cruz, M. Armengol. Control production of polyester resins by NIR spectroscopy. *Microchemical Journal*. 90, p. 118-123, (2008).
130. A.F. Santos, E.L. Lima, J.C. Pinto. In-line evaluation of average particle size in styrene suspension polymerizations using Near-Infrared spectroscopy. *Journal of Applied Polymer Science*. 70, p.1737-1745, (1998).
131. A.F. Santos, E.L. Lima, J.C. Pinto. Control and design of average particle size in styrene suspension polymerizations using NIRS. *Journal of Applied Polymer Science*. 77, p. 453-462, (2000).
132. Q. Zhou, Y. Xi, H. He, R.L. Frost. Application of near infrared spectroscopy for the determination of adsorbed p-nitrophenol on HDTMA organoclay—implications for the removal of organic pollutants from water. *Spectrochimica Acta Part A*. 69, p.835-841, (2008).
133. J. Madejová, M. Pentrák, H. Pállková , P. Komadel. Near-infrared spectroscopy: A powerful tool in studies of acid-treated clay minerals. *Vibrational Spectroscopy*. 49, p. 211-218, (2009).
134. R.L. Frost, H.J. Spratt, S.J. Palmer. Infrared and near-infrared spectroscopic study of synthetic hydrotalcites with variable divalent/trivalent cationic ratios. *Spectrochimica Acta Part A*. 72, p. 984-988, (2009).
135. R. Lui, R.L. Frost, W.N. Martens. Near infrared and mid infrared investigations of adsorbed phenol on HDTMAB organoclays. *Materials Chemistry and Physics*. 113, p. 707-713, (2009).

Chapter 2. Polymer-clay nanocomposites: a brief overview

136. J. Madejová, H. Pálková, P. Komadel. Behaviour of Li⁺ and Cu²⁺ in heated montmorillonite: Evidence from far-, mid-, and near-IR regions. *Vibrational Spectroscopy*. 40, p. 80-88, (2006).
137. R.L. Frost, J.T. Kloprogge, Z. Ding. Near-infrared spectroscopic study of nontronites and ferruginous smectite. *Spectrochimica Acta Part A*. 58, p. 1657-1668, (2002).
138. B.J. Reddy, R.L. Frost, M.J. Dickfos. Characterization of Ni silicate-bearing minerals by UV-vis-NIR spectroscopy: Effect of Ni substitution in hydrous Ni-Mg silicates. *Spectrochimica Acta Part A*. 71, p.1762-1768, (2009).
139. S. Petit, A. Decarreau, F. Martin, R. Buchet. Refined relationship between the position of the fundamental OH stretching and the first overtones for clays. *Physics and Chemistry of Minerals*. 31, p. 585-592, (2004).
140. A. Witschnigg, S. Laske, M. Kracalik, M. Feuchter, G. Pinter, G. Maier, W. Märzinger, M. Haberkorn, G.R. Langecker, C. Holzer. In-Line characterization of polypropylene nanocomposites using FT-NIR. *Journal of Applied Polymer Science*. 117, p. 3047-3053, (2010).
141. S. Laske, M. Kracalik, M. Feuchter, G. Pinter, G. Maier, W. Märzinger, M. Haberkorn, G.R. Langecker. FT-NIR as a determination method for reinforcement of polymer nanocomposites. *Journal of Applied Polymer Science*. 114, p. 2488-2496, (2009).

IN-LINE NEAR-INFRARED SPECTROSCOPY FOR THE CHARACTERIZATION OF DISPERSION IN POLYMER - CLAY NANOCOMPOSITES

3

In-line Near-Infrared spectroscopy (NIR) is used to monitor clay dispersion in the polymer matrix during the preparation of polymer nanocomposites by melt-mixing in a batch mixer. Based on chemometrics principles, various single parameter calibration models employing data obtained from widely used nanocomposites dispersion characterization techniques are developed and their quality is tested. Given the generally unsatisfactory outcome, multi-parameter calibration models are then assessed, a 7-parameter model encompassing factors derived from oscillatory rheometry, FT-IR and thermomechanical data yielding good results. Since the validity of the model outside the material / equipment / operating boundaries that were used to generate it was shown to be quite restricted, a second 7-parameter model is derived from a broader set of experimental data. Finally, the model is successfully applied to monitor in real time the evolution of clay dispersion with mixing time.

3.1. Introduction

Polymer nanocomposites based on layered silicate clays have found widespread practical application, as they possess good properties relative to the matrix even at low filler content [1 – 2]. However, since performance is determined by the morphology and degree of clay dispersion attained during compounding and processing [1 – 4], it is important to carefully monitor and control these characteristics during those manufacturing stages. Therefore, the development of fast-responsive and informative on-line techniques that are easy to operate, do not affect the existing material morphology at the monitoring location and that are sensitive even to minor changes in the material characteristics continues to be of great practical interest.

The authors have been using on-line oscillatory rheometry [5] for the characterization along the extruder of polymer-clay nanocomposites during compounding. Although a good correlation seems to exist between the rheological response and the existing morphology or the degree of mixing, in some cases it may not be possible to discriminate between different dispersion levels [6 – 7]. Thus, the search for alternative on-line techniques remains relevant. In recent years, developments in sensors and fiber optics brought up a renewed interest in near-infrared spectroscopy (NIR) as an in-line technique for process monitoring/control purposes [8 – 10]. NIR spectroscopy is routinely utilized in several industrial polymer processes such as polymerization reactions, controlled degradation and chemical modification [8, 11 – 12]. The use of NIR for in-line monitoring of the preparation of polymer matrix nanocomposites is recent and limited. Moghaddam *et al.* [13] fixed a NIR probe to a compounding mini-extruder and correlated mixing temperature, particle size and viscosity changes with spectral differences. This was achieved by applying Principal Component scores, but no calibration model was defined. In turn, Witschnigg *et al.* [14] interfaced a NIR probe between a laboratory twin-screw extruder and the die and studied the effect of screw speed and geometry on the final properties of the nanocomposites prepared. The authors developed single parameter calibration models, based on the Young's Modulus, interlayer distance and drawing force, i.e., they focused on the clay reinforcement effects. However, the quality of some of the models seems insufficient to enable a quantitative analysis.

Chapter 3. In-line NIR spectroscopy for the characterization of dispersion in polymer-clay nanocomposites

These efforts are encouraging in terms of exploring the possibility of correlating spectral differences of NIR data with clay dispersion levels. Due to the complexity of the spectra, NIR should rely on adequate chemometrics to extract from the data as much relevant information as possible [8 – 10]. Chemometrics represents both NIR major advantage and limitation. Indeed, a single calibration model could eventually provide information on multiple chemical, physical and morphological characteristics, enabling NIR to replace several other characterization techniques. Conversely, an adequate chemometric analysis often requires extensive experimental characterization and data treatment, as well as the development of multi-parameter calibration models [8 – 10, 15 – 16].

This work uses NIR to monitor clay dispersion within a polymer matrix, both in terms of evolution with time and final level attained. A commercial set-up is used and a wide-ranging calibration model is developed to correlate NIR spectral data with nanocomposites morphology/degree of mixing. To accomplish this, the usefulness of parameters derived from various well established characterization techniques is initially evaluated. A multi-parameter calibration model is then put forward. The preparation of a Polypropylene / Polypropylene grafted with Maleic Anhydride / Montmorillonite clay system (PP/PP-g-MA/C20A), using different PP-g-MA contents and operating conditions will be used as a case study. The compatibilizer content should impact on clay dispersion [22, 29, 31 – 32]. It has been reported that PP-g-MA contents of up to 15 % wt. may induce high dispersion levels, a further increase in percentage having a negligible effect [22, 31]. Similarly, different mixing speeds should bring about distinct degrees of dispersion [21 – 23, 28].

Chapter 3. In-line NIR spectroscopy for the characterization of dispersion in polymer-clay nanocomposites

3.2. Experimental

3.2.1. Materials and composites

The materials used in this work are listed in Table 3. 1, together with their main characteristics. They include a commercial polypropylene (injection molding grade), a polypropylene grafted with maleic anhydride and Cloisite 20A, a natural montmorillonite clay modified with dimethyl dehydrogenated tallow quaternary ammonium salt (2M2HT) in a concentration of 95 meq/100g of clay. Table 3. 2 presents the compositions of one set of PP/PP-g-MA/C20A nanocomposites containing the same amount of nanoclay (5 wt.%) and different PP-g-MA content (0 to 15 wt.%), all prepared in a batch mixer (Haake Rheomix OS600 - Thermo Scientific Inc.) at 200 °C and 50 rpm during 7 min, the ingredients being fed simultaneously. PP/PP-g-MA/C20A with 90/5/5 w/w/w was prepared using several rotor speeds (50, 100, 150 and 200 rpm).

Table 3. 1. Materials and main characteristics.

Material	Acronym	Producer	Grade	MFI/lamellar distance
Polypropylene	PP	Lyondell Basell	Moplen HP500N	12 g/10 min (230 °C/2.16 kg)
Compatibilizer	PP-g-MA	Crompton	Polybond 3200	115 g/10 min (190 °C/2.16 kg)
Montmorillonite clay	C20A	Southern Clay Products	Cloisite 20A	$d_{001} = 2.42$ nm

Table 3. 2. Compositions of the PP/PP-g-MA/C20A nanocomposites.

Material	Composition (wt.%)			
PP	95	90	85	80
PP-g-MA	0	5	10	15
C20A	5	5	5	5

Chapter 3. In-line NIR spectroscopy for the characterization of dispersion in polymer-clay nanocomposites

3.2.2. In-line set-up

The in-line NIR system comprises three main components (Figure 3. 1): (i) a diffuse reflectance probe (Axiom Analytical Inc.) with a sapphire window having a diameter of 5.7 mm; (ii) a Matrix® F (Bruker Optics) spectrophotometer and (iii) the OPUS® Quant2 (Bruker Optics) data acquisition and analysis software. The probe communicates with the spectrophotometer via a fiber optics cable and the spectrophotometer connects to the workstation by a LAN-type cable. A threaded hole with Dynisco-type tip geometry was machined in the front plate of the mixing chamber to accommodate the NIR probe.

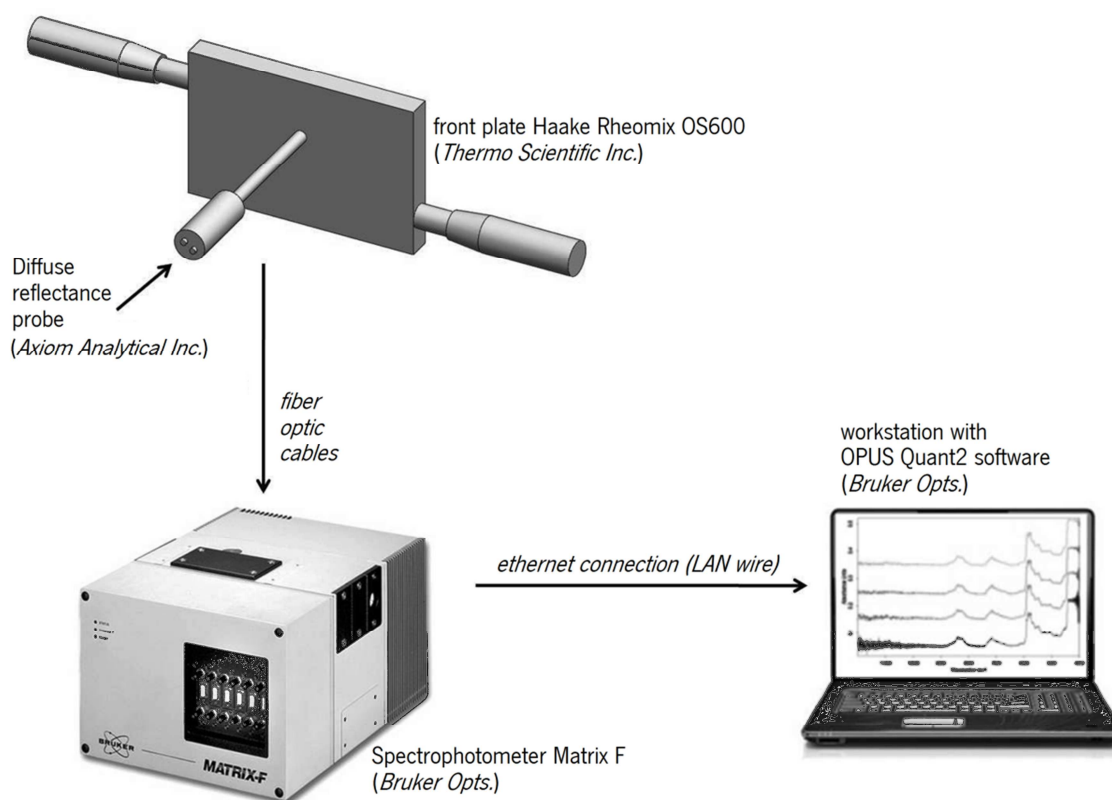


Figure 3. 1. In-line NIR set-up.

The NIR spectra were measured with a resolution of 8 cm^{-1} and accumulation of 4 scans, the acquisition time for each spectrum being less than 2 seconds. During the initial mixing stages, due to the melting of the matrix and the presence of large voids, the spectra were generally very noisy and had very low absorbance. Consequently, for chemometric purposes acquisition started once the

Chapter 3. In-line NIR spectroscopy for the characterization of dispersion in polymer-clay nanocomposites

onset of equilibrium torque was reached (this typically occurred after 2 minutes of mixing), as the calibration models were developed for the final composites. Thus, it was possible to collect 150 spectra during each mixing cycle. Figure 3. 2(a) illustrates typical torque and temperature curves for PP and composites 95/0/5 and 85/15/5. Predictably, changes in composition cause variations in the maximum and equilibrium torque, as well as in the time to reach the latter, but only the maximum torque exhibits significant deviations. This may be due to the offsetting rheological effects of the PP-g-MA (decreasing the viscosity of the system) and of the clay (increasing the viscosity). Figure 3. 2(b) displays examples of the corresponding NIR spectra. The spectra measured soon after the material is fed ($t = 2$ seconds) are also included.

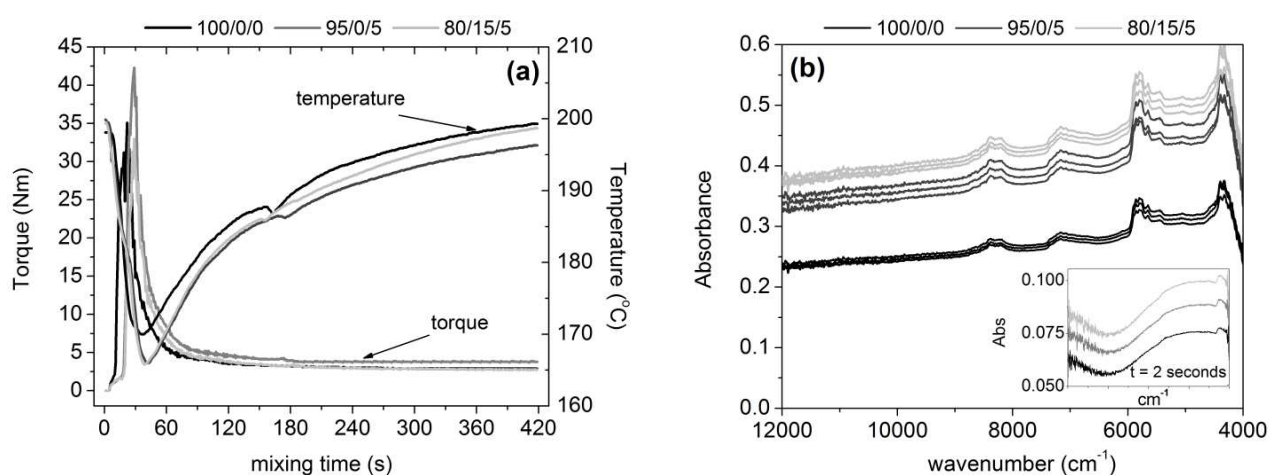


Figure 3. 2. (a) Typical batch mixer torque and temperature curves for samples 100/0/0, 95/0/5 and 80/15/5. (b) Examples of NIR spectra for the same materials.

3.2.3. Characterization of the Composites

Rotational Rheometry (AR-G2, TA Instruments) – The linear viscoelastic response of the samples at 200 °C was determined with oscillatory frequency sweeps from 0.1 to 100 rad/s, using parallel plates with a diameter of 25 mm and a 1 mm gap, performed under constant strain (1% for the matrix and 0.5 % for the composites). The disks were previously compression molded at 200 °C and 20 Tons. The complex viscosity vs. frequency curves were fitted to a modified Carreau-Yasuda model with yield stress, σ_0 (21 – 23):

Chapter 3. In-line NIR spectroscopy for the characterization of dispersion in polymer-clay nanocomposites

$$|\eta^*(\omega)| = \frac{\sigma_0}{\omega} + \eta_0 [1 + \lambda \omega^a]^{(b-1)/a} \quad (3.1)$$

and to a power law (6 – 7):

$$|\eta^*(\omega)| = A\omega^b \quad (3.2)$$

where the adjustable parameters are the zero shear viscosity (η_0), the relaxation time (λ), the Yasuda parameter (a), the power law index (b) and the power law consistency (A). The Origin® Pro8 software was used for this purpose. The values of G' (storage modulus) and G'' (loss modulus) at low frequency were also determined.

Medium FT-IR (FTIR4100, Jasco) – The organoclay was analyzed with a KBr mortar. The nanocomposite samples were compression molded into thin films ($\pm 75 \mu\text{m}$ thick) at 200 °C and analyzed in transmission mode, in a range between 4000 and 500 cm^{-1} using 12 scans and a resolution of 4 cm^{-1} . The wavelength region between 1300 and 750 cm^{-1} was fitted with the Pearson VII expression using the Origin® Pro8 software, with a 75 % Gaussian shape ($\mu = 4$) for the determination of the wavenumber shift for the 1050 cm^{-1} (Si-O in-plane) and 1080 cm^{-1} (Si-O out-of-plane) peaks.

X-ray diffraction, XRD (AXS Nanostar-D8 Discover, Bruker) – The diffraction patterns were obtained using a diffractometer equipped with a $\text{CuK}\alpha$ generator ($\lambda = 1.5404 \text{ \AA}$) at 40 kV and 40 mA, in a 2θ range from 0.08 – 10°. The organoclay was analyzed directly ($\theta = 1.82^\circ$, $d_{001} = 2.42 \text{ nm}$), whereas the nanocomposite samples were previously compression molded into disks with a diameter of 20 mm and a thickness of 4 mm.

Tensile tests (Universal Tester 4505, Instron) – The testing procedure followed generally the ASTM D-882 standard, using compression molded films ($\pm 250 \mu\text{m}$ thick), a 1 kN load cell, a 50 mm initial gauge and a drawing speed of 5 mm/min.

3.3. Development of the chemometric model

The measured NIR spectra are related with the clay dispersion state by means of a calibration model. To achieve this several aspects must be addressed, namely the selection of the parameters that most adequately describe the nanoclay dispersion (to be incorporated into the model), the determination of the minimum population size required to obtain a robust correlation and the definition of the best Validation/Calibration population size ratio, in order to minimize the monitoring time.

3.3.1. Chemometrics

Chemometrics is a step-by-step methodology aiming to develop a calibration model relating the NIR spectral data with the reference characterization parameters [8 – 10, 16]. It involves the actual model development and its validation, to guarantee effective predicting capabilities [10, 16]. The multivariate calibration technique uses the entire spectral structures instead of a single spectral data point to provide broader information, and thus detect even minute differences in the sample spectra [9, 16].

During model development, a pre-defined group of samples (commonly designated as “training samples”) is used to compute the calibration curve, which directly yields the analyte property from the respective spectra. To ensure precision, the degree of correlation between the spectral and reference data should be high. For this purpose, a cross-validation step attests the quality of the adjustment of the data points to the calibration curve. More specifically, a certain number of the training samples are selected and the predicted property is compared with the reference values [10, 16]. Finally, the calibration model can be used to predict the characteristics of unknown samples.

3.3.2. Quality of the model

A partial least squares (PLS) regression to the calibration data set was used, the model quality being assessed by the following parameters (9 – 11):

Chapter 3. In-line NIR spectroscopy for the characterization of dispersion in polymer-clay nanocomposites

- i. Error of prediction – the Root Mean Square Error is calculated for all samples:

$$\text{RMSE} = \sqrt{\frac{\sum_{i=1}^n (Y_{i\text{measured}} - Y_{i\text{predicted}})^2}{n}} \quad (3.3)$$

where Y_{measured} and $Y_{\text{predicted}}$ are the measured and predicted values, respectively. RMSE is usually labeled as Root Mean Square Error of Estimation (RMSEE) or as Root Mean Square Error of Prediction (RMSEP) when applied to model development or final independent validation, respectively. Both should be as low as possible.

- ii. Coefficient of Determination (R^2) – it yields the percentage of variance present in the component values, which is reproduced in the subsequent prediction:

$$R^2 = \left[1 - \frac{\sum_{i=1}^n (Y_{i\text{predicted}} - \overline{Y_{\text{predicted}}})^2}{\sum_{i=1}^n (Y_{i\text{measured}} - \overline{Y_{\text{measured}}})^2} \right] \times 100 \quad (3.4)$$

where $\overline{Y_{\text{predicted}}}$ and $\overline{Y_{\text{measured}}}$ are the predicted and measured average values, respectively. Ideally, R^2 should be higher than 95 %, but values above 90 % are well accepted for qualitative studies. Low R^2 ($\ll 90$ %) frequently result from inappropriate reference parameters, insufficient precision of the reference data and/or presence of outliers in the calibration data set.

- iii. Bias – is the systematic average deviation between the measured and predicted data sets, calculated by averaging all deviations in the data set:

$$\text{bias} = \frac{\sum_{i=1}^n (Y_{i\text{measured}} - Y_{i\text{predicted}})}{n} \quad (3.5)$$

Bias should be as small as possible.

- iv. Residual Prediction Deviation (RPD) – is the ratio between the standard deviation of the reference values and the bias-corrected mean error of the prediction (validation step):

$$\text{RPD} = \frac{\sqrt{\frac{1}{M-1} \times \sum_{i=1}^n (Y_{i\text{measured}} - \overline{Y_{\text{measured}}})^2}}{\sqrt{\frac{1}{M-1} \times \sum_{i=1}^n (Y_{i\text{measured}} - Y_{i\text{predicted}} - \text{bias})^2}} \quad (3.6)$$

where M is the size of the calibration set. Values above 5 are considered as adequate for quality control, whilst those over 8 indicate that the method is valid for analytical tasks.

Chapter 3. In-line NIR spectroscopy for the characterization of dispersion in polymer-clay nanocomposites

3.3.3. Model Parameters

In the present study chemometrics will be employed to develop a calibration model able to predict the level of clay dispersion in a molten polymer matrix. This requires a proper characterization of the polymer-clay nanocomposite, in order to find suitable reference parameters. Transmission Electron Microscopy (TEM) and X-ray diffraction (XRD) are probably the most commonly used techniques for this purpose [1 – 2, 17 – 19]. TEM provides a direct view of clay dispersion, enabling the determination of agglomerates/particle size and number of stacks/platelets per area. However, TEM analyses only very small areas, requires time consuming sample preparation and tedious data treatment. XRD presents a clear region of interest at low 2θ angles, due to the typical clay Bragg's diffraction peak, from which the clay spacing and stacks height may be estimated. Nonetheless, XRD data may be misinterpreted due to orientation and crystallinity effects [1 – 2, 17 – 18].

Several authors have successfully related the rheological response with the state of dispersion of clay nanocomposites [6 – 7, 20 – 24]. For example, Lertwimolnun and Vergnes [21 – 23] used a modified Carreau-Yasuda model with yield stress (equation 1) to describe the frequency dependence of the absolute complex viscosity and successfully related this with the exfoliation level. Other studies used a power law expression to describe the complex viscosity and storage modulus behavior at low frequency, with the exponent correlating with the state of clay dispersion [6 – 7]. However, the same dependence was found both for high clay loading in a poorly dispersed composite and for good clay dispersion at lower clay concentration [6 – 7]. Also, the moduli values (G' and G'') may provide a good perception of dispersion, the increase of their values having been related to a finer dispersion [22], while the formation of a plateau at low frequencies has been attributed to the deformation and recovery of the dispersed particles [3, 20, 24].

Medium IR analysis (FT-IR) has also been utilized to characterize the morphology of polymer nanocomposites [25 – 27] based on the principle that the clay band can be decomposed at least in four peaks, three being related to the Si-O in-plane vibrations (or bonds with basal oxygen) appearing at about 1120, 1050 and 1020 cm^{-1} , respectively, and the fourth with the Si-O out-of-plane vibration (with apical oxygen or hydroxyl group) appearing at about 1080 cm^{-1} . As the individual clay layers become more spaced, the peaks at 1050 cm^{-1} and 1080 cm^{-1} tend to shift. When the structure is ordered and intercalated, the peak at 1050 cm^{-1} will suffer a negative shift towards lower

Chapter 3. In-line NIR spectroscopy for the characterization of dispersion in polymer-clay nanocomposites

wavenumber, whilst for highly intercalated or partially exfoliated morphologies, the peak at 1080 cm^{-1} will shift to higher wavenumbers [26 – 27].

The mechanical properties (i.e., the practical material performance) should depend on the extent of dispersion, but the exact relation between them is much disputed [1 – 2, 28 – 30]. The clay reinforcement effect is influenced by the adhesion between filler and matrix, the nanoparticles aspect ratio (individual layers, stacked layers or tactoids) and also by the clay nucleating effect. For example, the role of the addition of a maleated compatibilizer [28, 29] and of the preferential orientation of the clay platelets [30] on the mechanical performance has been investigated.

The above methods probe different length and time scales, thus possibly providing complementary sensitivities in terms of the degree of dispersion of a polymer/clay nanocomposite. Four of them will be taken in as reference – XRD, rheology, FT-IR and tensile testing – as they are relatively simple to use and are readily available in most laboratories. Since, in principle, the final morphology of a polymer/clay system should result from the thermal and mechanical inputs during compounding/processing [21], it makes sense to include a thermomechanical index in this set. As a batch mixer is being used here, the maximum or the equilibrium torque per unit material were selected (the nominal values will be used, as the amount of composite in the mixing chamber was kept constant).

3.4. Results and Discussion

3.4.1. Single parameter models

In the following, the parameters from each of the characterization techniques selected in Section 3.3.3 will be considered separately in terms of developing chemometric models. The corresponding quality will be assessed by the measures presented in section 3.3.2. The experimental results obtained for the nanocomposites of Table 3. 2 are listed in Table 3. 3.

Chapter 3. In-line NIR spectroscopy for the characterization of dispersion in polymer-clay nanocomposites

Table 3. 3. Values of the parameters associated to the selected reference techniques.

		100/0/0	95/0/5	90/5/5	85/10/5	80/15/5
XRD	d_{001} (nm)	0.00	2.55	3.00	3.40	3.40
Rheology	G' (kPa)	0.073	0.118	0.186	1.061	1.003
	G'' (kPa)	0.294	0.409	0.508	0.992	2.111
	σ_0 (kPa)	0.000	0.037	0.129	1.356	2.250
	b	-0.194	-0.252	-0.240	-0.774	-1.000
FT-IR	1050 cm^{-1}	0.0	-3.1	-7.2	-8.4	-8.7
	1080 cm^{-1}	0.0	0.0	1.5	3.4	3.4
Tensile Testing	Young's Modulus (GPa)	1.200	1.180	1.135	1.124	1.103
	Maximum stress (MPa)	33.5	29.5	27.0	24.8	22.9
Torque	Maximum (Nm)	35.10	42.30	41.00	33.90	33.00
	Equilibrium (Nm)	2.98	3.80	3.47	3.23	2.89

Most parameters change monotonically with clay content, although some techniques seem to have difficulty in discriminating between the 89/10/5 and the 80/15/5 samples. Each calibration curve was determined with a partial least square regression on 150 spectra. Table 3. 4 lists the respective quality factors. The R^2 and RPD values for the interlayer spacing (d_{001} from XRD), Young's modulus and maximum tensile stress are inferior to the acceptable limits (90 % for R^2 and 5 for RPD), i.e., it is not possible to build good calibration models using them. The validation step used 60 spectra per sample, i.e., a validation/calibration population ratio of 40 %. As expected, interlayer spacing, Young's modulus and maximum tensile stress fail the validation step, as the predictive capability of the respective models is compromised by the low quality calibration results. As discussed above, even R^2 values above 90 % do not necessarily guarantee a chemometric model with quantitative predictive power. As shown in Figure 3. 3 for the maximum torque and peak shift at 1050 cm^{-1} , the R^2 values of the calibration lines exceed 90% but the final validation fails because the model cannot resolve the spectral differences of the samples. In both cases the validation yields high global errors

Chapter 3. In-line NIR spectroscopy for the characterization of dispersion in polymer-clay nanocomposites

(RMSEP) and bias, as well as R^2 values below 90%. Several factors may influence these results, such as the limited sensitivity of the reference technique, the error associated to the reference results, insufficient data, influence of environmental conditions (temperature, humidity) and sample preparation. The remaining parameters, namely rheology data, peak shift at 1080 cm^{-1} and equilibrium torque provide robust models, for which the quality of the calibration was supported by the validation results.

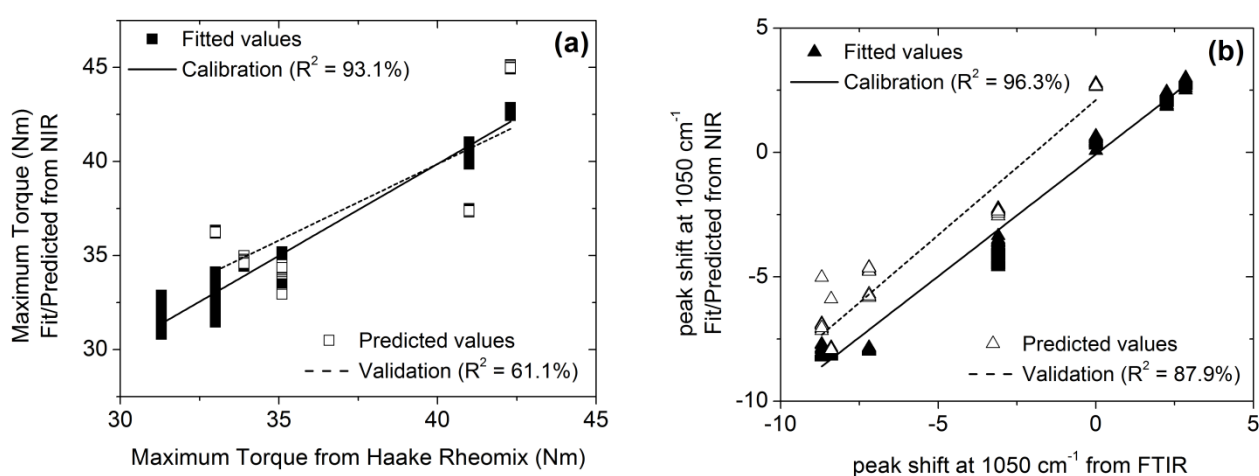


Figure 3. 3. Individual calibration models and their validation: (a) Maximum Torque; (b) peak shift at 1050 cm^{-1} .

Overall, these results express the ineffectiveness of single parameters like d_{001} , Young's Modulus and maximum tensile stress to describe the global state of clay dispersion in the polymer matrix, which confirms the possibility of secondary effects influencing the results, as discussed in section 3.3.3.

Chapter 3. In-line NIR spectroscopy for the characterization of dispersion in polymer-clay nanocomposites

Table 3. 4. Quality factors of the individual calibration models and respective validation.

		<i>XRD</i>		<i>Rheology</i>			<i>FT-IR</i>		<i>Tensile Testing</i>		<i>Torque</i>	
		d_{001}	G'	G''	σ_0	b	1050	1080	E	Stress	Maximum	Equilibrium
		(nm)	(kPa)	(kPa)	(kPa)		cm-1	cm-1	(GPa)	(MPa)	(Nm)	(Nm)
Calibration	RMSEE	0.192	0.068	0.096	0.118	0.063	0.682	0.083	0.012	2.320	0.768	0.087
	R^2 (%)	68.8	97.8	98.2	99.1	98.5	96.3	99.1	89.1	62.7	93.1	91.6
	RPD	0.8	8.8	10.7	15.9	11.3	10.6	16.8	1.2	0.8	8.7	8.1
	RMSEP	0.765	0.099	0.112	0.154	0.101	0.236	0.102	0.234	3.96	1.982	0.108
Validation	R^2 (%)	25.5	96.9	97.6	98.5	98.1	87.9	98.4	76.5	31.1	61.1	90.3
	bias	-2.86	0.16	0.12	0.10	-0.08	0.66	0.06	1.34	3.44	2.98	0.96

3.4.2. Population Size

Sampling size and ratio between the validation and calibration populations could influence the quality of the chemometric models. In order to investigate this, the single parameter models were recalculated for different population sizes. The 150 spectra registered initially were divided in two groups, one containing 100 spectra to be used for calibration and the other with 50 spectra to be used for validation. Assignment to the groups was done randomly. Subsequently, sub-groups formed from these rendered different calibration population sizes and validation/calibration population ratios. As far as calibration is concerned, the size of the population was found to influence little the chemometric values. For example, the R^2 of d_{001} ranges between 69.9 % and 68.8 % when the population size increases from 25 to 100, maintaining the value of 68.8 % for a population of 150. Similar conclusions could be reached for the remaining parameters. Table 3. 5 presents the R^2 and RMSEP values for the validation for several validation/calibration population ratios (ranging from 5 to 60 %). The Validation/Calibration population ratio does not affect the quality of the models. The exceptions are the torque parameters, particularly the Maximum torque, for which the decrease in the population ratio from 60 % to 5 % results in R^2 values to exceed the acceptable 90 %.

These data confirm the results presented in section 3.4.1 and show that the development of a reliable chemometric model does not rely on the sampling size of the calibration, but rather on the effectiveness of the parameters used.

Chapter 3. In-line NIR spectroscopy for the characterization of dispersion in polymer-clay nanocomposites

Table 3. 5. Validation of the chemometric models using different validation/calibration population ratios.

<i>Validation/Calibration (%)</i>		<i>5</i>	<i>15</i>	<i>25</i>	<i>60</i>
XRD	d_{001} (nm)	60.3 / 0.19	60.1 / 0.19	59.6 / 0.19	59.0 / 0.19
	G' (kPa)	95.7 / 0.11	95.2 / 0.10	94.4 / 0.11	93.1 / 0.12
Rheology	G'' (kPa)	96.9 / 0.17	96.4 / 0.14	95.6 / 0.17	95.5 / 0.20
	σ_0 (kPa)	97.5 / 0.09	97.4 / 0.10	96.7 / 0.09	95.8 / 0.11
	b	96.4 / 0.14	95.8 / 0.14	95.1 / 0.14	94.3 / 0.19
FT-IR	1050 cm^{-1}	94.1 / 0.07	93.8 / 0.06	93.5 / 0.06	92.2 / 0.06
	1080 cm^{-1}	96.4 / 0.12	95.9 / 0.11	95.6 / 0.13	94.9 / 0.13
Tensile Testing	Young's Mod. (GPa)	86.1 / 0.10	86.5 / 0.10	86.0 / 0.10	85.4 / 0.10
	Maximum stress (MPa)	59.0 / 2.34	59.4 / 2.32	59.2 / 2.37	58.6 / 2.42
Torque	Maximum (Nm)	91.7 / 0.91	90.7 / 0.70	88.9 / 0.77	88.9 / 0.98
	Equilibrium (Nm)	90.5 / 0.11	89.7 / 0.11	89.3 / 0.13	88.6 / 0.15

3.4.3. Multi-parameter models

The ineptitude of single model parameters based on d_{001} , Young's modulus and maximum tensile stress to describe the global state of clay dispersion in the polymer matrix having been demonstrated, the suitability of multi-parameter models was explored. In this case, each parameter was normalized as:

$$\text{Normalized Value (\%)} = \frac{(\text{Value} - \text{minimum})}{(\text{Maximum} - \text{minimum})} \times 100 \quad (3.7)$$

i.e., a score of 0% matches the polymer matrix, while 100% refers to the best dispersed nanocomposite. In turn, each model considered the average of the relevant normalized values. Table 3. 6 presents the calibration and validation quality factors of the various models tested combining

Chapter 3. In-line NIR spectroscopy for the characterization of dispersion in polymer-clay nanocomposites

from 2 to 11 parameters. A model joining more than one parameter, even if extracted from a single characterization technique, is taken here as multi-parameter.

Table 3. 6. Calibration and Validation results for the multi-parameter models.

Multi-parameter model	Calibration			Validation		
	R ² (%)	RMSEE	RPD	R ² (%)	RMSEP	bias
Torque	95.6	1.52	9.0	89.7	1.99	-3.09
FT-IR	98.5	0.23	12.8	98.1	0.47	0.81
Rheology	98.8	0.65	13.1	96.9	1.12	0.87
Rheology and XRD	94.0	2.09	8.0	90.1	4.15	1.14
Rheology and FT-IR	98.6	0.76	14.5	97.7	0.97	-0.75
Maximum torque, Rheology and FT-IR	99.8	0.85	27.8	99.5	1.01	0.64
Rheology, FT-IR and Tensile testing	90.4	1.67	8.1	88.2	2.14	1.08
All	51.7	10.1	1.8	38.5	22.3	-15.7

For a population of 150 spectra per sample and a validation/calibration population ratio of 15%, the torque parameters, merging Rheology and XRD, and grouping Rheology, FT-IR and tensile testing resulted in calibration lines with high coefficients of determination but poor validation outcomes. Combining the 11 parameters yields a chemometric model with very low calibration and validation R² values (51.7% and 38.5%, respectively).

Conversely, using the FT-IR parameters, the (four) Rheology parameters and the combination of both techniques yielded excellent calibration lines, with R² values above 98 % and very good validation performance. Figure 3. 4 shows the best result, which was obtained with a 7 parameter model encompassing the maximum torque, storage (G') and loss (G'') moduli, melt yield stress (σ_0), power law index (b) and peak shifts at 1050 and 1080 cm⁻¹. The calibration curve has a global error (RMSEE) of 0.85 %, a residual prediction deviation (RPD) of 27.8, and a R² value of 99.8 %. As for

Chapter 3. In-line NIR spectroscopy for the characterization of dispersion in polymer-clay nanocomposites

the validation, the results were also very good, with R^2 equal to 99.5%, a global error of 1.01 and a bias of 0.641.

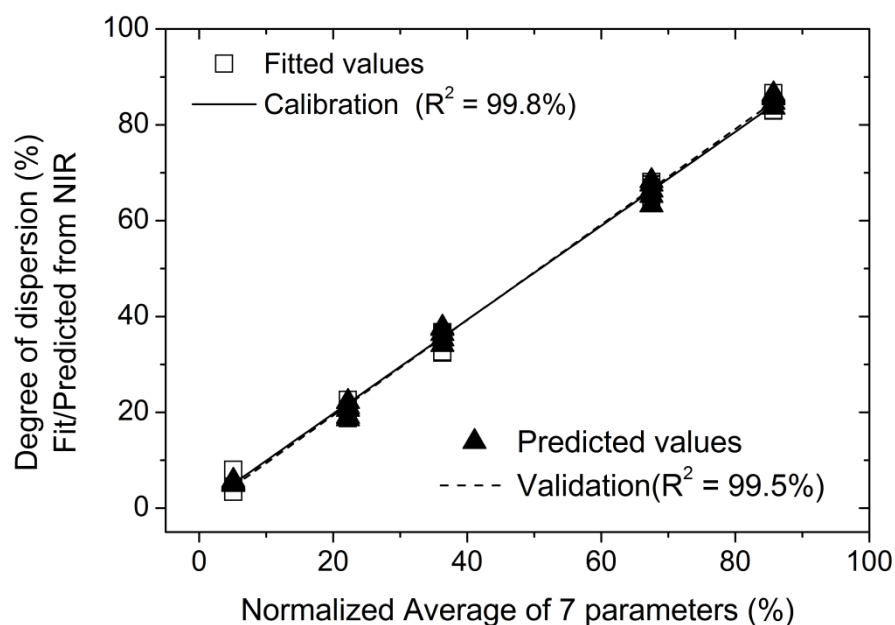


Figure 3. 4. Chemometric model using the normalized average of maximum torque, rheology and FT-IR.

These results could be foreseen taking into consideration those presented in section 3.4.1. If the parameters derived from XRD and tensile testing do not yield good quality single parameter models, using them in multi-parameter arrangements will compromise the quality of the final model. The same reasoning should be applicable to the higher quality models, which combine parameters that previously rendered good single parameter models.

The results above exhibit a number of interesting features:

- Despite the supporting rationality and the easiness in obtaining their parameters values, it seems that models attempting to adopt global energy inputs to the system upon mixing have difficulty in correlating them strongly with the resulting dispersion. Other authors have reported similar difficulties [21, 29, 31 – 32].

Chapter 3. In-line NIR spectroscopy for the characterization of dispersion in polymer-clay nanocomposites

- Parameters from well-established characterization techniques such as rheology (oscillatory rheometry) and FT-IR, but not XRD as seen above, can provide very good chemometric models and so does their combination.
- As expected, the combination of favorable techniques, such as rheology and FT-IR, with others yielding weaker chemometric models (e.g., XRD or tensile data) compromises the usefulness of the exercise; this is particularly noticeable in the 11 parameter model, which presented the worst quality.
- Conversely, developing multi-parameter models that incorporate sufficiently performing building blocks generates adequate chemometric models, such as the 7-parameter tested.

3.4.4. Validity limitations

The 7-parameter model discussed above and developed from samples prepared with different PP-g-MA content was employed to characterize the degree of dispersion of nanocomposites prepared with different rotor speeds. In Table 3. 7, the predictions show a good agreement with the measured values for 50 rpm, but the differences for the samples prepared at the remaining speeds range between 14 and 32 %. This is generally translated by the high RMSEP and bias. The good outcome for 50 rpm is explained by the fact that this condition was used in the two sets of nanocomposite samples (section 3.2.1). Thus, the 7-parameter model developed based on the effect of the PP-g-MA content is not suitable to analyze samples prepared under different operating conditions, i.e., NIR-based models should not be applicable outside the material/equipment/operating boundaries that were used to generate them. Although not shown here, the application of the 7-parameter model based on data from nanocomposites prepared under different rotor speeds would face identical limitations in characterizing the dispersion of nanocomposites with varying degrees of compatibilizer.

Chapter 3. In-line NIR spectroscopy for the characterization of dispersion in polymer-clay nanocomposites

Table 3. 7. Predicted final dispersion level of nanocomposites prepared using different rotor speeds.

	50 rpm	100 rpm	150 rpm	200 rpm
Measured (\pm error)	27.5 (\pm 3.3)	34.5 (\pm 4.7)	52.4 (\pm 6.1)	79.2 (\pm 9.7)
Predicted (\pm error)	27.6 (\pm 2.1)	45.6 (\pm 2.7)	60.5 (\pm 7.6)	90.2 (\pm 3.8)
RMSEP			22.4	
bias			20.6	

Given the above, it makes sense to use the data from the two sets of experiments (exploring the effects of PP-g-MA content and of rotor speed) to generate a new 7-parameter chemometric model. The normalized average values of all samples were recalculated, as the absolute minimum and maximum values of each parameter are now altered. Table 3. 8 summarizes the quality factors. The new global model exhibits a high quality standard, with a calibration curve with R^2 above 99 %, a low global error and a high RPD, and validation with a R^2 value above 90 %, low global error and a bias approaching zero. For example, when using the initial 7 – parameter model to predict the dispersion level of the samples prepared with different PP-g-MA content (Figure 3. 4), the differences between measurements and forecasts ranged in the interval 1.3 % to 3.9 %. The new global 7 – parameter produces discrepancies in the range 0.3 – 1.5 %.

Table 3. 8. Global 7-parameter model: calibration and validation quality factors.

<i>Calibration</i>			<i>Validation</i>		
R^2 (%)	RMSEE	RPD	R^2 (%)	RMSEP	bias
99.5	1.52	14.2	99.1	2.03	-0.013

3.5. Real-time prediction

The predictive ability of the global model in real-time NIR measurements will be used to monitor the evolution of dispersion upon mixing. Since the global model was developed taking in two variables – PP-g-MA content and rotor speed – these effects were studied independently. Thus, a new composite containing 7.5 wt.% of PP-g-MA (87.5/7.5/5) was prepared at a rotor speed of 50 rpm (the reference rotor speed). In turn, the 90/5/5 w/w/w composite (the reference composite) was prepared at 125 and 175 rpm. Spectra were collected every 2 seconds, Figure 3. 5 showing data for the 87.5/7.5/5 w/w/w nanocomposite. Figure 3. 6 presents the evolution in time of torque and the predicted dispersion level for the two case studies.

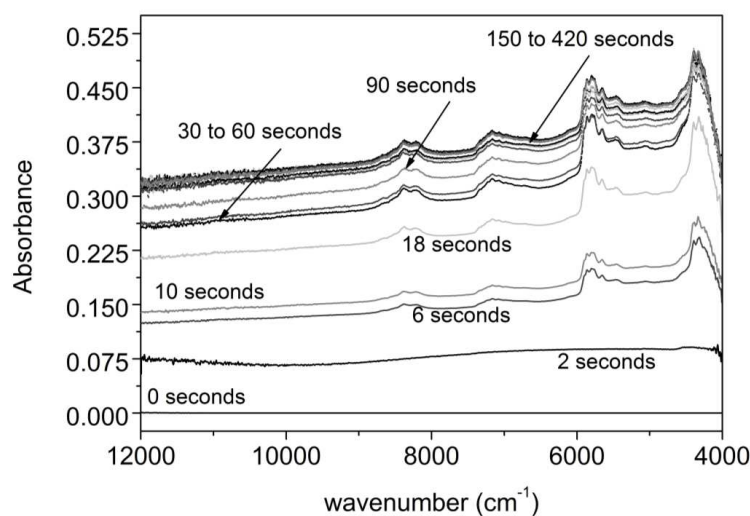


Figure 3. 5. Spectra measured during mixing for 87.5/7.5/5 w/w/w.

The initial spectrum (at 0 seconds) is close to zero. As mixing evolves, both the baseline and the signal intensity increase. As seen in the torque curve, melting starts around 10 – 20 seconds of mixing. The increase in torque is due to the conversion of a granular flow into that of a melt suspension with high solids content. Even in these initial moments, although the NIR signal is weak, the fundamental peaks are already visible, and clay dispersion is predicted to be initiated. The torque reaches its maximum at about 30 seconds and decreases thereafter, as melting progresses.

Chapter 3. In-line NIR spectroscopy for the characterization of dispersion in polymer-clay nanocomposites

Melting is probably completed at around 90 – 120 seconds, but it is only after mixing for 180 seconds that a torque plateau is reached, which most likely corresponds to little further changes in dispersion. In fact, it has been repeatedly reported for several systems melt mixed in batch mixers or twin-screw extruders that most of the dispersive mixing takes place upon melting, when the thermomechanical stresses are higher, little evolution being detected thereafter [33 – 34]. Differences in the NIR spectra are also higher in the same interval, whereas between 180 to 420 seconds the spectra are nearly superimposed. Thus, the rate of dispersion is predicted to be higher from 60 to 150 seconds and a plateau is foreseen beyond 180 seconds.

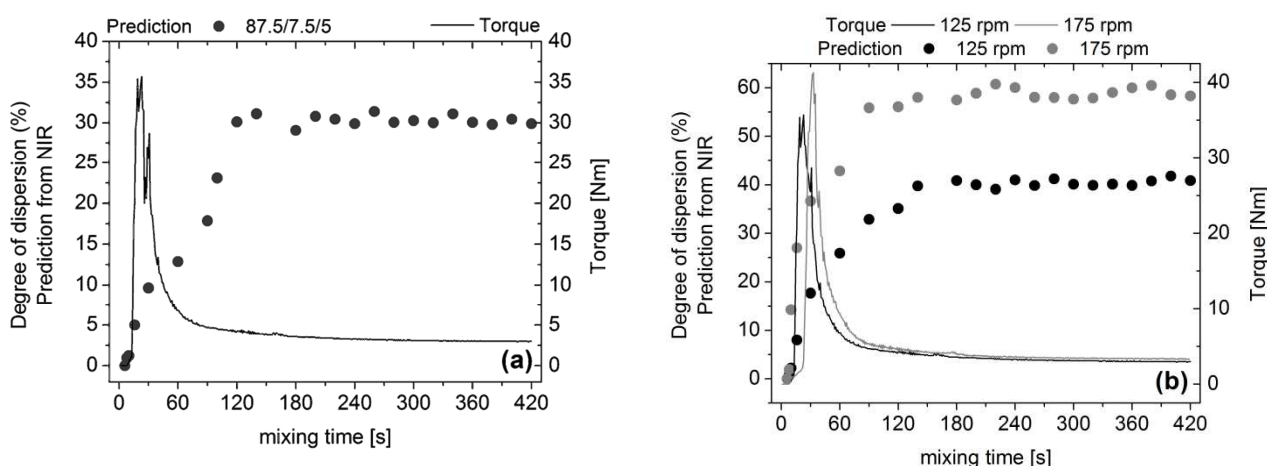


Figure 3. 6. Time evolution of torque and (predicted) dispersion: (a) 87.5/7.5/5 at 50 rpm (b) 90/5/5 at 125 and 175 rpm.

The final dispersion level (after 180 seconds) predicted by NIR for the sample with 7.5 wt.% of PP-g-MA is roughly 30 %, which connects well with the normalized average values of the samples with 5 % and 10 wt.% of PP-g-MA, 26.3 % and 36.9 %, respectively. It is also in agreement with reports relating the improvement of clay dispersion in polyolefin matrices with the increase in compatibilizer content [22, 29, 31 – 32]. In the case of the 90/5/5 w/w/w nanocomposite, the final dispersion level is predicted to increase with rotor speed (approximately 39 % and 59 % at 125 rpm and 175 rpm, respectively). Again, these values are in line with the normalized averages (23.5 %, 49.6 %, 77.2 % for 100, 150 and 200 rpm, respectively) and with reports showing an increase in dispersion with increasing rotor speed [21 – 23, 28].

3.6. Conclusions

The viability and effectiveness of using NIR for the in-line monitoring of clay dispersion during the preparation of clay nanocomposites by melt-mixing is demonstrated. Chemometrics can support the development of calibration models with good quality calibration and validation measures, but two requirements must be fulfilled. First, it is essential that models are built with parameters from dispersion characterization techniques that are really able to discriminate between distinct dispersion levels. In this respect, the implementation of single parameter calibration models from XRD, rheology, FT-IR, tensile testing or torque data was globally unsuccessful. Multi-parameter models showed greater potential, particularly when incorporating sufficiently performing individual building blocks. Specifically, a 7-parameter model incorporating parameters from oscillatory rheometry (G' , G'' , σ_0 , b), FT-IR (wavenumber shift of the peaks at 1050 and 1080 cm^{-1}) and thermomechanical data from the mixing equipment (maximum torque) yielded good results. Secondly, it was proven that the validity of the calibration model outside the material / equipment / operating boundaries that were used to create it is very limited. Therefore, it is important to use the broadest possible set of data. In the present case, the same 7-parameter model now based on results from nanocomposites produced at different rotor speeds and having different compatibilizer levels exhibited very good quality features. When applying this same calibration model to the real time monitoring of the evolution of dispersion upon mixing of nanocomposites under new operating conditions or of nanocomposites containing new levels of compatibilizer, not only distinct results were obtained, but they matched well the forecasted values.

Finally, an investigation of the effect of population size on the quality of the calibration model showed that when setting the Validation/Calibration population ratio at 15% there is no need to use an extensive sampling size.

3.7. References

1. M. Alexandre, P. Dubois. Polymer-layered silicate nanocomposites: preparation, properties and uses of a new class of materials. *Materials Science and Engineering* 28, p.1-63, (2000).
2. D.R. Paul, L.M. Robeson. "Polymer nanotechnology: Nanocomposites". *Polymer*. 49, p. 3187-3204, (2008).
3. S.S. Ray, M. Okamoto. Polymer/layered silicate nanocomposites: a review from preparation to processing. *Progress in Polymer Science* 28, p.1539-1641, (2003).
4. S. Pavlidou, C.D. Papaspyrides. A review on polymer-layered silicate nanocomposites. *Progress in Polymer Science* 33, p. 1119-1198, (2008).
5. S. Mould, J.M. Barbas, A.V. Machado, J.M. Nóbrega, J.A. Covas. Measuring the rheological properties of polymer melts with on-line rotational rheometry. *Polymer Testing*. 30, p. 602-610, (2011).
6. A. Durmus, A. Kasgoz, C.W. Macosko. Linear low density polyethylene (LLDPE)/clay nanocomposites. Part I: Structural characterization and quantifying clay dispersion by melt rheology. *Polymer*. 48, p. 4492-4502, (2007).
7. A. Vermogen, K. Masenelli-Varlot, R. Séguéla, J. Duchet-Rumeau, S. Boucard, P. Prele. Evaluation of the structure and dispersion in polymer-layered silicate nanocomposites. *Macromolecules*. 38, p. 9661-9669, (2005).
8. M. Blanco, I. Villarroya. "NIR spectroscopy: a rapid-response analytical tool". *Trends in Analytical Chemistry*. 21, p. 240-249, (2002)
9. D.A. Burns, E.W. Ciurczak (Eds.). *"Handbook of Near-Infrared Analysis"* CRC Press (2008).
10. H.W. Siesler, Y. Ozaki, S. Kawata, H.M. Heise (Eds.). *"Near-Infrared Spectroscopy: Principles, Instruments, Applications"* Willey-VCH, (2002).
11. A.F. Santos, E.L. Lima, J.C. Pinto. "In-line evaluation of average particle size in styrene suspension polymerizations using near-infrared spectroscopy". *Journal of Applied Polymer Science*. 70, p. 1737-1745, (1998)

Chapter 3. In-line NIR spectroscopy for the characterization of dispersion in polymer-clay nanocomposites

12. S.E. Barnes, M.G. Sibley, H.G.M. Edwards, P.D. Coates. "Process monitoring of polymer melts using in-line spectroscopy". *Transactions of the Institute of Measurement and Control*. 29, p. 453-465, (2007)
13. L.Moghaddam, D.J.Martin, P.J.Halley, P.M.Fredericks. "Vibrational spectroscopic studies of laboratory scale polymer melt processing: application to a thermoplastic polyurethane nanocomposite". *Vibrational Spectroscopy*. 51, p. 86-92, (2009)
14. A. Witschnigg, S. Laske, M. Kracalik, M. Feuchter, G. Pinter, G. Maier, W. Märzinger, M. Haberkorn, G.R. Langecker, C. Holzer. "In-line characterization of polypropylene nanocomposites using FT-NIR". *Journal of Applied Polymer Science*. 117, p. 3047-3053, (2010)
15. J. Workman Jr., L. Weyer. "Practical guide to interpretive Near-Infrared spectroscopy" CRC Press, (2007).
16. M.J. Adams. *Chemometrics in Analytical Spectroscopy* The Royal Society of Chemistry, (1995).
17. A.B.Morgan, J.W. Gilman. "Characterization of polymer-layered nanocomposites by Transmission Electron Microscopy and X-Ray Diffraction: a comparative study". *Journal of Applied Polymer Science*. 87, p. 1329-1338, (2003)
18. B.J. Nang, D. Wang, C.A. Wilkie. "Relationship between the solubility parameter of polymers and the clay dispersion in polymer/clay nanocomposites and the role of the surfactant". *Macromolecules*. 38, p. 6533-6543, (2005)
19. J. Bandyopadhyay, S.S. Ray. "The quantitative analysis of nano-clay dispersion in polymer nanocomposites by small angle X-ray scattering combined with electron microscopy". *Polymer*. 51, p. 1437-1449, (2010)
20. M.J. Solomon, A.S. Almusallam, K.F. Seefeldt, A. Somwangthanaroj, P. Varadan. "Rheology of Polypropylene/Clay hybrid materials". *Macromolecules*. 34, p. 1864-1872, (2001)
21. W. Lertwimolnun, B. Vergnes. "Influence of screw profile and extrusion conditions on the microstructure of polypropylene/organoclay nanocomposites". *Polymer Engineering and Science*. 47, p. 2100-2109, (2007)

Chapter 3. In-line NIR spectroscopy for the characterization of dispersion in polymer-clay nanocomposites

22. W. Lertwimolnun, B. Vergnes. "Influence of compatibilizer and processing conditions on the dispersion of nanoclay in a polymer matrix". *Polymer*. 46, p. 3462-3471, (2005)
23. W. Lertwimolnun, B. Vergnes. "Effect of processing conditions on the formation of polypropylene/organoclay nanocomposites in a twin-screw extruder". *Polymer Engineering and Science*. 46, p. 314-323, (2006)
24. P. Cassagnau. "Melt-rheology of organoclay and fumed silica nanocomposites". *Polymer*. 49, p. 2183-2196, (2008)
25. L. Yan, C.B. Roth, P.F. Low. "Changes in the Si-O vibrations of smectite layers accompanying the sorption of interlayer water". *Langmuir*. 12, p. 4421-4429, (1996)
26. L.S. Loo, K.K. Gleason. "Fourier transform infrared investigation of the deformation behavior of montmorillonite in nylon-6/nanoclay nanocomposite". *Macromolecules*. 36, p. 2587-2590, (2003)
27. K.C. Cole. "Use of Infrared spectroscopy to characterize clay intercalation and exfoliation in polymer nanocomposites". *Macromolecules*. 41, p. 834-843, (2008)
28. M. Modesti, A. Lorenzetti, D. Bon, S. Besco. "Effect of processing conditions on morphology and mechanical properties of compatibilized polypropylene nanocomposites". *Polymer*. 46, p. 10237-10245, (2005)
29. M.W. Spencer, L. Cui, Y. Yoo, D.R. Paul. "Morphology and properties of nanocomposites based on HDPE/HDPE-g-MA blends". *Polymer*. 51, p. 1056-1070, (2010)
30. M. Bousmina. "Study of intercalation and exfoliation processes in polymer nanocomposites". *Macromolecules*. 39, p. 4259-4263, (2006)
31. D.H. Kim, P.D. Fasulo, W.R. Rodgers, D.R. Paul. "Structure and properties of polypropylene-based nanocomposites: Effect of PP-g-MA to organoclay ratio". *Polymer*. 48, p. 5308-5323, (2007)
32. K. Chrissopoulou, S.H. Anastasiadis. "Polyolefin/layered silicate nanocomposites with functional compatibilizers". *European Polymer Journal*. 47, p. 600-613, (2011)

Chapter 3. In-line NIR spectroscopy for the characterization of dispersion in polymer-clay nanocomposites

33. J.A. Covas, O.S. Carneiro, J.M. Maia, S.A. Filipe, A.V. Machado. "Evolution of chemistry, morphology and rheology of various polymer systems along a twin-screw extruder". *The Canadian Journal of Chemical Engineering*. 80, p. 1065-1074, (2002)
34. J.K. Lee, C.D. Han. "Evolution of polymer blend morphology during compounding in an internal mixer". *Polymer*. 40, p. 6277-6296,(1999)

IN-LINE NEAR-INFRARED SPECTROSCOPY: A TOOL TO MONITOR THE PREPARATION OF POLYMER-CLAY NANOCOMPOSITES IN EXTRUDERS

4

In-line diffuse reflectance and on-line transmission Near-Infrared spectroscopy (NIR) measurements are performed at the same location of the barrel of a twin screw extruder during the preparation of a polypropylene/clay nanocomposite. Their performance is evaluated by means of a 7-parameter chemometric model using off-line rheological and structural (FT-IR) data obtained from samples prepared under different screw speed, compatibilizer content and clay loading, as well as a process-related thermomechanical index. Despite the higher variability of the diffuse reflectance signal, the two models present analogous high quality indices. The aptness of the reflectance measurements is thus validated, which has direct practical advantages, since this probe can be fixed in any typical melt pressure transducer port. The probe is then used for the real-time in-line monitoring of the production of the same nanocomposite, but now using different throughputs, and the chemometric-based predictions are compared with experimental off-line characterization data. The non-linear effect of throughput is correctly anticipated.

J.M. Barbas, A.V. Machado, J.A. Covas, Journal of Applied Polymer Science, in press (2012)

4.1. Introduction

Polymer-clay nanocomposites exhibit excellent physical and mechanical performance at clay contents typically lower than 5 % in weight [1 – 2]. It is currently well established that their properties are determined by the morphology and clay dispersion level and that these are strongly influenced by the conditions used for the compounding and processing stages [1 – 7]. However, correlations between dispersion and processing conditions remain unclear [3 – 7], which continue to make difficult process set-up, optimization, control and scale-up.

Real time monitoring of material characteristics upon compounding and processing of these materials is thus of great interest. On-line oscillatory rheometry [8] was successfully used for the characterization of polymer-clay nanocomposites along a twin screw extruder. Correlations between the rheological response and the degree of mixing could be established, but it has been reported that in some cases rheology is unable to discriminate between different dispersion levels. [6, 9] Also, rheological measurements take typically a few minutes, i.e., they are not performed in real time.

Spectroscopic techniques, Near-Infrared (NIR) in particular, have found a remarkable development due to the recent advances in probes, sensor technology and equipment construction [10 – 14]. On-line NIR during polymer processing (usually extrusion) is mostly performed in transmission mode, using flow-cell fixtures inserted between extruder and die [13 – 19]. However, acquiring NIR spectra by means of reflection probes [20 – 23] can be more convenient, as fixing them to the processing equipment, inclusive along its axis, should be easier and allow monitoring the evolution of dispersion along the screw. Rohe *et al.* [20] used prototype transmittance and reflection probes during blending of polyethylene with polypropylene in a twin screw extruder and found out that they produced comparable results, even if the authors had to develop a complex optical bypass system. Curiously, most previous on-line NIR monitoring of the preparation of clay nanocomposites has been performed using reflection probes, but these have been located between extruder and die. Moghaddam *et al.* [21] correlated temperature, particle size and viscosity changes of polymer-clay nanocomposites with spectral differences. Witschnigg *et al.* [22] studied the effect of screw speed and geometry on the final composite performance. Fischer *et al.* [23] correlated the spectral data with the degree of exfoliation of melt that was detoured from the main stream before crossing the die. These pioneering

Chapter 4. In-line NIR spectroscopy: a tool to monitor the preparation of polymer-clay nanocomposites in extruders

studies focused essentially on the clay reinforcement effects and applied a simplified chemometric analysis. The authors [24] monitored the evolution of clay dispersion during compounding in a batch mixer and attempted to develop appropriate chemometric models. For this purpose, they tested models of different complexity using parameters derived from various well established dispersion characterization techniques. Eventually, a 7-parameter model comprising data from oscillatory rheometry, Fourier Transform Infra-Red spectroscopy (FT-IR) and a thermomechanical process-related index provided good predictive capacity.

Carrying out Diffuse Reflectance measurements along the axis of a twin-screw extruder could involve a few complications. The periodic exposure of the probe to the rotating surfaces of the tips of the screw elements, the eventual presence of large clay solid particulates that may act as diffuse reflectors, the complex three-dimensional flow pattern developing in mixing zones and the possibility that the screws will not work fully filled at the measuring point could interfere with the spectra measurement.

This work aims at investigating the effectiveness of diffuse reflectance to monitor the preparation of a Polypropylene/Polypropylene grafted with Maleic Anhydride/Organo-Montmorillonite (PP/PP-g-MA/D67G) system in a twin-screw extruder using commercial probes and appropriate chemometrics. In-line (not on-line) measurements at the extruder barrel are targeted, i.e., without affecting material flow and performed as upstream in the process as possible. The quality of the spectra acquired by transmission and diffuse reflectance probes is first compared. Then, 7-parameter chemometric models are built for each measurement mode on the basis of characterization data from nanocomposites prepared with different screw speed, compatibilizer content and clay content. The aptness of the two probes is compared by assessing quantitatively the quality of each model. Ultimately, the diffuse reflection probe is used for the real-time in-line monitoring of samples prepared using different throughputs, the predictions being compared with experimental off-line characterization data.

4.2. Experimental

4.2.1. Materials and composites

The materials used in this work are listed in Table 4. 1. They include an injection molding grade Polypropylene (PP), a Polypropylene grafted with Maleic Anhydride (PP-g-MA) and Dellite 67G (D67G), a natural Montmorillonite clay modified with dimethyl dihydrogenated tallow quaternary ammonium salt (2M2HT). Table 4. 2 presents the compositions of the PP/PP-g-MA/D67G nanocomposites prepared in a modular co-rotating intermeshing twin-screw extruder Leistritz LSM 30.34. As NIR spectra are quite sensitive to temperature variations [16], the barrel and die set temperature were kept constant at 200 °C for all the extrusion runs. The feed rate (Q) was always set at 3 kg/h by a Moretto Dosing System DVM18-L and the reference screw speed was 100 rpm. In the case of the 90/5/5 wt.% nanocomposite, various screw speeds were used (50, 100, 200 and 300 rpm).

Table 4. 1. Materials used in the work.

<i>Material</i>	<i>Acronym</i>	<i>Producer</i>	<i>Grade</i>	<i>MFI/lamellar distance</i>
Polypropylene	PP	Lyondell Basell	Moplen HP500N	12 g/10 min (230 °C/2.16 kg)
Compatibilizer	PP-g-MA	Crompton	Polybond 3200	115 g/10 min (190 °C/2.16 kg)
Montmorillonite clay	D67G	Laviosa	Dellite 67G	$d_{001} = 3.70$ nm

Table 4. 2. Composition of the various PP/PP-g-MA/D67G nanocomposites prepared.

<i>Variable</i>	<i>PP (%wt.)</i>	<i>PP-g-MA (%wt.)</i>	<i>D67G (%wt.)</i>
Reference	90	5	5
% PP-g-MA	95	0	5
	85	10	5
% clay	94	5	1
	93	5	2
	92	5	3
	87.5	5	7.5

4.2.2. Process monitoring set-up

The NIR process monitoring system used is depicted in Figure 4. 1 and comprises three main components:

- i. Two commercial sensors, a Diffuse Reflectance probe FDR-650 and a Transmission probe FPT-850 (both from Axiom Analytical Inc.). The first has a sapphire window with a diameter of 5.7 mm, for an illuminated area with a diameter of 3.2 mm and a field depth of 3 mm. It uses an 80 fiber bundle cable that splits in two 40 fiber bundles to connect to the analyzer inlet and outlet channels. The background signal is acquired prior to installation, using a Spectralon diffuse reflection standard target (Bruker Optics) with a reflectivity index of 99%. The transmission probe has a physical rectangular gap of 5 mm, corresponding to the probe optical path length. The probe's inner duct is pressurized at 4 bar with N₂ to prevent humidity condensation inside the light guide channels. It uses two fiber optic cables for the transmitting and receiving signals with a core fiber diameter of 600 μm. The background is acquired using a loop of an identical fiber optic cable.
- ii. A Matrix® F (Bruker Optics) spectrometer with an InGaAs detector and a HeNe laser emitting at 633 nm at 1mW. The scanner rate is 10 kHz.
- iii. A PC with the OPUS® Quant2 software (Bruker Optics) for data acquisition and analysis, communicating with the spectrometer by a LAN-type cable.

Chapter 4. In-line NIR spectroscopy: a tool to monitor the preparation of polymer-clay nanocomposites in extruders

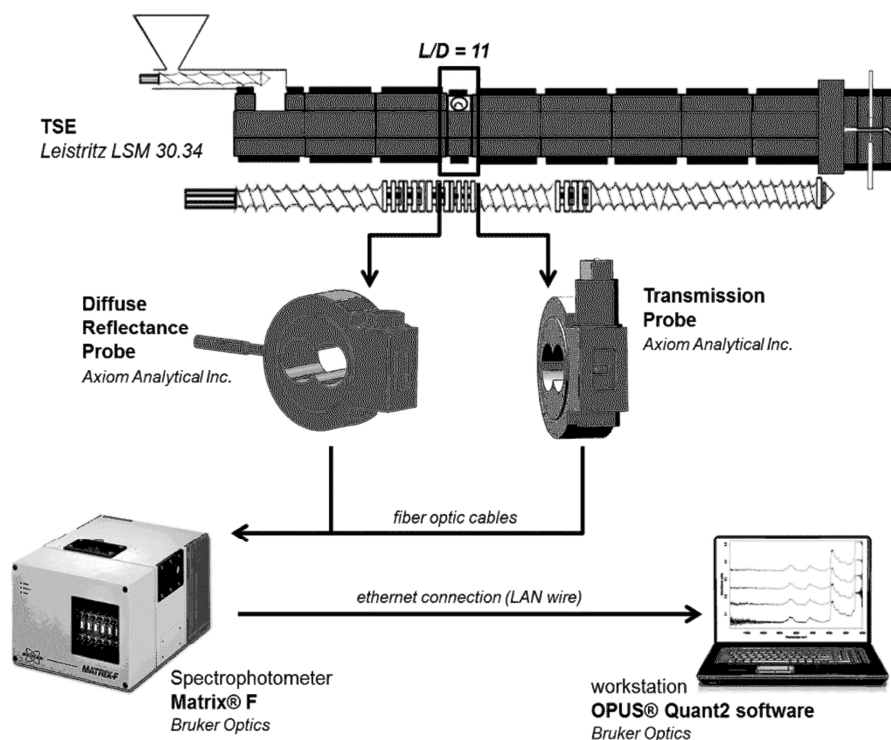


Figure 4. 1. In-line set-up.

The Diffuse Reflectance probe has a standard tip (with a 1/2 UNF thread) that enables its setting in any available conventional pressure sensor port along the extruder. The probe contacts directly the melt stream, no modifications to the extruder or die being required. The Transmission probe is inserted in a modified extruder segment [25], which consists of a bypass system developed in-house. Whenever measurements are to be performed, a rotary valve is actuated to divert melt from within the extruder into the gap of the probe at low shear rate, in order to avoid any changes in morphology upon collection and measurement. In a few situations, the combined effect of the residence time in the gap and heat transfer from the cold probe surfaces (despite the sensor being embedded into a heated barrel segment) may cause cooling of the material and problems in spectra acquisition.

In the experiments reported here, the two probes were positioned at a barrel location ($L/D = 11$) corresponding to the downstream region of the first mixing zone of the screw. The barrel segment also allows the quick collection (in circa 1 second) of material samples from within the extruder, which were then quenched and stored for subsequent off-line characterization. Thus, it could be

Chapter 4. In-line NIR spectroscopy: a tool to monitor the preparation of polymer-clay nanocomposites in extruders

readily confirmed that at this relatively upstream location in the process the polymer is already fully molten. Therefore, one would not only anticipate that here the evolution of dispersion is far from complete, but also that the effects of material changes and processing conditions are probably more significant [3 – 5]. In addition, the presence of a molten matrix is important for the subsequent rheological measurements (in fact, any remaining solids present in the sample would probably melt upon compression molding discs for the rheological measurements, i.e., the morphology of the sample upon collection would be destroyed).

4.2.3. Characterization of the Composites

NIR Spectroscopy (Matrix F, Bruker Optics) – The NIR spectra were measured from 12000 – 4500 cm^{-1} with a resolution of 8 cm^{-1} and accumulation of 4 scans, the acquisition time for each spectrum being less than 2 seconds. For comparison purposes the spectra acquisition conditions were the same in both modes. For each sample, a total of 50 spectra were measured during 30 minutes of a continuous extrusion run. The NIR spectra discussed throughout this work are an average of these, without performing any further processing or signal correction.

Rotational Rheometry (AR-G2, TA Instruments) – The linear viscoelastic response of the samples at 200 °C was obtained from oscillatory frequency sweeps from 0.1 to 100 rad/s, using parallel plates with a diameter of 25 mm and setting a 1 mm gap, performed under a constant strain (1 % for the polymer and 0.5 % for the composites). The disks had been previously compression molded at 200 °C and 20 Tons. Considering the association between the increase of melt yield stress (σ_0) and clay exfoliation proposed by Lertwimolnun and Vergnes [3 – 5] and between a power law exponent (b) at low frequencies and the state of clay dispersion suggested by others [6, 9], the complex viscosity vs. frequency curves were fitted to a modified Carreau-Yasuda model with yield stress: [3 – 5]

$$|\eta^*(\omega)| = \frac{\sigma_0}{\omega} + \eta_0 \left[1 + \lambda \omega^a \right]^{\frac{b-1}{a}} \quad (4. 1)$$

and to a power law: [6, 9]

$$|\eta^*(\omega)| = A \omega^b \quad (4. 2)$$

Chapter 4. In-line NIR spectroscopy: a tool to monitor the preparation of polymer-clay nanocomposites in extruders

where the adjustable parameters are the zero shear viscosity (σ_0), the relaxation time (λ), the Yasuda parameter (a), the power law exponent (b) and the power law consistency (A). The Origin® Pro8 software was used for this purpose. The values of G' (storage modulus) and G'' (loss modulus) at low frequency were also determined [3, 26], as they are considered to provide a good perception of clay dispersion, with the increase of their values relating to a finer dispersion [3, 26] and the formation of a plateau at low frequencies being attributed to the deformation and recovery of the dispersed particles [26, 27]

Medium FT-IR (FTIR4100, Jasco) – The organoclay was analyzed with a KBr mortar. The nanocomposite samples were compression molded at 200 °C into $\pm 75 \mu\text{m}$ thick films and analyzed in transmission mode, in the 4000 – 500 cm^{-1} wavenumber range with a resolution of 4 cm^{-1} , using 32 scans. The wavenumber accuracy of the FT-IR was checked prior to the measurements using the absorption peak of CO_2 at 668 cm^{-1} (background measurement, with resolution of 2 cm^{-1} , accumulation of 16 scans and apodization set to Boxcar, according to instructions of the manufacturer) for which the acceptance criterion is $\pm 2 \text{ cm}^{-1}$. Also the wavenumber repeatability was validated using a standard Polystyrene film (Jasco) with thickness of 40 μm (resolution of 2 cm^{-1} , accumulation of 16 scans and apodization set to Cosine), for which the acceptance criterion is that every reference peak is within $\pm 1 \text{ cm}^{-1}$.

The region between 1300 and 750 cm^{-1} was fitted with the Pearson VII expression utilizing the Origin® Pro8 software, adjusting a 75 % Gaussian shape ($\mu = 4$) for the determination of the wavenumber shift for the 1050 cm^{-1} (Si-O in-plane) and 1080 cm^{-1} (Si-O out-of-plane) peaks [28]. The clay Si-O bond region can be decomposed at least in four peaks, three being related to the in-plane vibrations (1120, 1050 and 1020 cm^{-1}) and the fourth to the out-of-plane vibrations (1080 cm^{-1}) [28 – 29]. As the individual clay layers become more spaced, the peaks at 1050 cm^{-1} and 1080 cm^{-1} tend to shift. When the structure is ordered and intercalated, the peak at 1050 cm^{-1} will suffer a negative shift towards a lower wavenumber, whilst for highly disordered or partially exfoliated morphologies the peak at 1080 cm^{-1} will shift to higher wavenumbers [28 – 29].

4.2.4. Chemometrics

The molecular absorbance of NIR radiation is weaker than that of medium IR, enabling an analysis without sample preparation [18, 30 – 32]. Conversely, since the response of the molecules to the exposure to NIR radiation results in complex spectra, one must rely on adequate chemometrics to extract from the data as much relevant information as possible. The correlation between the NIR spectra and the state of clay dispersion is obtained by means of a calibration model. Using the methodology developed previously and taking in its main conclusions [24], the calibration model will include parameters derived from oscillatory rheometry (G' , G'' , σ_0 , b), FT-IR (wavenumber shift of the peaks at 1050 and 1080 cm^{-1}) and a process-related thermomechanical index, specifically the specific mechanical energy (SME), calculated as the ratio between the mechanical power consumed by the extruder (Amp) and the corresponding throughput [33]. In this study two 7-parameter models will be calculated using either the transmission or the reflection spectra, both being built from the characterization of nanocomposites prepared with different screw speed, compatibilizer content and clay content. A partial least squares (PLS) regression will be applied to the calibration data set and the quality of the model is assessed using the parameters previously described in section 3.3.2 of this thesis [20, 22, 30 – 32].

4.3. Results and discussion

4.3.1. Analysis of the NIR spectra

The signal of each spectrum (Figure 4. 2) depends both on the chemical (molecular absorbance) and physical (scattering /reflective) characteristics of the sample, as well as on the optical measurement geometry [30]. The organic phase of the clay and the PP matrix have common spectral features [34 – 35], particularly in the region between 6000 – 5000 cm^{-1} assigned to the first overtone of the stretching vibrations of the CH_2 and CH_3 groups. In the PP matrix spectrum, the band at 7160 cm^{-1} is assigned to the combination of first overtones and fundamental vibrations also of the CH_2 and CH_3 groups, whilst the band between 8400 – 8200 cm^{-1} corresponds to the second and

Chapter 4. In-line NIR spectroscopy: a tool to monitor the preparation of polymer-clay nanocomposites in extruders

third overtones of the same CH bonds [35]. The peak around 5250 cm^{-1} in the organoclay spectrum is due to the combination of stretching and bending of the water molecules. At wavelengths higher than 6500 cm^{-1} the organoclay shows a prominent band between $7200 - 6800\text{ cm}^{-1}$ related to OH stretching and bending of both H_2O molecules and hydroxyls of the cationic surfactant [34]. The peak at 8230 cm^{-1} is assigned to the CH stretching vibrations of the organic phase. Due the overlapping of typical peaks and also to the low concentration of organoclay used, direct analysis of the NIR spectra of the resulting nanocomposites is sometimes difficult.

Figure 4. 2 displays the 50 spectra as measured in transmittance and in diffuse reflectance modes for the 90/5/5 nanocomposite prepared at 3 kg/h and 100 rpm (the results are identical for the remaining samples). The stability and repeatability of the NIR signal are good, even in the region with lower signal-to-noise ratio (above 10000 cm^{-1}). The amplitude between the maximum and minimum absorbance values is about 12 % and 20 % in transmission and reflection, respectively. Measurements with the Diffuse Reflectance probe were performed on an empty extruder operating at the same condition and the maximum absorbance values were less than 0.1 % of those measured for the melt. Thus, the influence of the rotation of the screw mixing elements is negligible. Consequently, the higher variability of the diffuse reflectance signal can be attributed to scattering effects caused by clay size, number and distribution [30, 32]. The lower information depth of the diffuse reflectance signal as compared to the transmission path length may enhance this effect.

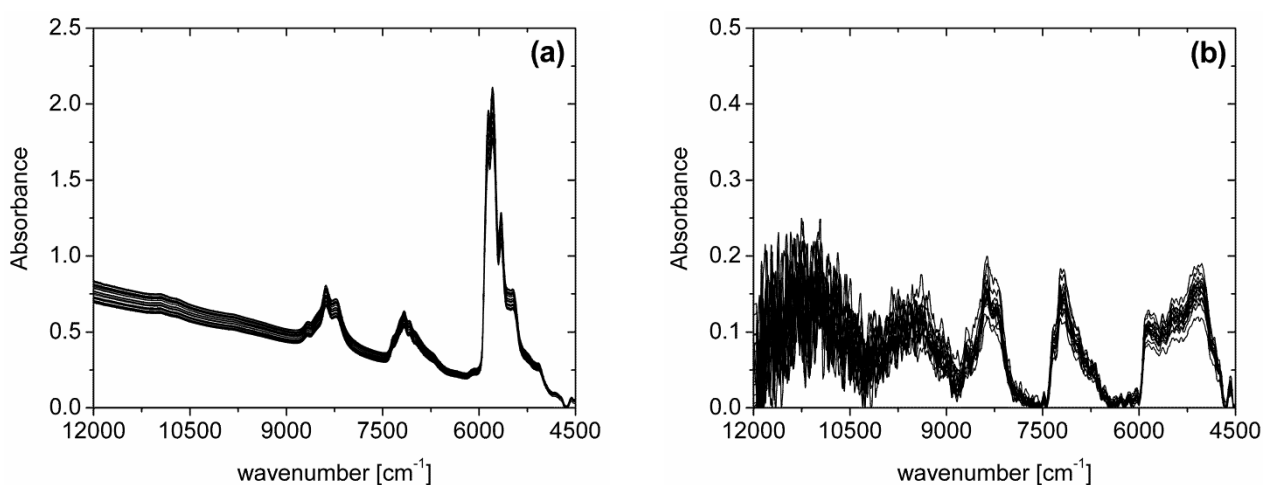


Figure 4. 2 Spectra acquired for the 90/5/5 nanocomposite prepared at 3 kg/h and 100 rpm: (a) Transmission (b) Diffuse reflectance.

Chapter 4. In-line NIR spectroscopy: a tool to monitor the preparation of polymer-clay nanocomposites in extruders

Figures 4. 3 to 4. 5 show the average spectra in transmission and reflectance modes, without any normalization, for all the nanocomposites prepared. Figure 4. 3 refers to PP/PP-g-MA/D67G 90/5/5 wt.% prepared under different screw speeds, Figure 4. 4 to compositions with varying compatibilizer content (from 0 to 10 wt.%) and Figure 4. 5 to nanocomposites with diverse clay content (from 1 to 7.5 wt.%).

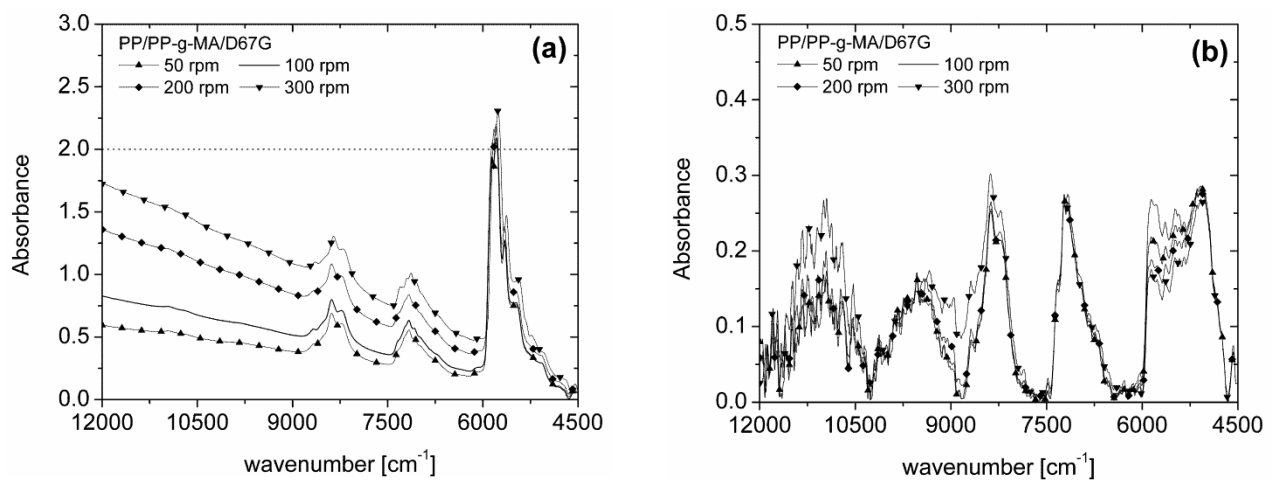


Figure 4. 3. Spectra acquired for the composites prepared with different screw speeds: (a) Transmission (b) Diffuse reflectance.

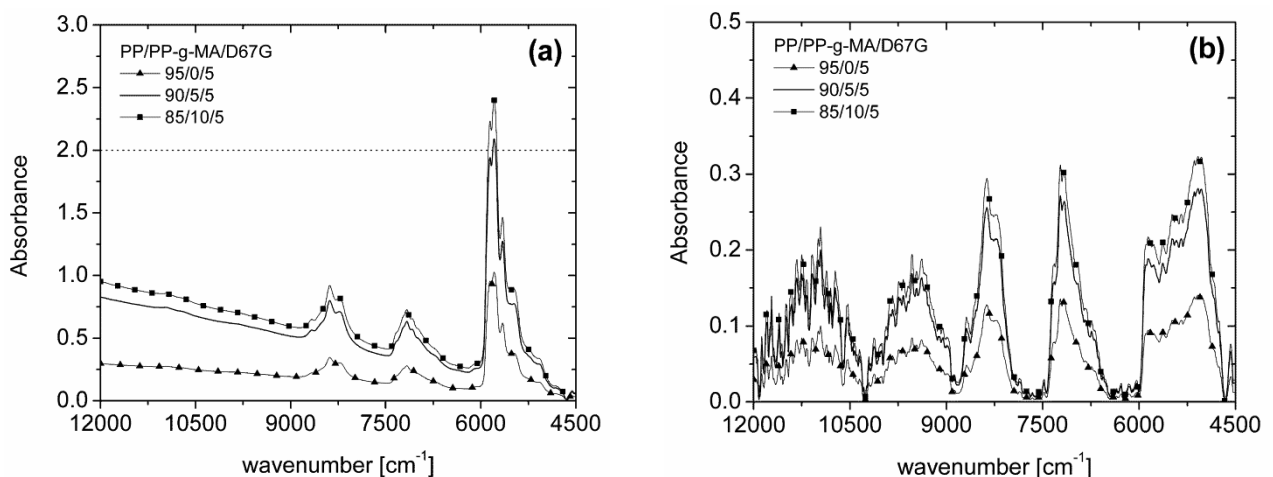


Figure 4. 4. Spectra acquired for the composites prepared with different PP-g-MA content: (a) Transmission (b) Diffuse reflectance.

Chapter 4. In-line NIR spectroscopy: a tool to monitor the preparation of polymer-clay nanocomposites in extruders

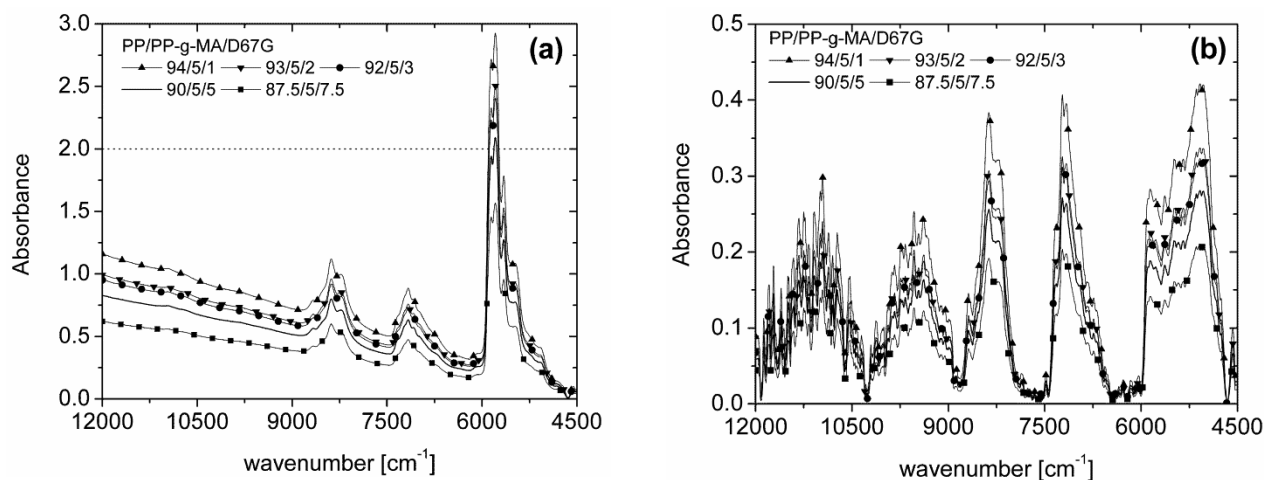


Figure 4. 5. Spectra acquired for the composites prepared with different clay content: (a) Transmission (b) Diffuse reflectance.

The region between 9000 and 5000 cm^{-1} is similar in the two modes, nonetheless signal variations in transmission are more pronounced. In the lower wavenumber region (6000 – 4500 cm^{-1}) the reflection spectra have worse definition, whilst the transmission signal shows some saturation (absorbance above 2.0). This is particularly noticeable in Figure 4. 3(a) for the nanocomposites prepared at 200 and 300 rpm, in Figure 4. 4(a) for the nanocomposite prepared with 10 wt.% PP-g-MA and in Figure 4. 5(a) for the nanocomposite prepared with 1 % in weight of D67G.

Usually, scattering increases with decreasing particle size resulting in signal losses in transmission mode and in the decrease of the signal-to-noise ratio in diffuse reflectance. Therefore, reflective losses may originate significant signal changes that are not directly related to chemical information but rather to particle distribution [30]. The spectral differences may result from a combination of clay intercalation/exfoliation, which generate a larger number of particles (clay stacks) with smaller sizes and higher inter-lamellar distance. In transmission mode, the baseline has a tendency to rise with increasing screw speed, increasing PP-g-MA content and decreasing clay content. Anyway, the two signals become more intense with increasing screw speed, increasing PP-g-MA content and decreasing clay content, which not only demonstrates the sensitivity of the spectra to changes in the extent of dispersion, but also supports the general idea that the higher the degree of dispersion the more intense the signal becomes. Since the aim is to compare the signals obtained with the two

Chapter 4. In-line NIR spectroscopy: a tool to monitor the preparation of polymer-clay nanocomposites in extruders

probes, to establish whether diffuse reflectance can provide the same bulk information as transmission, the analysis of the NIR spectra at this point is only qualitative.

4.3.2. Determining the model parameters

The chemometric model relates the spectral data with the clay dispersion level by means of a number of parameters that are derived from reference characterization techniques. This section presents and discusses the rheological response and medium infra-red spectra obtained by the off-line characterization of the samples collected during compounding.

As an example of the results obtained, Figure 4. 6 presents the isothermal (at 200 °C) linear viscoelastic response of the nanocomposites prepared under different mixing speeds. Table 4. 3 brings together the values of the dynamic moduli (G' and G'') at a constant frequency of 0.1 rad/s, melt yield stress (σ_0) and power law exponent (b) – see Equation 4. 1 and 4. 2 – for all the experiments performed, which were designed to uncover the effect of screw speed, compatibilizer content and clay percentage on dispersion.

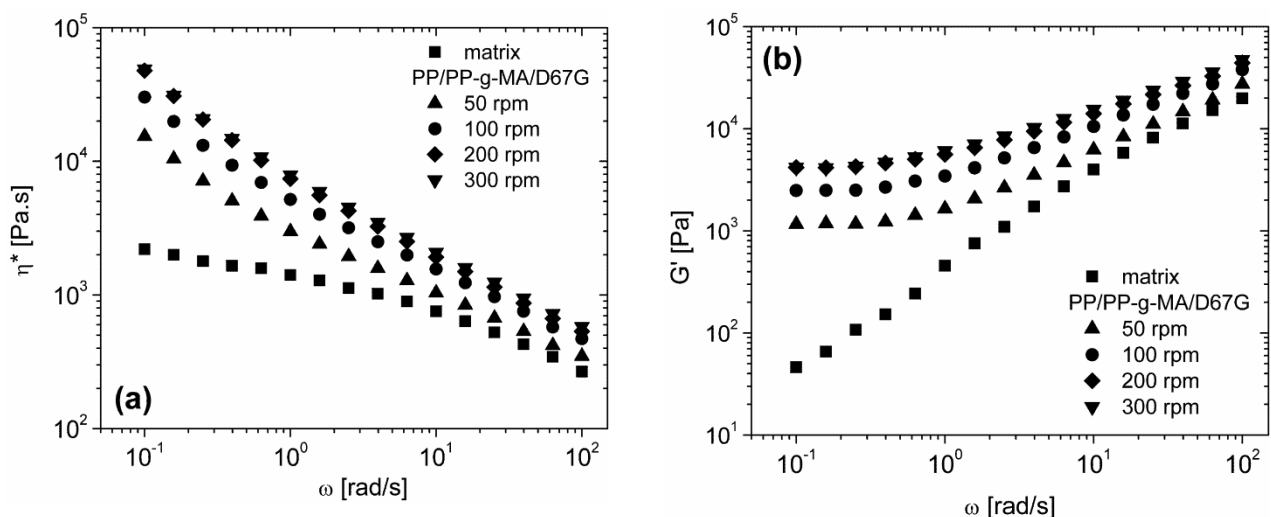


Figure 4. 6. Linear viscoelastic response against frequency of the nanocomposites prepared with different screw speeds: (a) complex viscosity and (b) storage modulus.

Chapter 4. In-line NIR spectroscopy: a tool to monitor the preparation of polymer-clay nanocomposites in extruders

The data for G' show the development of a plateau at low frequencies, a simultaneous vanishing of the Newtonian viscosity plateau at low deformation rates, as well as an increase in the overall modulus with increasing screw speed up to 200 rpm, which are usually taken as indicators of increasing dispersion levels [1, 3, 26]. Indeed, the solid-like behavior at low frequencies is generally attributed to the development of a percolating physical clay network [27] that can be attained with increasing dispersion and/or increasing clay content. Table 4. 3 demonstrates that melt yield stress (σ_0) and power law exponent (b) have a similar dependence, i.e., their absolute values increase with increasing speed up to 200 rpm, no differences being perceived for 300 rpm. This probably means that the effect of the higher dynamic stresses at the highest speed is offset by the decrease of the time the material is subjected to them.

For the same samples of Figure 4. 6, Figure 4. 7 represents the FT-IR spectra in the region of interest (Si-O bond) and the resultant peaks after fitting. Table 4. 3 lists the wavenumber shifts at 1050 and 1080 cm^{-1} . FT-IR seems to be little sensitive to changes in screw speed. The peak at 1050 cm^{-1} shifts towards lower wavenumbers when the speed increases from 50 to 100 rpm, which is often associated with the presence of an ordered and intercalated structure [28 – 29], no other evolution being observed for higher screw speeds. The peak at 1080 cm^{-1} shows a very small positive shift that sustains the same conclusion. Nanocomposites with lower clay content (from 1 to 3 wt.%) show a pronounced negative shift of the peak at 1050 cm^{-1} , which can be related to higher levels of intercalation. The same samples exhibit higher shifts of the peak at 1080 cm^{-1} , indicating that partial exfoliation was attained. This suggests that the majority of samples prepared have ordered intercalated structures, but when the clay content decreases the morphologies seem to be more disordered and with higher intercalation levels, or even partially exfoliated clay platelets.

Chapter 4. In-line NIR spectroscopy: a tool to monitor the preparation of polymer-clay nanocomposites in extruders

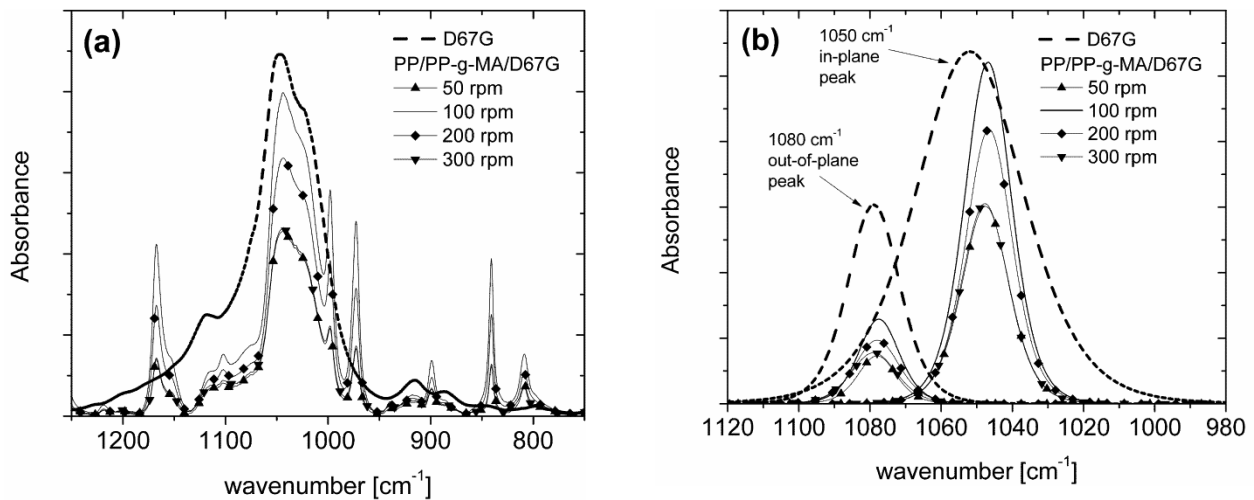


Figure 4. 7. FT-IR spectra in the Si-O band region of the nanocomposites prepared with different screw speeds: (a) as measured; (b) 1050 and 1080 cm^{-1} fitted peaks.

Finally, Table 4. 3 also contains data on SME, the specific mechanical energy index. The nature of this parameter is quite different from the remaining, as it integrates the mechanical power consumed along the entire screw length – which in principle should be proportional to the mixing intensity, hence to the dispersion level, divided by the mass output for normalization purposes. Taking again screw speed for discussion, SME increases from 2.0 to 2.7 A.Kg.h^{-1} as it goes from 50 to 300 rpm. The same type of variation was detected for the other effects studied.

A detailed analysis of Table 4. 3 may evidence some incoherency between the data trends indicated by the different techniques. This can be due to differences in the area analyzed, to the length scale probed by the characterized parameter, or to its particular correlation with clay dispersion. Therefore, the information provided by the various techniques selected for the 7 parameter model is complementary and offers a broad insight into the state of clay dispersion. To develop the chemometric models each parameter in Table 4. 3 was normalized according to:

$$\text{Normalized Value (\%)} = \frac{(\text{Value} - \text{minimum value})}{(\text{Maximum value} - \text{minimum value})} \times 100 \quad (4. 7)$$

i.e., a score of 0% matches the polymer matrix, while 100% refers to the most dispersed nanocomposite. Table 4. 4 lists the normalized averages (representing the relative degree of dispersion) for all nanocomposites and compounding conditions used to set the calibration models.

Chapter 4. In-line NIR spectroscopy: a tool to monitor the preparation of polymer-clay nanocomposites in extruders

An analysis of the effect of using weights affecting the parameters linked to Rheology, FTIR and SME revealed that a simple average of the seven parameters would yield the best results. Yet, as the number of parameters associated to each technique is different, the 7-parameter model inherently attributes more importance to rheological data and less to SME. In a separate study [24], it was demonstrated that this 7-parameter model has higher quality features than models purely based on rheology or FT-IR data.

Table 4. 3. Values of the properties of the 7-parameter model for the range of compounding runs.

Sample	G' (kPa)	G'' (kPa)	σ_0 (kPa)	b	1050 cm^{-1}	1080 cm^{-1}	SME (A.kg.h ⁻¹)	
matrix	0.046	0.215	0	-0.099	0	0	2.0	
Reference	2.489	1.586	2.736	-0.832	-5.6	1	2.3	
N (rpm)	50	1.162	0.992	1.337	-0.774	-4.6	0.8	2.0
	200	4.173	2.297	4.393	-0.863	-5.6	0.8	2.3
	300	4.179	2.547	4.480	-0.859	-4.6	0.7	2.7
PP-g-MA (%wt.)	0	0.118	0.409	0.007	-0.102	-5.1	0	2.7
	10	1.386	1.231	1.468	-0.641	-6.3	1.4	2.3
Clay (%wt.)	1	0.0731	0.294	0.072	-0.198	-13.8	1.4	2.0
	2	0.432	0.694	0.793	-0.489	-14.2	2.3	2.0
	3	0.572	0.716	1.027	-0.526	-14	1.5	2.3
	7.5	5.726	3.022	5.786	-0.893	-5.8	0.3	2.7

Table 4. 4. Normalized average values associated to each of the nanocomposites prepared.

			PP-g-MA (%wt.)		Clay (%wt.)					N (rpm)		
	matrix	reference	0	10	1	2	3	7.5	50	200	300	
Normalized average (%)	0.0	51.0	20.7	43.1	25.0	41.0	43.6	79.1	31.8	62.3	70.3	

4.3.3. Transmission vs. Reflection On-line measurements

When applying a PLS regression to the development of a chemometric model, the optimization of its performance may include different strategies. One is to apply data preprocessing techniques, such as corrections and normalizations, to maximize the analyte specific information or the spectra distinctive features. Another is to select the spectral region that provides better selectivity. It is also important to define the optimal matrix dimension (number of factors, ranging between 1 and 10) for adequate calibration and predictive performance [30 – 31]. Due to the differences in signal quality pointed out in section 4. 4. 1, the calibration model for Transmission the mode uses 4 PLS factors in the spectral region between 9597.7 and 4497.4 cm^{-1} after applying vector normalization as signal correction, whilst for Diffuse Reflectance mode 7 PLS factors are used and the region of interest ranges from 7502.1 to 4597.7 cm^{-1} , with a multiplicative scattering correction of the original signal. Vector normalization eliminates the effects of material density, sample thickness and others that may influence the bands height, resulting in inaccurate information related to signal intensity. The multiplicative scattering correction is often applied to diffuse reflectance measurements to reduce the drift effects discussed in section 4. 4. 1 [22, 30]. The Opus® Quant2 software was used to run the optimization algorithms, identify the potentially best procedure, set the number of factors (pairs of scores and loadings) of the spectral matrix, select the spectral region, perform signal correction and pinpoint eventual outliers in the test series.

Table 4. 5 shows the quality factors of the models for the two measurement modes. The corresponding calibration and validation curves are illustrated in Figure 4. 8. The Validation/Calibration population ratio was kept at 15 % [24]. The two measurement modes yielded good quality models, with R^2 values higher than 95 % for calibration and validation. The RMSEP values are low and very similar, while the RPD values are identical and above 8 (as desired), the same applying to bias. These results demonstrate the feasibility of using the diffuse reflectance probe for in-line real time monitoring of the preparation of polymer-clay nanocomposites directly at the barrel of the extruder, upon its steady-state operation.

Chapter 4. In-line NIR spectroscopy: a tool to monitor the preparation of polymer-clay nanocomposites in extruders

Table 4. 5. Calibration and Validation results for the 7-parameter models.

	Calibration			Validation		
	R2 (%)	RMSEE	RPD	R2 (%)	RMSEP	bias
Transmission	98.9	1.18	11.7	98.7	1.26	-0.901
Reflection	98.9	1.21	11.6	97.8	1.45	-0.945

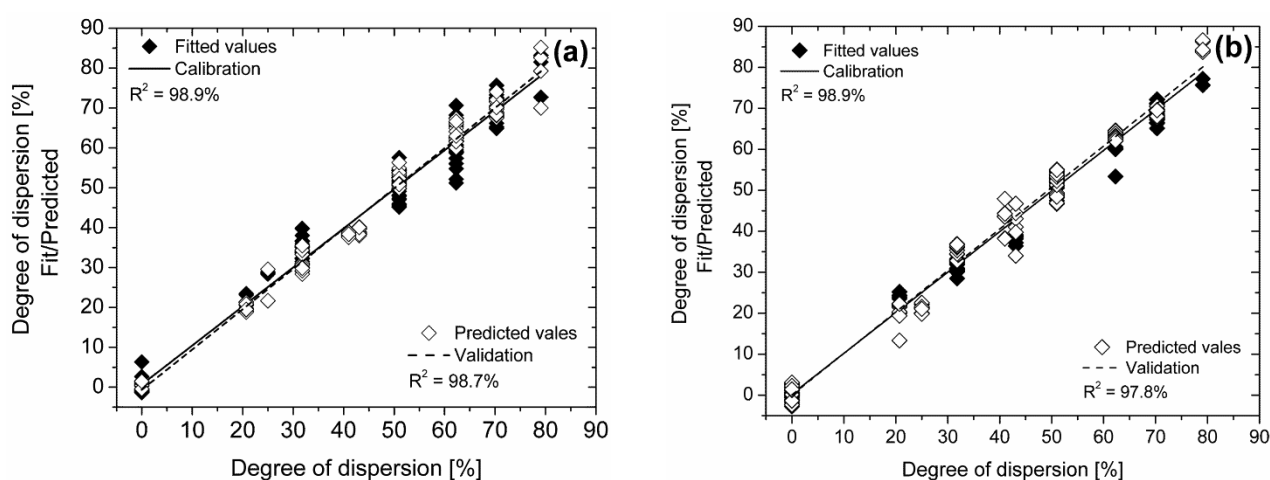


Figure 4. 8. Calibration models: (a) Transmission; (b) Reflection.

4.4.4. Real-time monitoring with Diffuse Reflectance

Given the good results reported above, the diffuse reflectance probe was used to monitor in real-time (at the same location as before) the manufacture of the PP/PP-g-MA/D67G 90/5/5 wt.% composite with three distinct feed rates (1.5, 6 and 9 kg/h), the other operating conditions remaining constant (barrel and die set to 200 °C, screw speed of 100 rpm). As before, 50 spectra were acquired per sample. Although it is well-known that chemometric models should not be extended to materials or processing conditions laying outside the range utilized to create them [30 – 31], the same model is used here, since one would anticipate that throughput variations will produce an effect on clay dispersion similar to that of screw speed, i.e., both are variables influencing the same dispersion mechanism. Table 4. 6 ranks the predicted relative degree of dispersion of the samples. Dispersion should not increase strictly with output, a maximum being anticipated at intermediate throughputs.

Chapter 4. In-line NIR spectroscopy: a tool to monitor the preparation of polymer-clay nanocomposites in extruders

Similarly to the effect of screw speed, this behavior could be due to the conflicting effects of higher hydrodynamic stresses and lower residence times with increasing feed rate. Nevertheless other factors may also come into play, as the higher shear rates associated to the higher outputs boost viscous dissipation and this may trigger polymer degradation. In turn, the degraded material will become less viscous and could outflow from between the clay platelets, thus delaying or even reducing dispersion.

Table 4. 6. Final dispersion levels of nanocomposites prepared using different throughputs.

	<i>Relative degree of dispersion (\pm error) –%</i>			
Q (kg/h)	1.5	3	6	9
NIR Prediction	32.0 (\pm 1.7)	51.6 (\pm 1.1)	73.0 (\pm 3.5)	35.4 (\pm 4.2)
Normalized average	30.1 (\pm 3.8)	51.0 (\pm 3.2)	70.1 (\pm 3.8)	40.4 (\pm 4.0)

At the same location of the in-line measurement, samples were collected from the extruder and characterized off-line. Rheology (complex viscosity, storage modulus) and FT-IR data (absorbance) are depicted in Figure 4. 9 and 10, respectively. The SME, σ_0 and b values are shown in Table 4. 7.

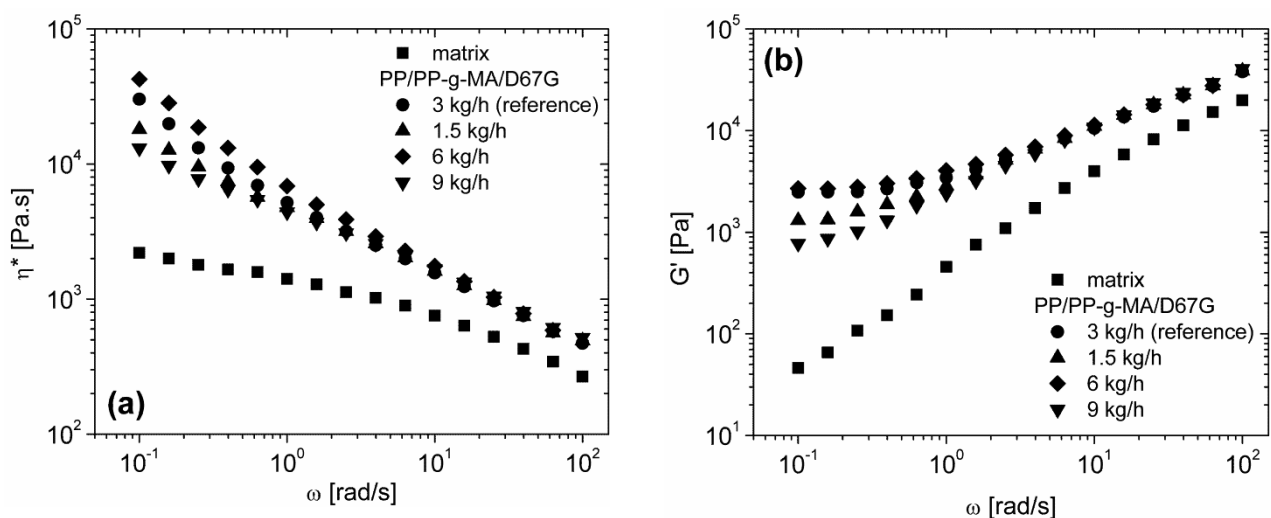


Figure 4. 9. Linear viscoelastic response against frequency of the PP/PP-g-MA/D67G 90/5/5 w/w/w nanocomposite prepared with different feed rates. (a) complex viscosity; (b) storage modulus.

Chapter 4. In-line NIR spectroscopy: a tool to monitor the preparation of polymer-clay nanocomposites in extruders

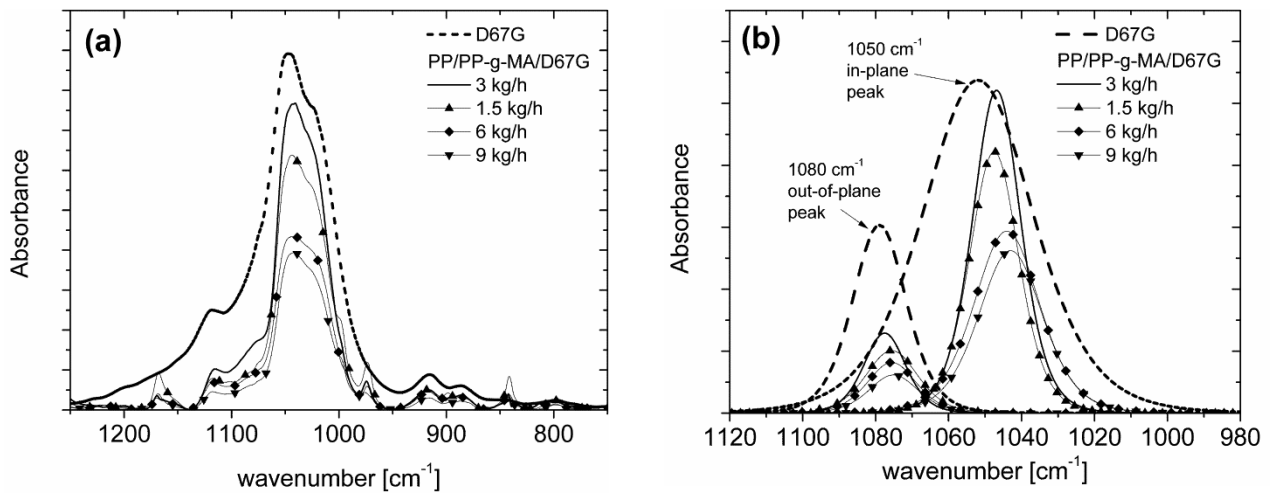


Figure 4. 10. FT-IR spectra in the Si-O band region of the PP/PP-g-MA/D67G 90/5/5 w/w/w nanocomposite prepared with different feed rates: (a) as measured; (b) 1050 and 1080 cm⁻¹ fitted peaks.

At low frequencies, the rheological parameters increase with feed rate up to 6 kg/h and decrease for 9 kg/h (Figure 4. 9); identical results are shown for melt yield stress (σ_0) and power law exponent (b). These results are in agreement with those reported by Lertwimolnun and Vergnes [5] for post-mortem samples collected along a twin screw extruder. FT-IR data (Figure 4. 10) demonstrates that the samples prepared at 6 and 9 kg/h have identical peak shifts. An XRD analysis of these samples could not detect any significant changes of the clay diffraction pattern with increasing feed rate. However, it is worth to stress again that these techniques used explore different length scales.

Table 4. 7. SME, σ_0 and b for the PP/PP-g-MA/D67G 90/5/5 w/w/w nanocomposite prepared with different feed rates.

Q (kg/h)	1.5	3	6	9
SME (Amp/Q)	2	2.3	2.7	2.7
σ_0 (kPa)	1.305	2.736	3.812	0.745
b	-0.625	-0.832	-0.840	-0.487

Chapter 4. In-line NIR spectroscopy: a tool to monitor the preparation of polymer-clay nanocomposites in extruders

In view of the experimental data of Figures 4. 9 and 4. 10 and Table 4. 7, the matching between the NIR predictions and the measured values (Table 4. 6) is quite satisfactory, the maximum in dispersion and its value being well predicted.

4.5. Conclusions

The practical feasibility of using diffuse reflectance NIR for the in-line monitoring along the axis of an extruder of the level of clay dispersion during the manufacture of polymer-clay nanocomposites is demonstrated. Consequently, the utilization of several of these probes positioned along the screw axis and die will characterize the evolution of clay dispersion upon compounding, which would be quite relevant for process set-up, composition tuning, optimization and control.

Although thus far transmission probes have been preferred for NIR monitoring of polymer melt processes, modern commercial diffuse reflectance probes can be made available with a Dynisco-type threaded tip that enables their simple fixing at any available pressure sensor port of the extruder or die. However, the spectra measurement could be affected by the periodic rotation of the tips of the screw elements, the presence of large clay solid particulates (more likely immediately upon polymer melting) acting as diffuse reflectors, the complex three-dimensional flow pattern in the screw channel and the possibility that the screws will not work locally fully filled. Measurements performed on an empty extruder operating normally demonstrated the maximum absorbance values were less than 0.1% of those measured for the melt, discarding the first effect above.

The performance of transmission and diffuse reflectance measurements for the same clay nanocomposite recipes and operating conditions was evaluated. By means of chemometrics, a 7-parameter calibration model was developed for each, using the same off-line characterization data (from oscillatory small amplitude rheology, FTIR and a process-related thermomechanical index). Despite the higher variability of the diffuse reflectance signal due to scattering effects, both models exhibited similar high quality measures.

Chapter 4. In-line NIR spectroscopy: a tool to monitor the preparation of polymer-clay nanocomposites in extruders

When the diffuse reflectance probe was used for the real-time monitoring of the effect of feed rate on the dispersion level of the same nanocomposite, the non-linear effect measured off-line was readily detected.

4.6. References

1. S.S. Ray, M. Okamoto. Polymer/layered silicate nanocomposites: a review from preparation to processing. *Progress in Polymer Science* 28, p.1539-1641, (2003).
2. S. Pavlidou, C.D. Papaspyrides. A review on polymer-layered silicate nanocomposites. *Progress in Polymer Science* 33, p. 1119-1198, (2008).
3. W. Lertwimolnun, B. Vergnes. Influence of compatibilizer and processing conditions on the dispersion of nanoclay in a polymer matrix. *Polymer*. 46, p. 3462-3471, (2005).
4. W. Lertwimolnun, B. Vergnes. Effect of processing conditions on the formation of polypropylene/organoclay nanocomposites in a twin-screw extruder. *Polymer Engineering and Science* 46, p. 314-323, (2006)
5. W. Lertwimolnun, B. Vergnes. Influence of screw profile and extrusion conditions on the microstructure of polypropylene/organoclay nanocomposites. *Polymer Engineering and Science*. 47, p. 2100-2109, (2007).
6. A. Vermogen, K. Masenelli-Varlot, R. Séguéla, J. Duchet-Rumeau, S. Boucard, P. Prele. Evaluation of the structure and dispersion in polymer-layered silicate nanocomposites. *Macromolecules*. 38, p. 9661-9669, (2005).
7. M. Modesti, A. Lorenzetti, D. Bon, S. Besco. Effect of processing conditions on morphology and mechanical properties of compatibilized polypropylene nanocomposites. *Polymer* 46, p. 10237-10245, (2005).
8. S. Mould, J.M. Barbas, A.V. Machado, J.M. Nóbrega, J.A. Covas. Measuring the rheological properties of polymer melts with on-line rotational rheometry. *Polymer Testing*. 30, p. 602-610, (2011).
9. A. Durmus, A. Kasgoz, C.W. Macosko. Linear low density polyethylene (LLDPE)/clay nanocomposites. Part I: Structural characterization and quantifying clay dispersion by melt rheology. *Polymer*. 48, p. 4492-4502, (2007).
10. I. Alig, B. Steinhoff, D. Lellinger. Monitoring of polymer melt processing. *Measurement Science and Technology*. 21, p. 1-19, (2010).

Chapter 4. In-line NIR spectroscopy: a tool to monitor the preparation of polymer-clay nanocomposites in extruders

11. T.R. Rodd. Fiber-optic probes for near-infrared spectrometry. J.M. Chalmers, P.R. Griffiths (Eds.). Handbook of Vibration Spectroscopy, vol.2 – Sampling Techniques: John Willey & Sons Ltd, (2002).
12. J. D. Tate, P. Chauvel, R.D. Guenard, R. Harner. Process monitoring by mid- and near-infrared Fourier transform spectroscopy. J.M. Chalmers, P.R. Griffiths (Eds.). Handbook of Vibration Spectroscopy, vol.4 – Applications in Industry, Materials and the Physical Sciences: John Willey & Sons Ltd, (2002).
13. P.D. Coates, S.E. Barnes, M.G. Sibley, E.C. Brown, H.G. Edwards, I.J. Scowen. In-process vibrational spectroscopy and ultrasound measurements in polymer melt extrusion. *Polymer*. 44, p. 5937-5949, (2003).
14. G. George, N. Hynard, G. Cash, L. Rintoul, M. O'Shea. Spectroscopic probes for real-time monitoring of polymer modification and degradation reactions. *Comptes Rendus Chimie*. 9, p. 1433-1443, (2006)
15. M.G. Hansen, S. Vedula. In-line fiber-optic Near-Infrared spectroscopy: monitoring of rheological properties in an extrusion process. Part I. *Journal of Applied Polymer Science*. 68, p. 859-872, (1998)
16. T. Nagata, M. Oshima, M. Tanigaki. In-Line Monitoring of Polyethylene Density Using Near Infrared (NIR) Spectroscopy. *Polymer Engineering and Science*. 40, p. 1107-1113 (2000)
17. I. Alig, D. Fischer, D. Lellinger, B. Steinhoff. Combination of NIR, Raman, Ultrasonic and Dielectric spectroscopy for in-line monitoring of the extrusion process. *Macromolecular Symposia*. 230, p.51-58, (2005).
18. C. Barrès, V. Bounor-Legaré, F. Melis, A. Michel. In-line near infrared monitoring of esterification of a molten ethylene–vinyl alcohol copolymer in a twin screw extruder. *Polymer Engineering and Science*. 46, p. 1613-1624, (2006).
19. S.E. Barnes, M.G. Sibley, H.G. Edwards, P.D. Coates. Process monitoring of polymer melts using in-line spectroscopy. *Transactions of the Institute of Measurement and Control*. 29, p.453-465, (2007).

Chapter 4. In-line NIR spectroscopy: a tool to monitor the preparation of polymer-clay nanocomposites in extruders

20. T. Rohe, S. Kölle, C. Stern, N. Eisenreich. In-line near infrared (NIR) spectroscopy for application in polymer extrusion processes. *Recent Research Developments in Pure & Applied Analytical Chemistry*. 3, p. 13-26 (2001)
21. L. Moghaddam, D.J. Martin, P.J. Halley, P.M. Fredericks. Vibrational spectroscopic studies of laboratory scale polymer melt processing: Application to a thermoplastic polyurethane nanocomposite. *Vibrational Spectroscopy*. 51, p. 86-92, (2009).
22. A. Witschnigg, S. Laske, M. Kracalik, M. Feuchter, G. Pinter, G. Maier, W. Märzinger, M. Haberkorn, G.R. Langecker, C. Holzer. In-line characterization of polypropylene nanocomposites using FT-NIR. *Journal of Applied Polymer Science*. 117, p. 3047-3053, (2010)
23. D. Fischer, J. Müller, S. Kummer, B. Kretzschmar. Real time monitoring of morphologic and mechanical properties of polymer nanocomposites during extrusion by near infrared and ultrasonic spectroscopy. *Macromolecular Symposia*. 35, p. 10-17, (2011).
24. J.M. Barbas, A.V. Machado, J.A. Covas. In-line Near-Infrared spectroscopy for the characterization of dispersion in polymer-clay nanocomposites. *Polymer Testing* 31, p. 527-536, (2012)
25. A.V. Machado, J.A. Covas, M. van Duin. Evolution of morphology and of chemical conversion along the screw in a corotating twin-screw extruder. *Journal of Applied Polymer Science* 71, p. 135-141, (1999)
26. P. Cassagnau. Melt-rheology of organoclay and fumed silica nanocomposites. *Polymer*. 49, p. 2183-2196, (2008).
27. R. Krishnamoorti, E.P. Giannelis. Rheology of end-tethered polymer silicate nanocomposites. *Macromolecules* 30, p. 4097-4102, (1997)
28. K.C. Cole. Use of Infrared spectroscopy to characterize clay intercalation and exfoliation in polymer nanocomposites. *Macromolecules*. 41, p. 834-843, (2008).
29. L. Yan, C.B. Roth, P.F. Low. Changes in the Si-O vibrations of smectite layers accompanying the sorption of interlayer water. *Langmuir*. 12, p. 4421-4429, (1996)
30. D.A. Burns, E.W. Ciurczak (Eds.). *Handbook of Near-Infrared Analysis*. CRC Press, USA (2008).

Chapter 4. In-line NIR spectroscopy: a tool to monitor the preparation of polymer-clay nanocomposites in extruders

31. D. Xiang, R. LoBrutto, J. Cheney, B.W. Wabuye, J. Berry, R. Lyon, H. Wu, M.A. Khan, A.S. Hussain. Evaluation of transmission and reflection modalities for measuring content uniformity of pharmaceutical tablets with Near-Infrared Spectroscopy. *Applied Spectroscopy* 63, p. 33-47, (2009)
32. M. Saeed, L. Probst, G. Betz. Assessment of diffuse transmission and reflection modes in Near-Infrared quantification, Part 2: Diffuse reflection information depth. *Journal of Pharmaceutical Sciences*. 100, p. 1130-1140, (2011)
33. K. Kohlgruber. Co-rotating twin-screw extruders: Fundamentals, technology and applications. Carl Hanser Verlag, Germany (2008)
34. J. Madejová, M. Pentrák, H. Pálková, P. Komadel. Near-infrared spectroscopy: A powerful tool in studies of acid-treated clay minerals. *Vibrational Spectroscopy* 49, p. 211-218, (2009)
35. O. Dumitrescu, D.C. Baker, G.M. Foster, K.M. Evans. Near infrared spectroscopy for in-line monitoring during injection moulding. *Polymer Testing* 24, p. 367-375, (2005)

THE EVOLUTION OF DISPERSION ALONG THE EXTRUDER DURING THE MANUFACTURE OF POLYMER-ORGANOCLAY NANOCOMPOSITES

5

For polymer-clay nanocomposites the relation between clay dispersion and processing conditions is still vague. The possibility of monitoring the dispersion the extruder axis upon compounding provides a better understanding of the mechanism, enabling faster and proper actions of process optimization. This work uses both on-line rheometry and in-line near-infrared spectroscopy (NIR) for monitoring the evolution of dispersion of a PP/PP-g-MA/D67G system along the twin screw extruder axis. For the second half of the extruder length, the on-line rheology shows a pronounced decrease of the viscoelastic response, while in-line NIR shows the effects of decreasing light scattering interferences. Process monitoring was complemented by adequate off-line characterization and the overall results show a reversion of the clay dispersion, which has been attributed to the effect of degradation of the clay surfactant and of the polymer matrix.

5.1. Introduction

Mixing a small amount (typically less than 5 wt.%) of clay particles with a thermoplastic polymer matrix is often performed directly in the melt, due to effectiveness of the intercalation – exfoliation levels attained [1 – 4] and the suitability of this route for industrial scale production [2 – 3]. Many authors investigated the effects of the molecular weight of the matrix [5 – 7], the chemical affinity of the polymer-clay interface [7 – 9] and the compatibilizer/clay ratio [10 – 12] on the dispersion and properties of the resulting nanocomposites. It also became evident that the type of mixer, the mixing protocol [2 – 3, 13 – 14], as well as the operating conditions [3, 15 – 17] strongly influence the dispersion levels attained and, therefore, the properties. A balance between mechanical shear and residence time is required to achieve proper dispersion [2 – 3, 11, 13, 15, 17]. Lertwimolnun and Vergnes [15] showed that although the extrusion conditions (screw speed, feed rate and temperature) have little impact on intercalation, they influence the final exfoliation levels, which is favoured by high screw speeds (N) and low feed rates (Q).

Clay dispersion in the polymer melt combines the diffusion of the polymer chains within the clay interlayer spacing (intercalation) and the delamination of the individual platelets (exfoliation) due to the application of mechanical stresses, followed by their diffusion into the melt [3, 11]. The role of the process parameters on the onset and kinetics of these steps has been the subject of debate. Bousmina [11] coupled an X-Ray instrument to a rotational rheometer and showed that the diffusion of the polymeric chains inside the clay galleries is best obtained under mild shearing conditions (or in a medium to low viscosity matrix) applied during sufficient time, whereas extensive exfoliation requires a high level of shearing/deformation. Understandably, the evolution of clay dispersion along the axis of an extruder, where a complex non-isothermal 3D flow develops, seems less well understood. Using oscillatory rheometry and X-ray diffraction, Lertwimolnun and Vergnes [15, 17] characterized post-mortem samples collected from various locations along a co-rotating twin screw machine. Based upon previously proposed correlations between the rheological response and the dispersion of nanocomposites, they concluded that both intercalation and exfoliation could reach relatively high levels immediately after melting. They also observed that less restrictive screw profiles yielded better dispersion levels. Furthermore, depending on the combination of screw profile and operating conditions, dispersion could develop, remain constant, or apparently revert along the

Chapter 5. The evolution of dispersion along the extruder during the manufacture of polymer-organoclay nanocomposites

screw axis, the latter being attributed to matrix degradation, even if no experimental evidence of the latter was provided.

Although these phenomena do not jeopardize the well established global correlations between processing conditions and final dispersion levels, they make more difficult practical process set-up, optimization and scale-up. The experimental procedure adopted by Lertwimolnun and Vergnes [17] is complex and time consuming, and may eventually induce thermal degradation and/or morphology changes during material collection and sample preparation (e.g., compression moulding of the post-mortem samples into disks, followed by re-heating prior to rheological testing). Therefore, the use of on-line or in-line monitoring techniques to follow the evolution of clay dispersion along the extruder axis seems particularly useful.

The authors have developed, and validated, a prototype on-line oscillatory rheometer [20], which when operated in small amplitude oscillatory shear (SAOS) mode, is capable of measuring rheological parameters such as the storage and loss moduli, G' , G'' , and melt yield stress, σ_0 , which have been correlated with the degree of dispersion by several authors [7 – 8, 15, 17, 31 – 32]. The device was able to discriminate the rheological response of a Polypropylene/Polypropylene grafted with Maleic Anhydride/Organo-Montmorillonite (PP/PP-g-MA/D67G) composite at several locations along the extruder [20].

An in-line Near-Infrared (NIR) spectroscopy set-up using a reflection probe has also been made available. Using adequate chemometrics, the absorbance spectra acquired could be related to the level of dispersion via a 7-parameter model, which combines four rheological parameters (G' , G'' , melt yield stress and power law index), two medium Fourier transformed-Infrared spectroscopy (FT-IR) parameters (wavenumber shifts for the peaks at 1050 cm^{-1} and 1080 cm^{-1} , usually associated to intercalation and exfoliation respectively [26 – 28]) and a thermomechanical index related to the mechanical energy input to the system (specific mechanical energy) [24]. The probe was used for the real-time in-line monitoring of the preparation of a PP/PP-g-MA/D67G system in a twin-screw extruder under different throughputs, the results correlating well with the experimental off-line characterization measurements.

Thus, on-line rheometry and in-line NIR can be used to characterize samples collected at several locations along the extruder during normal process operation, avoiding subjecting the material to

Chapter 5. The evolution of dispersion along the extruder during the manufacture of polymer-organoclay nanocomposites

subsequent thermal cycles and, therefore, eliminating one of the possible causes that could explain the apparent reversal of dispersion. This work uses these two techniques to monitor the evolution along the extruder of the dispersion of a PP/PP-g-MA/D67G system. Three screw profiles with distinct restrictive character are used, under constant processing conditions. In order to better understand the results obtained the morphology of the nanocomposites is observed via scanning transmission electron microscopy (STEM), and the thermal stability of the system is analysed by thermal gravimetric analysis (TGA). Reversibility of intercalation was observed in the downstream region of the extruder, having apparently been originated by the degradation of the organoclay surfactant.

5.2. Experimental

5.2.1. Materials

The materials used are identified in Table 5. 1. They include an injection moulding grade Polypropylene (PP), a Polypropylene grafted with Maleic Anhydride (PP-g-MA) to function as compatibilizer and Dellite 67G (D67G), a natural montmorillonite clay modified with dimethyl dihydrogenated tallow quaternary ammonium salt (2M2HT). It has a cation exchange capacity of 115 meq/100 g and the dry particle sizes are between 20 and 40 μm [25]. The PP/PP-g-MA/D67G composition was kept constant at 90/5/5 % in weight. The organoclay was dried overnight in a vacuum oven at 80 °C, before compounding.

Table 5. 1. Materials used in the work.

Material	Acronym	Producer	Grade	MFI/lamellar distance
Polypropylene	PP	Lyondell Basell	Moplen HP500N	12 g/10 min (230 °C/2.16 kg)
Compatibilizer	PP-g-MA	Crompton	Polybond 3200	115 g/10 min (190 °C/2.16 kg)
Montmorillonite clay	D67G	Laviosa	Dellite 67G	$d_{001} = 3.70 \text{ nm}$

Chapter 5. The evolution of dispersion along the extruder during the manufacture of polymer-organoclay nanocomposites

5.2.2. Preparation of the nanocomposites

The nanocomposites were prepared in a Leistritz LSM 30.34 modular co-rotating intermeshing twin-screw extruder, under fixed operating conditions (100 rpm, 3 kg/h and uniform barrel/die temperature set to 200 °C). The extruder layout is shown in Figure 5. 1.

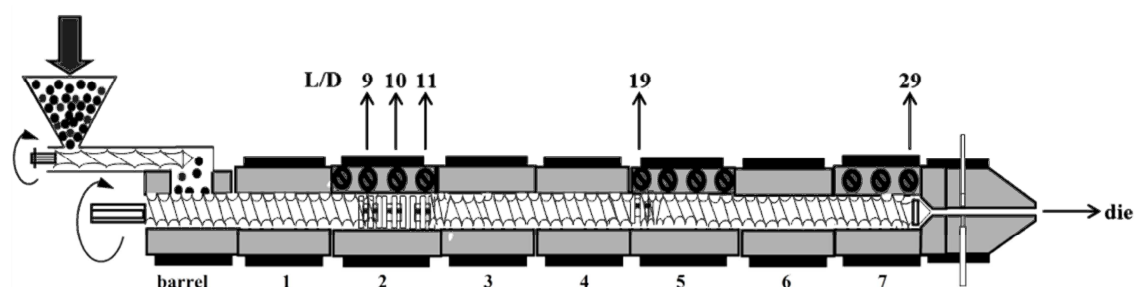


Figure 5. 1. Layout of the twin-screw extruder.

Three screw profiles (coded as SC1, SC2 and SC3) were utilized. Their construction is presented in Table 5. 2, where $xxRy$ denotes a conveying element (xx being the pitch (mm) and $R=120/y$ being the length (mm)), $xxKDy^\circ$ is a kneading block (xx is the number of individual discs (KD) and y° is their staggering angle) and $xxRyL$ is a left-handed element (L standing for the pitch (mm)). Each screw contains two mixing blocks in between arrays of conveying elements. The geometries differ in the configuration of the mixing block upstream, where polymer melting and a varying degree of clay intercalation and exfoliation are expected to take place. SC1 and SC3 contain 13 disks followed by a left handed element, while the latter is not present in SC2. In the case of SC1, the first 4 disks are staggered positively, the following 5 are neutral and the last four are staggered negatively. Thus, this geometry should gradually create higher hydrodynamic stresses. The mixing block of SC2 is highly restrictive, but it does not include a left handed element. SC3 consists of 13 disks staggered at 90° (this geometry being usually associated to distributive mixing) followed by a left handed element. The extruder was fitted with modified barrel segments (Figure 5. 1 – barrel segments 2, 5 and 7) designed to allow for material sampling and/or on-line measurements, as explained in more detail below. The use of sample collecting devices made possible a local visual check of the presence of solid vs. molten material, operation under full vs. partial channel filling, the measurement of the

Chapter 5. The evolution of dispersion along the extruder during the manufacture of polymer-organoclay nanocomposites

average melt temperature (by sticking a fast response thermocouple in the freshly collected melt) and an estimation of the minimum residence time (by counting the time elapsed between feeding a pigment tracer into the screws and identifying a local colour change in the melt stream).

Table 5. 2. Screw profiles used in the preparation of the PP/PP-g-MA/D67G nanocomposites.

Screw Profile	1	60R/60R4/45R2/30R2/4KD+60°/5KD90°/4KD-60°/30R4L/30R/30R4/20R2/6KD90°/20R4L/45R/30R/30R2
	2	60R/60R4/45R2/30R2/13KD-30°/20R4/30R/30R4/20R2/6KD90°/20R4L/45R/30R/30R2
	3	60R/60R4/45R2/30R2/13KD90°/30R4L/30R/30R4/20R2/6KD90°/20R4L/45R/30R/30R2

As seen in Table 5. 3, up to $L/D=11$ (this location corresponds approximately to the downstream edge of the mixing blocks for SC1 and SC3 – see also Figure 5. 1, that of SC2 being shorter), differences in the rate of melting, melt temperature and residence time are more notorious, then fading towards the die exit. As expected, melting is delayed in screw SC1 and so is melt temperature build up. Local and global residence times seem higher. Conversely, SC2 melts the polymer quickly and causes significant melt temperature raise. Since its upstream mixing block is shorter, the screws work partially filled at $L/D=11$ and melt temperature and residence times measurements were not feasible. SC3 seems to induce the same melting as SC2, but the melt temperatures up to $L/D=11$ are lower (but higher than those for SC1). Therefore, SC1, SC2 and SC3 should create distinct thermomechanical stresses, and thus influence the diffusion and shearing processes.

Chapter 5. The evolution of dispersion along the extruder during the manufacture of polymer-organoclay nanocomposites

Table 5. 3. Process monitoring parameters registered during compounding with the different screw profiles.

	Melt Temperature (°C)						Residence time (s)		SME (A.Kg.h ⁻¹)
	L/D 9	L/D 10	L/D 11	L/D 19	L/D 29	die	L/D 11	die	
SC1	(a)	194.0 ± 0.6	198.2 ±1.4	204.9 ±0.8	198.9 ±0.5	207.9 ±0.4	27 ± 2.0	138 ± 3.0	3.00
SC2	198.7 ±0.4	202.6 ± 0.5	(b)	207.8 ±0.3	199.1 ±0.4	212.0 ±0.3	(b)	149 ± 2.6	2.78
SC3	189.4 ±0.3	198.5 ± 0.2	203.8 ±1.3	208.9 ±0.2	200.2 ±0.3	211.9 ±0.4	23.7 ± 0.6	148.7 ± 2.1	2.89

(a) Melting is not completed

(b) Partially filled screw channels

5.2.3. Sample collection and On-line/In-line Monitoring

At each sampling location identified in Figure 5. 1, material from the plasticating chamber can flow outwards through lateral channels machined in the barrel wall. A rotating valve can divert the sample to a chamber for sample collection (or temperature measurement), or to the on-line rheometer.

The on-line rheometer prototype set-up uses a DSR301 rheometer head (Anton Paar) and has been validated and described in detail elsewhere [20]. When measurements are to be performed, the rotating valve is actuated to divert melt from within the extruder into the measuring chamber at low shear rate, in order to avoid any changes in morphology upon collection. The temperature inside the test chamber is controlled by means of a thermocouple embedded in the lower plate. Sample collection takes about 30 seconds, corresponding to a cycle of purging, collection and setting the gap, followed by thermal stabilization at the test temperature. The measurements were performed at L/D = 9, 10, 11 and 19 (see Figure 5. 1). They consisted of isothermal (at 200 °C) frequency sweeps from 0.1 to 100 rad/s, using parallel plates with a diameter of 20 mm and a 1 mm gap, under a constant strain (1 % for the PP matrix and 0.5 % for the nanocomposites).

A NIR spectroscopy Diffuse Reflectance (DR) probe for polymer extruders (from Hellma Analytics) having a sapphire window (with a diameter of 5.7 mm, for an illuminated area with a diameter of 2 mm and a field depth of 3 mm) was directly fixed to the extruder at L/D = 9, 10, 11, 19, 29 and die

Chapter 5. The evolution of dispersion along the extruder during the manufacture of polymer-organoclay nanocomposites

by a Dynisco-type thread. The probe contacts directly the melt stream, no modifications to the extruder or die being necessary. The connection with the NIR spectrometer (Matrix F, Bruker Optics) is made by fibre optic cables (the illumination cable has 7 fibres with 400 μm core diameter, whilst the detection cable has a single fibre with 600 μm core diameter). The NIR spectra were measured from 12000 – 4500 cm^{-1} with a resolution of 8 cm^{-1} and accumulation of 4 scans, the acquisition time for each spectrum being approximately 2 seconds. The background signal is acquired prior to installation, using a *Spectralon*[®] diffuse reflection standard target (Bruker Optics) with a reflectivity index of 99 %. At each location, a total of 50 spectra were measured during regular intervals of continuous extrusion runs. The NIR spectra discussed throughout this work are averages of these, without performing any further processing or signal correction.

5.2.4. Off-line Characterization of the Composites

Medium FT-IR

The FT-IR analyses were performed with a spectrometer FTIR-4100 (Jasco). The organoclay was analysed with a KBr mortar. The nanocomposite samples were compression moulded at 200 °C into $\pm 75 \mu\text{m}$ thick films and analysed in transmission mode, in the 4000 – 500 cm^{-1} wavenumber range with a resolution of 4 cm^{-1} , using 32 scans. To eliminate interferences due to preferential orientation of the clays [26 – 28], the beam was polarized using a KRS-5 grid polarizer lens (SPECAC). At least 3 films were analysed per sample. The wavenumber accuracy and repeatability of the instrument were checked prior to the measurement and the procedure is described elsewhere [24]. Fitting of the Si-O band region (between 1250 and 750 cm^{-1}) [27– 28] for the determination of the wavenumber shift for the 1050 cm^{-1} (Si-O in-plane) and 1080 cm^{-1} (Si-O out-of-plane) peaks is described elsewhere [23 – 24].

Chapter 5. The evolution of dispersion along the extruder during the manufacture of polymer-organoclay nanocomposites

Electron Microscopy

Scanning transmitted electron microscopy (STEM) observations of the composites were performed with a NanoSEM Nova200 (Fei), using an acceleration voltage of 15kV. Ultra-thin sections (± 80 nm) were cut, under cryogenic conditions (-60 °C) from samples collected from the extruder using the UC6 ultra-microtome (Leica) equipped with a diamond knife.

Thermal Gravimetric Analysis

Thermal gravimetric analysis (TGA) of the organoclay (D67G), polymer matrix (PP/PP-g-MA 95/5wt.%) and nanocomposites were carried out on a Q500 (TA Instruments) under different conditions. Dynamic tests were used a heating rate of 10 °C/min from 50 to 650 °C under a constant flow of nitrogen (60 ml/min).

The clay and matrix were also subjected to isothermal tests at 150° and 200 °C (set processing temperature) for 10 min, under a constant flow of nitrogen (60 ml/min).

Color Measurements

Measurements were used with a Datacolor 400™ colorimeter (Datacolor), using an illuminated spot with a diameter of 6.6 mm. Colour levels were measured using compression moulded disks with a diameter of 25 mm and a thickness of 1 mm. All samples were measured against a white background standard, including the reference sample (extruded polypropylene) to minimize transparency effects. The CIELAB colour coordinates, L^* for darkness and b^* for yellowness, were registered according to the procedure described in the ASTM E313 standard test method. Three replicas were used for each sample.

5.3. Results and discussion

5.3.1. Evolution of clay dispersion

Several authors [7 – 8, 15, 21 – 22, 31 – 32] used the rheological response of polymer-clay nanocomposites (usually performed in SAOS mode) and established correlations with the state of dispersion of the organoclay. The increase of the storage (G') and loss (G'') moduli has been related to a finer dispersion [7 – 8, 31 – 32], providing a good perception of the quality of dispersion. Also, the formation of a plateau at low frequencies has been attributed to the deformation and recovery of the dispersed particles [7, 8, 22, 31 – 32]. Lertwimolnun and Vergnes [15, 17] used a modified Carreau-Yasuda model with yield stress (σ_0 – equation 5. 1) to describe the frequency (ω) dependence of the absolute complex viscosity (η^*) and successfully related this with the exfoliation level.

$$|\eta^*(\omega)| = \frac{\sigma_0}{\omega} + \eta_0 [1 + \lambda \omega^a]^{(b-1)/a} \quad (5. 1)$$

Other studies used a power law expression to describe the complex viscosity behavior at low frequency and correlated the exponent (b – equation 5. 2) with the state of clay dispersion [21 – 22].

$$|\eta^*(\omega)| = A\omega^b \quad (5. 2)$$

According to the correlations previously established, Figure 5. 2 and 5. 3 show the curves of the complex viscosity and storage modulus measured during isothermal frequency sweeps, using the on-line rheometer. The prepared nanocomposites exhibit higher viscoelastic response than the respective matrix. Also, it is visible for all G' curves, the formation of a plateau at lower frequencies, suggesting the existence of a 3D structure typical of this type of materials [2, 7 – 8, 22, 31 – 32]. The material prepared with SC1 (Fig. 5. 2(a) and 5. 3(a)) shows minor differences between L/D 10 and L/D 19, however at L/D 11 the rheological behaviour is slightly higher. Figures 5. 2(b) and 5. 3(b) show that along the first kneading block, the material prepared with SC2 exhibits a pronounce solid-like behaviour (curve slope close to 1), typical of a well dispersed nanocomposite. However at L/D 19 a pronounce decrease of the rheological response indicates reversion of the dispersion.

Chapter 5. The evolution of dispersion along the extruder during the manufacture of polymer-organoclay nanocomposites

Using SC3 (Fig. 5. 2(c) and 5. 3(c)) the viscoelastic behaviour increases until L/D 19, suggesting a steady evolution of the dispersion levels along the extruder.

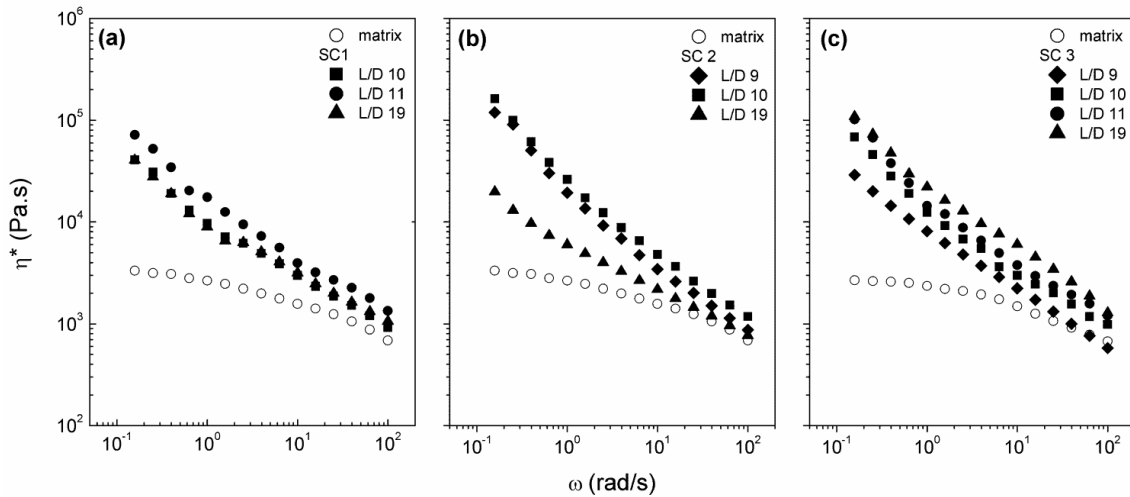


Figure 5. 2. Complex viscosity (η^*) over frequency at different locations for all screw profiles used: (a) SC 1, (b) SC 2 and (c) SC 3.

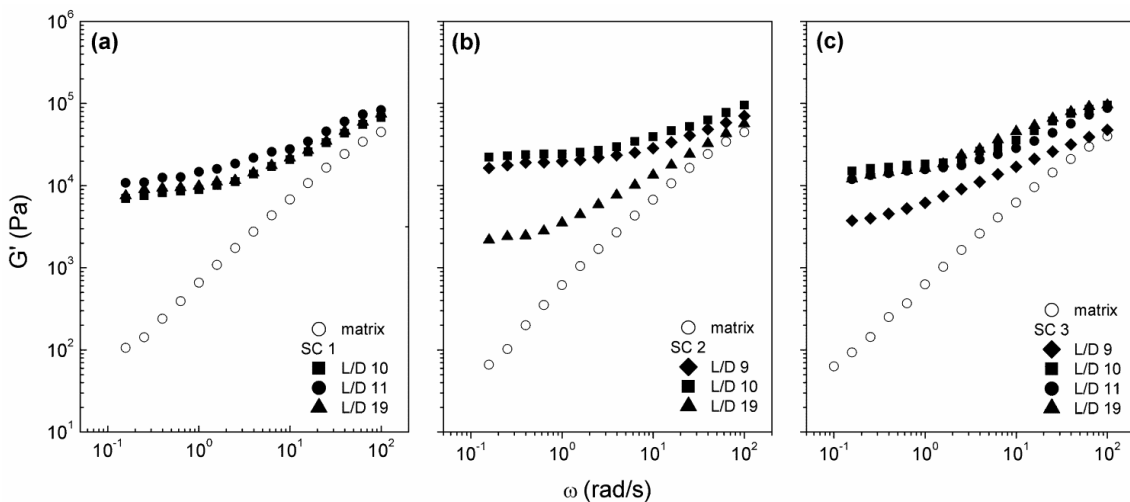


Figure 5. 3. Storage modulus (G') over frequency at different locations for all screw profiles used: (a) SC 1, (b) SC 2 and (c) SC 3.

Figure 5. 4 shows in more detail the evolution of the rheological behaviour along the extruder. Specifically Figure 5. 4(a) depicts the low frequency values of G' and Figure 5. 4(b) shows the calculated values of the melt yield stress. The fitting of the complex viscosity curves to the modified

Chapter 5. The evolution of dispersion along the extruder during the manufacture of polymer-organoclay nanocomposites

Carreau-Yasuda model is described elsewhere [15, 17, 24]. Both rheological parameters show that the dispersion levels are higher at the end of the first kneading block (L/D 11), after which a more or less pronounced reversion is detected. SC1 shows increase of G' and yield stress from L/D 10 to 11; downstream, at L/D 19 the values are slightly lower, particularly the melt yield stress, suggesting a decrease of the exfoliation. Along the first mixing zone SC2 exhibits higher values of G' and melt yield stress than the remaining configurations. However beyond L/D 11 both parameters exhibit a sudden drop. Rheologically, SC3 appears as the most favourable screw configuration. According to Lertwimolnun and Vergnes [15, 17] the melt yield stress is related to the degree of exfoliation, and SC3 shows a steady increase of the melt yield stress between L/D 9 and L/D 11, beyond which it remains approximately constant. Curiously, SC1 and SC3 present similar G' responses at L/D 11 and L/D 19, but the melt yield stress values set these profiles apart, suggesting that lower levels of exfoliation are attained with SC1. The meaning of this sudden decrease of the rheological behaviour at locations downstream L/D 11 is not clear yet. However, identical results were obtained by off-line rheometry measurements (not shown). These results are not entirely unexpected, since Lertwimolnun and Vergnes [34] have reported the reversion of dispersion along the extruder, which was attributed to degradation of the polymer matrix. However, the decrease of the viscoelastic response of polymer-clay nanocomposites has also been attributed to other factors. Fornes et al [5] suggested that the decrease of the rheological properties may be related to higher levels of exfoliation and decrease of particles sizes. The authors explain that the platelets on a nanometer scale can be easily aligned under flow, resulting in a negligible contribution of the solid particulates to the viscoelastic behaviour of polymer-clay nanocomposites, which can occur even during small amplitude oscillatory shear experiments [32, 34]. This relates to an earlier work by Vaia et al [1] claiming that the initially randomly and misaligned structure of the nanocomposite, can become oriented and organized exhibiting a liquid-like behaviour due to the lubrication effects of the clay particles, which can be compared to those of sliding disks. Kim et al [6] concluded that the diffusion of the polymer chains into the gallery of the silicate is a major factor for occurring delamination. When exfoliation increases less intercalated stacks remain, justifying the decrease of the rheological properties.

Chapter 5. The evolution of dispersion along the extruder during the manufacture of polymer-organoclay nanocomposites

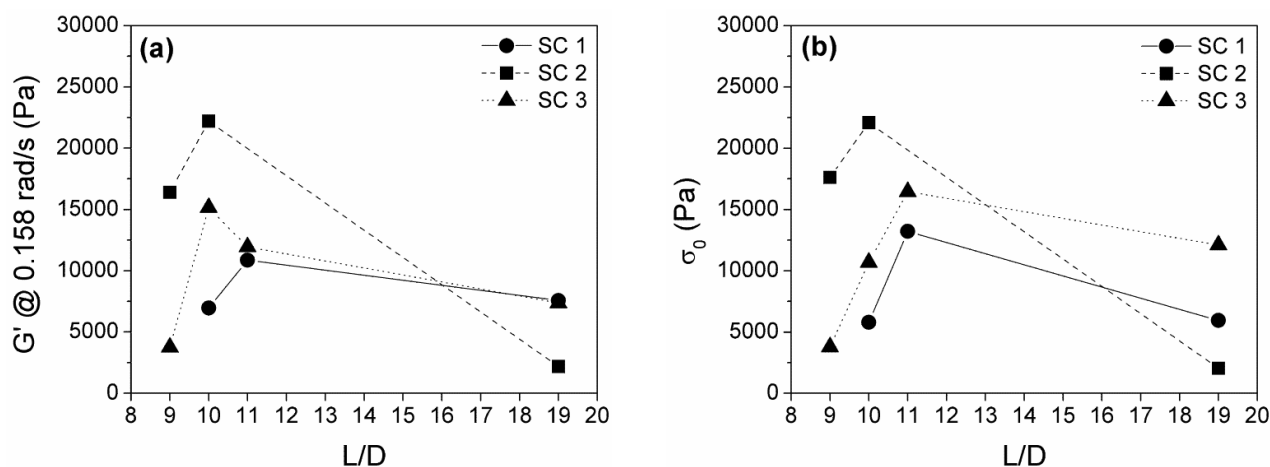


Figure 5. 4. On-line rheometry data along the extruder: (a) storage modulus (G') at 0.158 rad/s; (b) calculated melt yield stress.

In-line NIR spectroscopy was used simultaneously with on-line rheometry, but it enabled measurements in locations where using the rheometer was not feasible. Figure 5 displays the average NIR spectra for each extruder position, without further signal corrections, and the only differences detected are related to the baseline shifts. The shift of the baseline in reflection mode can be associated with the quality of dispersion [24, 33]. The increase of dispersion generates a larger number of particles (clay stacks and/or individual platelets) with smaller sizes and higher inter-lamellar distance [24], which enhances the light scattering effects causing the baseline off-set to higher values.

For SC1 (Figure 5. 5(a)) rising of the NIR baseline is detected between L/D 9 and L/D 11. Beyond L/D 11 the baseline consistently drops until the die exit. SC2 (Figure 5(b)) spectra show minor differences between L/D 9 and L/D 29, but a pronounced decrease of the spectra baseline occurs at the die. SC3 (Figure 5. 5(c)) shows an increase of the spectra baseline until L/D 19, yet again reversion occurs at L/D 29. The increase of dispersion, along the first half of the extruder, originates a larger volume of smaller particles that enhance light scattering thus the baseline offsets to higher values. Along the second half of the extruder the baseline decreases noticeably. Overall, the evolutions detected by in-line NIR are in agreement with the ones found by on-line rheometry.

Chapter 5. The evolution of dispersion along the extruder during the manufacture of polymer-organoclay nanocomposites

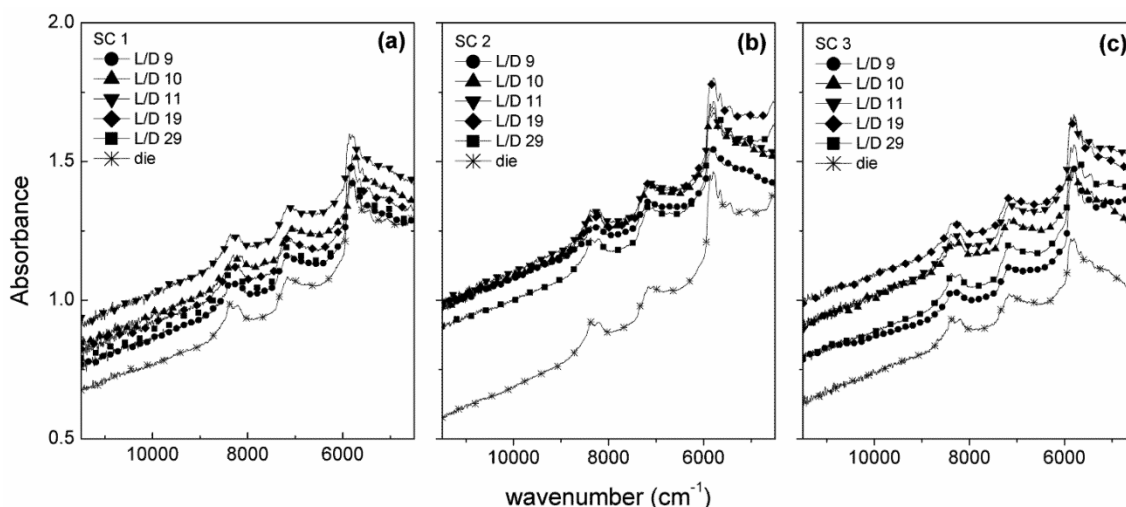


Figure 5. 5. NIR spectra along the extruder barrel for all screw profiles used: (a) SC 1, (b) SC 2 and (c) SC 3.

However, NIR enables also a quantitative assessment of the clay dispersion in real-time. This is done by means of a chemometric model, relating the spectral differences and reference parameters often used to describe the clay dispersion. The model encompasses 7 parameters derived from oscillatory rheometry (G' , G'' , σ_0 , b), FT-IR (wavenumber shift of the peaks at 1050 and 1080 cm^{-1}) and a process-related thermomechanical index, specifically the specific mechanical energy (SME) [23 – 24]. The model used here, was previously developed [24] to study the effect of throughput at the end of the first mixing zone (L/D 11), the calibration samples, having different levels of dispersion, were obtained by varying the clay loading, the compatibilizer content and the screw speed. The quality of the NIR predictions is assessed by the Root Mean Square Error of Prediction (RMSEP) and the bias. The statistical meaning, calculations and acceptance limits of these quality factors are explained elsewhere [23 – 24]. Although it is well-known that chemometric models should not be extended to conditions laying outside the calibration range, this model is applied here because the different constructions of the first mixing zone are expected to influence the hydrodynamic stresses, residence times and viscous dissipation effects, generating similar effects as screw speed and throughput variations.

The NIR predictions of the relative degree of dispersion are shown in Figure 5. 6, plotted as function of the extruder location, and listed in Table 5. 4 with the respective errors and quality parameters (RMSEP and bias). As it was anticipated, some of the locations yield higher degree of dispersion

Chapter 5. The evolution of dispersion along the extruder during the manufacture of polymer-organoclay nanocomposites

than the ones previously obtained at L/D 11 [24], therefore these extrapolated values have higher associated error, yielding higher global errors of prediction (RMSEP) and higher bias values. In spite of this, the NIR predictions of the relative degree of dispersion match well the on-line rheometry results.

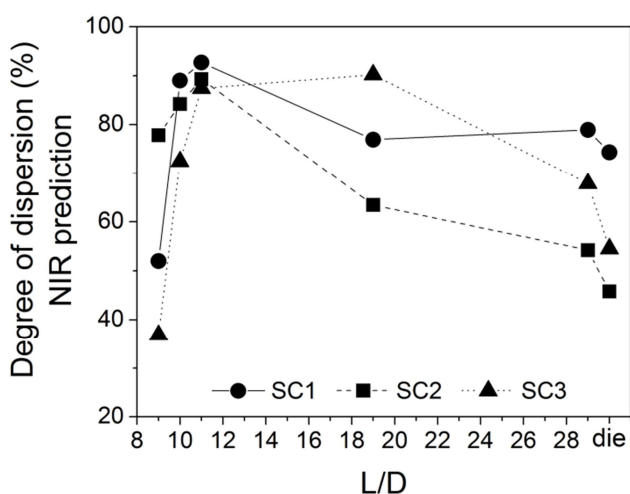


Figure 5. 6. NIR real-time predictions of the degree of dispersion for the different screw profiles used.

Table 5. 4. NIR real-time predictions of the degree of dispersion of the nanocomposites prepared using different screw geometries.

	<i>Relative degree of dispersion (\pm error) –%</i>		
	SC1	SC2	SC3
L/D 9	52.0 \pm 2.1	77.8 \pm 3.2	36.9 \pm 1.1
L/D 10	89.0 \pm 6.5	84.2 \pm 5.7	72.4 \pm 1.1
L/D 11	92.7 \pm 14.3	89.3 \pm 6.2	87.4 \pm 10.5
L/D 19	76.9 \pm 2.1	63.4 \pm 2.1	90.2 \pm 18.6
L/D 29	78.9 \pm 1.4	54.2 \pm 2.7	67.8 \pm 2.3
die	74.3 \pm 1.8	45.8 \pm 1.6	54.5 \pm 2.1
RMSEP (%)	14.1	5.1	15.6
bias	5.1	1.1	5.8

Chapter 5. The evolution of dispersion along the extruder during the manufacture of polymer-organoclay nanocomposites

Table 5. 4 confirms that for all screw profiles dispersion evolves fast along the first mixing zone (L/D 9 – L/D 11) and beyond L/D 11 it remains constant or reverts. For SC1, dispersion increases about 40% between L/D 9 and L/D 11, at L/D 19 dispersion is slightly lower but remains constant until the die exit. Using SC2 at L/D 9 the dispersion levels are higher than for SC1, and increase further (circa 12 %) until L/D 11, beyond which the values decrease to levels that are lower than the initial ones. With SC3 dispersion is apparently delayed and the value at L/D 9 is lower than for the other 2 profiles, dispersion continues to increase until L/D 19. At L/D 29 and die exit a significant reversion (about 35 %) is detected.

Overall, the results suggest the existence of an intermediate structure (intercalated with some level of exfoliation) for most of the analysed samples, which is common for polymer-clay nanocomposites prepared by melt-mixing [2 – 3, 11, 15, 17].

On-line rheology and in-line NIR indicate that a more or less pronounced reversion of dispersion occurs along the second half of the extruder (beyond L/D 11), which can be attributed to coalescence of the clay particles and/or degradation of the polymer matrix. Also, because NIR is a spectroscopic technique the results are sensitive to orientation effects, so it is reasonable to assume the existence of orientational interferences due to the trichroic nature of the clay [27 – 28].

5.3.2. Towards a dispersion model

Thus far, both on-line rheometry and in-line NIR indicate a marked reversion of dispersion after L/D 11, for all screw profiles tested. Some theories can be considered for this reversion:

- the unstable thermodynamics of the structure developed causes the clay particles to coalesce under the less intensive flow taking place downstream of the first mixing zone;
- the organoclay surfactant degrades due to excessive temperature, causing the interface clay-polymer to be less favourable thus explaining the collapse or re-agglomeration of the clay particles;
- the polymer matrix suffers the effects of thermo-oxidative degradation, resulting in lower viscosity due to chain scission;

Chapter 5. The evolution of dispersion along the extruder during the manufacture of polymer-organoclay nanocomposites

- possible orientation of the dispersed phase within the matrix causing the decrease of the viscoelastic response.

Because the viscoelastic response includes the effects of dispersion, chemical affinity and thermal stability, and the direct analysis of the NIR spectra does not provide enough chemical information on the effects of degradation, some off-line characterization was necessary, to better explain the obtained results.

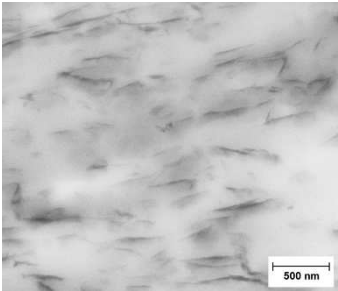
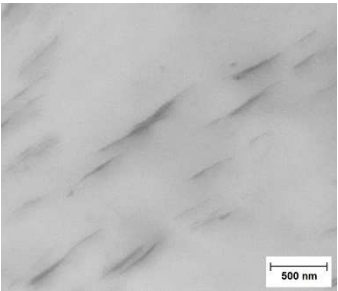
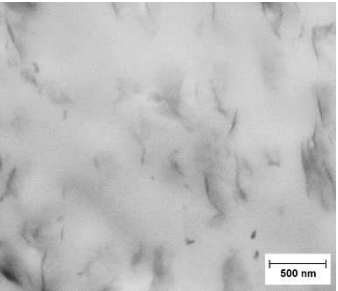
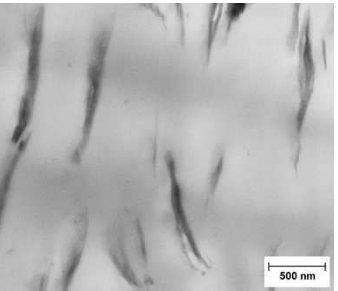
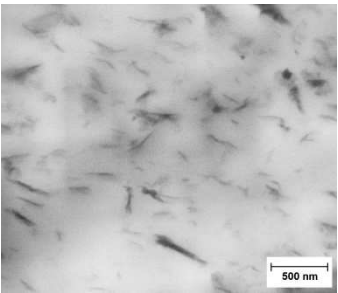
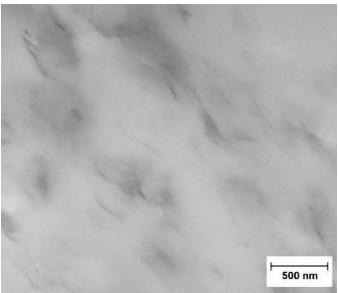
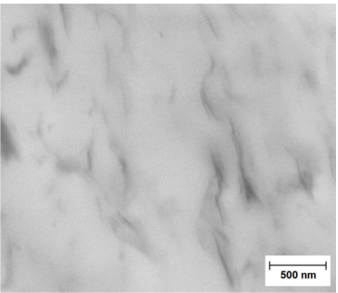
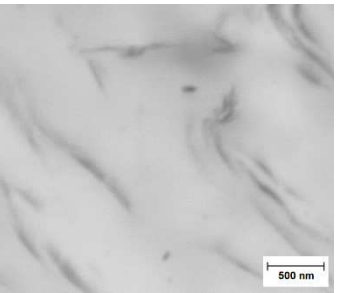
STEM was used for observation of the nanocomposites structure, providing a qualitative evaluation of the clay dispersion. Table 5. 5 shows the attained micrographs where the darker areas are the clay particles. Only the samples of the nanocomposites prepared with SC1 and SC2 were analysed, because they include the two types of dispersion evolution detected, increasing along the first mixing zone, followed by stabilization (SC1) or reversion (SC2). In both cases, dispersion develops between L/D 10 and L/D 19. Dispersion in the first mixing zone is identical for both screw profiles. At L/D 19 the dispersion of SC2 is seemingly better, as the blurred appearance of the image suggests the presence of more clay particles with smaller sizes. Downstream, at L/D 29, the filler appears to re-aggregate and both screw profiles present analogous dispersion levels. However at the die exit, the clay particles size is larger for SC1.

In addition, some level of orientation exists at L/D 19 and at the die, confirmed by the alignment of the clay particles. At L/D 19 samples are being collected from a kneading block, where the non-parallel flow lines mimic an extensional flow, which is recognised [35] as favourable for the clay particle dispersion. But, it may also induce a preferential orientation, similar to what happens at the die exit.

Overall, the images show an increase of the clay dispersion along the first half of the screw (between L/D 10 and L/D 19), but filler aggregates become coarser towards the die exit.

Chapter 5. The evolution of dispersion along the extruder during the manufacture of polymer-organoclay nanocomposites

Table 5. 5. Scanning transmitted electron microscopy images of the nanocomposites prepared with SC1 and SC2.

	L/D 10	L/D 11	L/D 19	L/D 29	die
SC 1	x				
SC 2		x			

Chapter 5. The evolution of dispersion along the extruder during the manufacture of polymer-organoclay nanocomposites

Considering the STEM images, the reversion detected from L/D 11 forward cannot be explained solely on the basis of orientation effects. Hence, the hypothesis of degradation, of the polymer matrix, the clay surfactant or a combination of both, must be explored.

The FT-IR spectra of the organoclay and of the nanocomposites show a pronounced band between 1250 and 750 cm^{-1} due to the Si-O bonds of the silicate. It has been demonstrated [26 – 28] that this band can be decomposed in at least four peaks, three being related to the Si-O in-plane vibrations appearing at about 1120, 1050 and 1020 cm^{-1} , and the fourth with the Si-O out-of-plane vibration appearing at about 1080 cm^{-1} . As the individual clay layers become more spaced, the peaks at 1050 cm^{-1} and 1080 cm^{-1} tend to shift. The negative shift of the peak at 1050 cm^{-1} is related to the penetration of the polymer chains inside the clay galleries, whilst the positive shift of the peak at 1080 cm^{-1} is attribute to delamination of the clay platelets (exfoliation) [26 – 27]. Accordingly, FT-IR was used to discriminate between the intercalation and exfoliation levels attained with the different screw profiles. Figure 5. 7 shows the evolution along the extruder of the FT-IR peak shifts. For SC1 and SC2, the FT-IR shift of the peak at 1050 cm^{-1} (Figure 5. 7(a)) indicates the increase of intercalation until L/D 19, after which the intercalation levels off for SC1 and decreases for SC2. At L/D 11, SC3 shows higher levels of intercalation, but downstream a marked reversion occurs. The shift of the peak at 1080 cm^{-1} (Figure 5. 7(b)) for SC1 suggests an exfoliated structure at L/D 10, but the regular decrease of the peak shift until the die exit is consistent with re-agglomeration, and with the increase of intercalation. For SC2 the positive shift of the peak at 1080 cm^{-1} , indicates a steady increase of exfoliation from L/D 9 to L/D 29, showing a minor decrease at the die exit. Between L/D 9 and L/D 11, SC3 exhibits a sharp increase of exfoliation that remains constant until the die exit.

Chapter 5. The evolution of dispersion along the extruder during the manufacture of polymer-organoclay nanocomposites

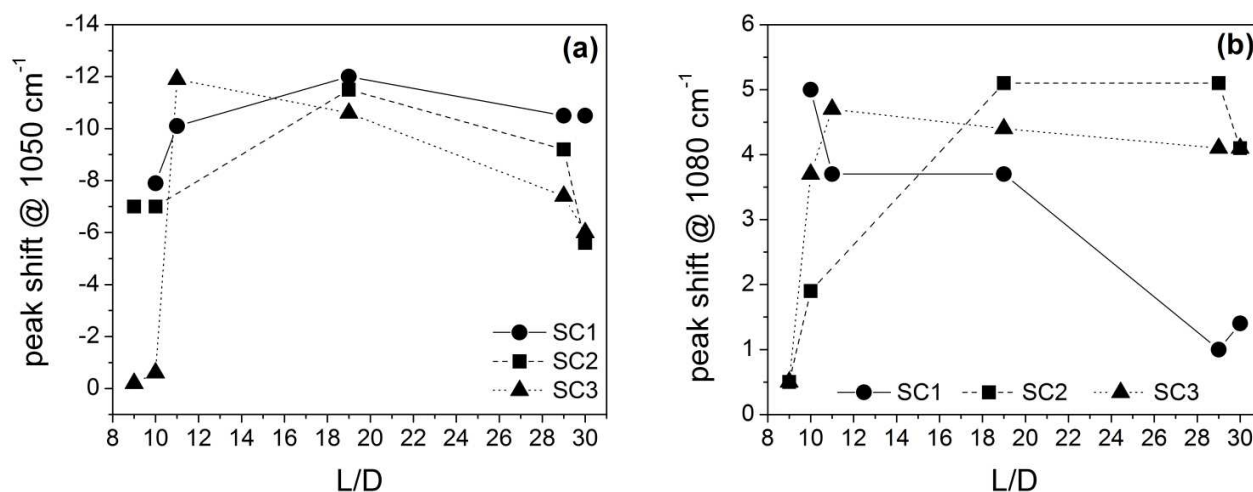


Figure 5. 7. Off-line FTIR analysis: (a) in-plane peak (1050 cm⁻¹) shift; (b) out-of-plane peak (1080 cm⁻¹) shift.

FT-IR suggests that for SC1 the generated stresses along the first mixing zone (L/D 9 to 11) are enough to prompt exfoliation, but as melting completes relaxation phenomena are also occurring, resulting in what appears to be the platelets re-agglomeration beyond L/D 11 [3, 15, 17]. In the case of SC2 and SC3, the decrease of intercalation appears to be associated with the increase of exfoliation [3, 11]. The FT-IR results are not influenced by the orientation of the dispersed particles because of the polarization of the beam [26 – 28]; nevertheless, this is still a plausible explanation for the conflicting results observed between rheology (Figure 5. 4(b)) and FT-IR (Figure 5. 7(b)) of SC2 and SC3. Although seemingly incoherent, rheometry, NIR and FT-IR results are in agreement with previous findings [3, 15, 17] showing that dispersion occurs fast, and high levels of intercalation (sometimes even exfoliation) are reached during the initial melting phase, hence the swift increase between L/D 9 and L/D 11 for all screw profiles tested.

The visual appearance of the collected samples suggests that some level of thermo-oxidative degradation occurs during the mixing process in the TSE. The CIELab luminosity (L^*) and yellowness (b^*) coordinates were measured and the results are depicted in Figure 5. 8. Figure 5. 8(a) shows that all nanocomposites are darker ($\Delta L^* < 0$) than the polymer matrix. The increase of darkness has been attributed to the incorporation of the organoclay [29 – 30] but also to the degradation effects of the polymer matrix, the organoclay modifier or to a combination of both phenomena [29, 30]. Moreover, Fornes et al [29] established a correlation between the increase of darkness and the

Chapter 5. The evolution of dispersion along the extruder during the manufacture of polymer-organoclay nanocomposites

exfoliation levels, stating that a higher number of individual platelets will render higher contact between the clay surface and the polymer matrix enhancing the colour formation. Accordingly, given the L^* variations, the nanocomposite prepared with SC1 should have the highest level exfoliation. However, the results obtained this far for SC1 show that this screw profile yields lower levels of exfoliation, as such we consider that the decrease of L^* is mainly related to degradation phenomena.

Figure 5. 8(b) shows that the yellowness index ($\Delta b^* > 0$) of the nanocomposites is higher than that of the polymer matrix. Also b^* increases along the extruder and all screw profiles exhibit comparable yellowness values. The yellowness index is unequivocally related to the degradation of the nanocomposite [30], and its increase indicates the formation of unsaturated bonds, usually associated to thermo-oxidative degradation. Actually, Fornes et al [29] propose a Hoffmann-type elimination reaction for the degradation of quaternary ammonium compounds. In the case of D67G, the dimethyl dihydrogenated tallow degradation would result in a dimethylamine ($\text{NH} - (\text{CH}_3)_2$) and also an alpha-olefin ($\text{CH}_2 = \text{CH} - (\text{CH}_2)_n - \text{CH}_3$).

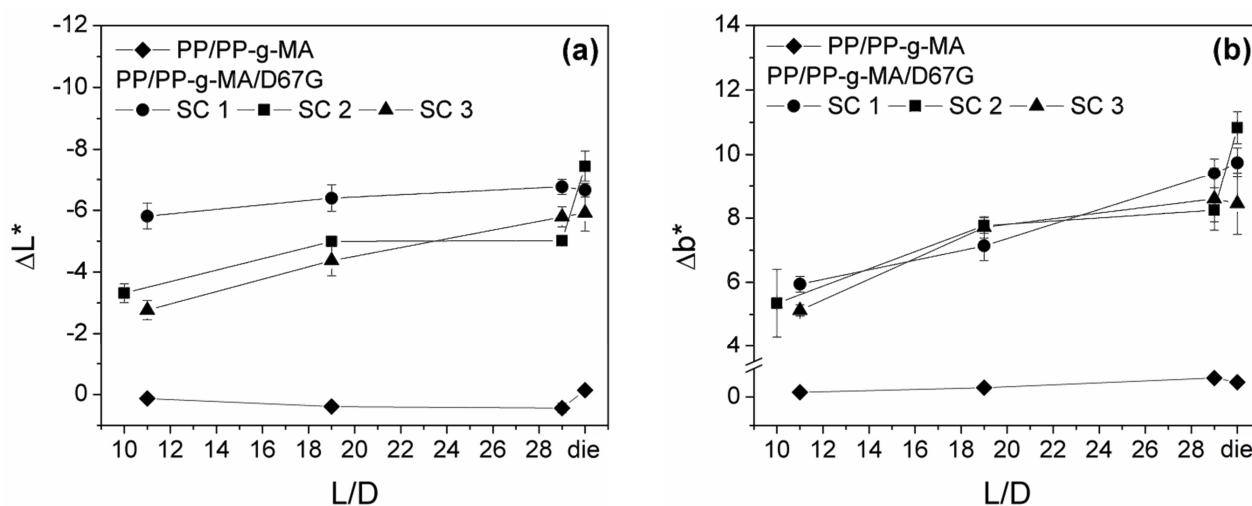


Figure 5. 8. CIELab colour coordinates (a) luminosity and (b) yellowness.

Although confirming degradation, it is not possible to discriminate if it affects preferentially the clay surfactant or the polymer matrix. But, the thermal behaviour of the nanocomposite and its components (organoclay and polymer matrix) provides some useful insight on the thermal stability. The TGA results are shown in Figure 5. 9.

Chapter 5. The evolution of dispersion along the extruder during the manufacture of polymer-organoclay nanocomposites

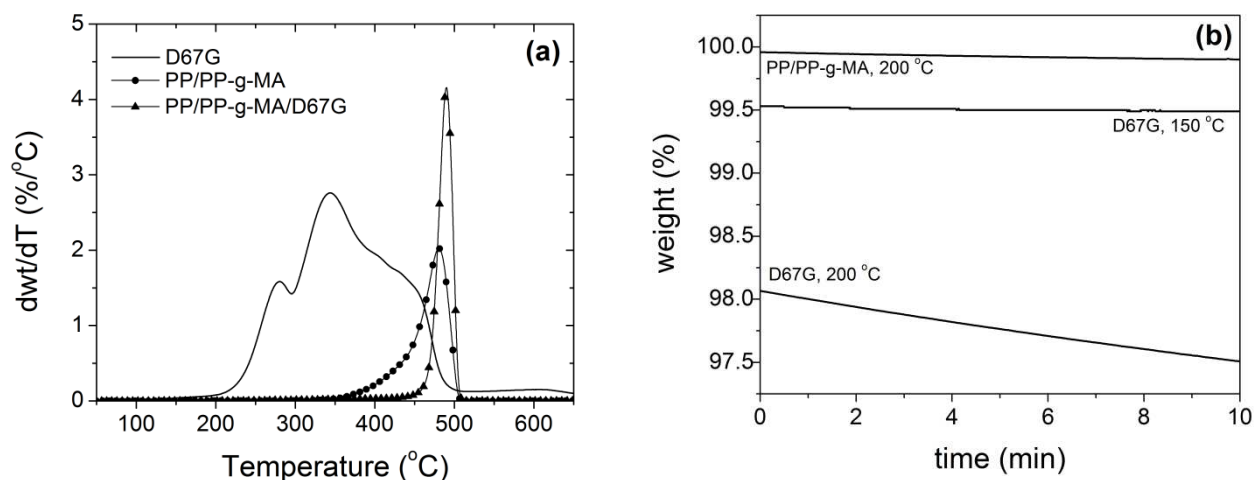


Figure 5. 9. (a) Dynamic TGA derivative curves of the organoclay (D67G), the polymer matrix (PP/PP-g-MA) and the nanocomposite (PP/PP-g-MA/D67G) prepared with SC2. (b) Isothermal TGA curves of the organoclay and the polymer matrix.

From Figure 5. 9(a), it is obvious that significant weight changes start at different temperatures, specifically 246 °C for the organoclay, 444 °C for the polymer matrix and 478 °C for the nanocomposite. This shows that as expected the nanocomposite is more thermally stable than its individual components. However, Bertini et al [36] propose that the onset of degradation for these materials should be considered at 1 % weight loss. Hence, degradation starts at 213 °C for the organoclay, 360 °C for the polymer matrix and 330 °C for the nanocomposite. Using Bertini's method [36] the nanocomposite weight loss begins 30 °C before the degradation of the matrix, which can be explained by the degradation of the clay organic modifier that induces minor changes to the DTGA signal due to the low clay loading. To confirm this interpretation of the data, both the polymer matrix and the organoclay were submitted to isothermal tests (Figure 5. 9(b)) and the results show that after 10 minutes at 150 °C in a non-oxidative environment the weight loss of the clay is about 0.5 % but at 200 °C increases to 2.5 %. The PP/PP-g-MA matrix remains stable, even at 200 °C, presenting a minor weight loss of 0.1 %. The organoclay weight changes in this temperature range are due to the volatilization of lower molecular weight components derived from degradation of the organic modifier. Similar results were reported by other authors [30, 36 – 38]. Shah and Paul [37] studied the degradation of different organoclays during melt processing of polyethylene based nanocomposites, and concluded that clays modified with multi alkyl tails (like the surfactant 2M2HT) have greater thermal stability. However, the respective nanocomposites show

Chapter 5. The evolution of dispersion along the extruder during the manufacture of polymer-organoclay nanocomposites

greater weight loss (due to degradation of the surfactant) during melt compounding, than that determined by TGA analysis of the organoclay. The authors conclude that thermodynamics of the extrusion process enhances the solubility of the alpha-olefins in the polyolefin matrix, expediting the removal of these degradation products from the organoclay, and making its release easier than by volatilization during TGA [37]. Moreover, Xie *et al* [38] showed that the metallic cations of the original silicate structure have a catalytic effect on degradation of both the surfactant and the polymer matrix. They also state that the unsaturated olefinic degradation products of the surfactant may lead to unfavourable interfacial plasticization (or advantageous cross-linking depending on the matrix) reaction with the polymer, explaining the often unexpected rheological behaviour of these materials [38].

Given the results, thermal degradation of the clay surfactant (and subsequent polymer matrix degradation) appears a good explanation for the reversion of dispersion detected by the on-line/in-line techniques. Degradation should have different influence on the mechanism of dispersion, depending on which of the organic parts is affected. If degradation of the clay surfactant is the main event, the polymer-clay interface is affected and the diffusion of the polymer melt within the clay layers is hindered [3, 11]. However, until degradation of the surfactant reaches the critical point, time has passed during which some level of dispersion is reached. Therefore, as STEM and FT-IR data suggest, the already exfoliated particles may not be affected, but the remaining clay stacks will not evolve to a well dispersed structure. Eventually, the intercalated clay particles may collapse due to the decrease of the interlayer spacing by removal of the surfactant [29, 37 – 38] and/or re-agglomerate due to the attractive electrostatic forces between the silicate sheets [8, 34]. Xu *et al* [8] established a correlation between these interfacial phenomena and the viscoelastic behaviour. The authors claim that depending on the type of polymer-clay bond established, a highly dispersed nanocomposite may show a liquid-like behaviour, explained by the long-term unstable thermodynamics of the generated structure. This appears a realistic explanation for the reversion of the rheological behaviour of SC2 and SC3 (Figure 4), while keeping the high exfoliation levels detected by the FT-IR (Figure 7(b)) and the dispersion levels seen by STEM (Table 5) for SC2.

If degradation of the clay surfactant actually prompts the degradation of the polymer matrix, the decrease of the molecular weight and of the viscosity, interfere with the global thermodynamics of

Chapter 5. The evolution of dispersion along the extruder during the manufacture of polymer-organoclay nanocomposites

dispersion process. At this point, the hydrodynamic stresses exerted by the polymer matrix may not be enough to overcome the inherent attractive forces between the clay layers, thus even if some level of exfoliation was achieved the clay particles tend to the initial aggregated state [8, 34]. Actually, this is a plausible explanation for the results obtained with SC1, indicating a highly intercalated and partially exfoliated structure formed at the end of the first mixing zone. Then, as the intercalation levels appear to slightly increase from L/D 11 forward (Figure 5. 7(a)), the shift of the 1080 cm^{-1} peak (Figure 5. 7(b)) decreases to a non-exfoliated level, suggesting that the initial levels of exfoliation could not be supported.

These observations suggest that the dispersion mechanism involves two phases, one related to the dispersion itself and another dependent of degradation. After melting, the polymer chains begin to penetrate inside the clay galleries. Depending on the given residence time and the matrix viscosity, the diffusion of the polymer chains develops and the gallery spacing increases (intercalation); ultimately, due to the increase of the melt viscosity (stress/strain) and/or time, delamination of the platelets occurs (exfoliation). It is likely that some erosion takes place during this stage, caused by a combination of shear and strain. Eventually, given long residence time and/or high temperatures, degradation of the clay surfactant takes place, triggering the degradation of the polymer matrix. It is likely, that the exfoliated particles are unaffected, but due to decrease of viscosity and of the hydrodynamic stresses the clay layers may collapse or re-agglomerate.

5.4. Conclusions

On-line oscillatory rheometry and in-line NIR were used to study the evolution of the dispersion of a PP/PP-g-MA/D67G system. Overall, the results show that regardless of the screw profile, a significant contribution to the final dispersion is given by the initial melting and mixing stage (until L/D 11). However, both techniques indicated that the increase of dispersion along the first mixing zone is followed by a reversion downstream.

Further off-line analysis by STEM revealed that dispersion evolves until L/D 19, after which the clay particles appear as coarser agglomerates. For SC1 the FT-IR analysis revealed that beyond L/D 11 the increase of the intercalation levels is complemented by the decrease of exfoliation. Conversely, for the other two screw profiles the decrease of intercalation appears compensated by the increase of exfoliation. These results clarified some discrepancies between the on-line rheology data and the in-line NIR predictions. Finally colour measurements and TGA confirmed the degradation of the nanocomposites and the thermal instability of the organoclay, confirming that degradation of the clay surfactant is likely to occur, triggering the degradation of the polymer matrix.

As such, the reversion of dispersion was attributed to the degradation of the clay surfactant, affecting the polymer-clay interface, and of the polymer matrix, causing the decrease of the hydrodynamic stress levels, enabling relaxation of the polymer matrix. Ultimately, these lead to the collapse of the clay structure and/or re-agglomeration of the clay particles.

5.5. References

1. R.A Vaia, H. Ishii, E.P. Giannelis. Synthesis and properties of two-dimensional nanostructures by direct intercalation of polymer melt in layered silicates; *Chemistry of Materials*, 5 p. 1694-1696 (1993)
2. J.W. Cho, D.R. Paul. Nylon 6 nanocomposites by melt compounding; *Polymer* 42 p. 1083-1094 (2001)
3. H.R. Dennis, D.L. Hunter, D. Chang, S. Kim, J.L. White, J.W. Cho, D.R. Paul. Effect of melt processing conditions on the extent of exfoliation in organoclay-based nanocomposites; *Polymer* 42 p. 9513-9522 (2001)
4. S. Pavlidou, C.D. Papaspyrides. A review on polymer-layered silicate nanocomposites. *Progress in Polymer Science*. 33 p. 1119-1198 (2008)
5. T.D. Fornes, P.J. Yoon, H. Keskkula, D.R. Paul. Nylon 6 nanocomposites: the effect of matrix molecular weight. *Polymer* 42 p. 9929-9940 (2001)
6. S.W. Kim, W.H. Jo, M.S. Lee, M.B. Ko, J.Y. Jho. Effects of shear on melt exfoliation of clay in preparation of Nylon 6/Organoclay nanocomposites, *Polymer Journal* 34 p. 103-111 (2002)
7. S. Tanoue, L.A. Utracki, A. Garcia-Rejon, J. Ttibouet, K.C. Cole, M. R. Kamal. Melt compounding of diferente grades of Polystyrene with Organoclay. Part 1: Compounding and Characterization; *Polymer Engineering and Science* 44 p. 1046-1060 (2004)
8. L. Xu, H. Nakajima, E. Manias, R. Krishnamoorti. Tailored nanocomposites of Polypropylene with layered silicates; *Macromolecules* 42 p. 3795-3803 (2009)
9. M. Modesti, A. Lorenzetti, D. Bon, S. Besco. Effect of processing conditions on morphology and mechanical properties of compatibilized polypropylene nanocomposites. *Polymer*. 46 p. 10237-10245 (2005)
10. M.W. Spencer, L. Cui, Y. Yoo, D.R. Paul. Morphology and properties of nanocomposites based on HDPE/HDPE-g-MA blends. *Polymer*. 51 p. 1056-1070 (2010)

Chapter 5. The evolution of dispersion along the extruder during the manufacture of polymer-organoclay nanocomposites

11. M. Bousmina. Study of intercalation and exfoliation processes in polymer nanocomposites. *Macromolecules*. 39 p. 4259-4263 (2006)
12. K. Chrissopoulou, S.H. Anastasiadis. Polyolefin/layered silicate nanocomposites with functional compatibilizers. *European Polymer Journal*. 47 p. 600-613 (2011)
13. M.A. Treece, W. Zhang, R.D. Moffit, J.P. Oberhauser. Twin-screw extrusion of Polypropylene-Clay nanocomposites: Influence of masterbatch processing, screw rotation mode and sequence; *Polymer Engineering and Science* 47 p. 898-911 (2007)
14. P. Médéric, J. Ville, J. Huitric, M. Moan, T. Aubry. Effect of processing procedures and conditions on structural, morphological and rheological properties of Polyethylene/Polyamide/Nanoclay blends; *Polymer Engineering and Science* 51 p. 969-978 (2011)
15. W. Lertwimolnun, B. Vergnes. Effect of processing conditions on the formation of polypropylene/organoclay nanocomposites in a twin-screw extruder. *Polymer Engineering and Science*. 46 p. 314-323 (2006)
16. P. Peltola, E. Valipakka, J. Vourinen, S. Syrjala; K. Hanhi. Effect of rotational speed of twin screw extruder on the microstructure and rheological and mechanical properties of nanoclay-reinforced polypropylene nanocomposites; *Polymer Engineering and Science* 46 p. 995-1000 (2006)
17. W. Lertwimolnun, B. Vergnes. Influence of screw profile and extrusion conditions on the microstructure of polypropylene/organoclay nanocomposites. *Polymer Engineering and Science*. 47 p. 2100-2109 (2007)
18. K. Kohlgruber. *Co-rotating twin-screw extruders: Fundamentals, technology and applications*; Carl Hanser Verlag, Munich, Germany (2008)
19. A.V. Machado, J.A. Covas, M. van Duin. Evolution of morphology and of chemical conversion along the screw in a corotating twin-screw extruder; *Journal of Applied Polymer Science*, 71 p. 135-141 (1999)

Chapter 5. The evolution of dispersion along the extruder during the manufacture of polymer-organoclay nanocomposites

20. S. Mould, J.M. Barbas, A.V. Machado, J.M. Nóbrega, J.A. Covas. Measuring the rheological properties of polymer melts with on-line rotational rheometry. *Polymer Testing*. 30 p. 602-610 (2011)
21. A. Durmus, A. Kasgoz, C.W. Macosko. Linear low density polyethylene (LLDPE)/clay nanocomposites. Part I: Structural characterization and quantifying clay dispersion by melt rheology. *Polymer*. 48 p. 4492-4502 (2007)
22. A. Vermogen, K. Masenelli-Varlot, R. Séguéla, J. Duchet-Rumeau, S. Boucard, P. Prele. Evaluation of the structure and dispersion in polymer-layered silicate nanocomposites. *Macromolecules*. 38 p. 9661-9669 (2005)
23. J.M. Barbas, A.V. Machado, J.A. Covas. In-line Near-Infrared spectroscopy for the characterization of dispersion in polymer-clay nanocomposites; *Polymer Testing* 31 p. 527-536 (2012)
24. J.M. Barbas, A.V. Machado, J.A. Covas. In-line Near-Infrared spectroscopy: a tool to monitor the preparation of polymer-clay nanocomposites in extruders, *article in press*, *Journal of Applied Polymer Science*. DOI: 10.1002/app.38106 (2012)
25. R. Zouari, T. Domenech, B. Vergnes, E. Peuvrel-Disdier. Time evolution of the structure of organoclay/polypropylene nanocomposites and application of the time-temperature superposition principle; *Journal of Rheology*, 56 p. 725-742 (2012)
26. K.C. Cole. Use of Infrared spectroscopy to characterize clay intercalation and exfoliation in polymer nanocomposites". *Macromolecules*. 41 p. 834-843 (2008)
27. L. Yan, C.B. Roth, P.F. Low. Changes in the Si-O vibrations of smectite layers accompanying the sorption of interlayer water. *Langmuir*. 12 p. 4421-4429 (1996)
28. W.L. IJdo, S. Kemnetz, D. Benderly. An Infrared method to assess organoclay delamination and orientation in organoclay polymer nanocomposites. *Polymer Engineering and Science* 46 p. 1031-1039 (2006)
29. T.D. Fornes, P.J. Yoon, D.R. Paul. Polymer matrix degradation and color formation in melt processed nylon 6/clay nanocomposites; *Polymer* 44 p. 7545-7556 (2003)

Chapter 5. The evolution of dispersion along the extruder during the manufacture of polymer-organoclay nanocomposites

30. L. Cui, J.E. Bara, Y. Brun, Y. Yoo, P.J. Yoon, D.R. Paul. Polyamide and polycarbonate based nanocomposites prepared from thermally stable imidazolium organoclay; *Polymer* 50 p. 2492-2502 (2009)
31. P. Cassagnau. Melt-rheology of organoclay and fumed silica nanocomposites. *Polymer*. 49 p. 2183-2196 (2008)
32. R. Krishnamoorti, E.P. Giannelis. Rheology of end-tethered polymer silicate nanocomposites; *Macromolecules* 30 p. 4097-4102 (1997)
33. D.A. Burns, E.W. Ciurczak (eds). *Handbook of Near-Infrared Analysis* CRC Press, Florida, USA (2008).
34. J. Ren, B.F. Casanueva, C.A. Mitchel, R. Krishnamoorti. Disorientation kinetics of aligned polymer layered silicate nanocomposites; *Macromolecules* 36 p. 4188-4194 (2003)
35. L.A. Utracki. Clay-containing polymeric nanocomposites – vol. 1. Part 2. Basic elements of polymeric nanocomposite technology, p. 158-160; Rapra Technology Limited, Shropshire, UK (2004)
36. F. Bertini, M. Canetti, G. Leone, I. Tritto. Thermal behaviour and pyrolysis of modified organo-layered silicates as intermediates for in situ polymerization; *Journal of Analytical and Applied Pyrolysis*, 86 p. 74-81 (2009)
37. R.K. Shah, D.R. Paul. Organoclay degradation in melt processed polyethylene nanocomposites, *Polymer* 47 p. 4075-4084 (2006)
38. W. Xie, Z. Gao, W-P. Pan, D.L. Hunter, A. Singh, R. Vaia. Thermal degradation chemistry of alkyl quaternary ammonium montmorillonite, *Chemistry of Materials* 13 p 2979-2990 (2001)

THE EFFECT OF THE PROCESSING CONDITIONS ON THE EVOLUTION OF DISPERSION OF DIFFERENT POLYMER-CLAY NANOCOMPOSITES

6

Twin screw extrusion remains the preferred technique to prepare polymer-clay nanocomposites by direct melt intercalation. Although general correlations between processing conditions and clay dispersion have been established, the actual evolution of dispersion along the extruder axis seems less well understood. In-line monitoring of the structure development along the extruder provided better understanding about the influence of the operating conditions on the dispersion phenomena. This work uses in-line Near-Infrared Spectroscopy (NIR), and adequate chemometric analysis, to assess in real time the evolution of dispersion of polymer-clay nanocomposites prepared under different conditions. Using a polypropylene matrix system and a nylon-6 matrix system, which were prepared with different screw speeds and feed rates, the work analyses the role of stress, shear and residence time on the onset and evolution of the intercalation/exfoliation mechanism. Results show that depending on the chemical affinity between polymer and clay, and on the applied processing conditions, dispersion may evolve, remain constant or revert. Suitable off-line characterization data confirms that under the same conditions the dispersion in a nylon-6 matrix is better and both systems exhibit an optimum set of conditions that maximize the level of dispersion.

J.M. Barbas, A.V. Machado, J.A. Covas (under preparation)

6.1. Introduction

Direct melt intercalation remains the method of choice for the preparation of polymer-clay nanocomposites, due to the effectiveness of the dispersion levels attained and the suitability for industrial scale production [1 – 3]. In addition to the chemical affinity between the polymer and the organoclay [4 – 9], there are also ample evidences that the mixing equipment and melt processing conditions [1 – 2, 6 – 8, 10 – 18] play a significant role in the dispersion of polymer-clay nanocomposites.

It is well established that the dispersion mechanism combines the process of diffusion of the polymer chains within the clay interlayer spacing (intercalation) and proper mechanical effort to delaminate the individual platelets (exfoliation) [2, 18].

Regardless of the polymeric matrix, it is well accepted that the increase of screw speeds results in better dispersion [1, 6, 11 – 17, 19 – 20]. Actually, Homminga *et al* [19] have shown that for highly compatible systems (like polyamides) the role of the shear forces in melt mixing is to expedite the intercalation process, by breaking up the original large sized clay agglomerates. This has also been suggested by other authors [2, 10]. However, some studies [5, 21 – 22] reported that high shear rates yield lower dispersion and lower exfoliation levels, attributing this to the effect of erosion. The influence of feed rate has also been studied [2, 3, 13, 23 – 24] and the results show that lower feed rates result in significant improvements of the exfoliation levels attained, which is has been attributed to the increase in residence time. Moreover, Lertwimolnun and Vergnes [3, 13] showed that this parameter has little effect on the state of intercalation. The effects of residence time and temperature have also been considered [1 – 2, 7, 20, 23 – 24]. It is general agreement that better exfoliation is achieved with higher residence times and that high temperature is often prejudicial, probably due to degradation of the clay surfactant.

Despite the validity of these findings, the effect of these parameters on the initiation and evolution of dispersion is still controversial. Associating these thermodynamic effects, particularly the balance between time (for diffusion) and shear (for delamination) proposed by Bousmina [18], to the evolution dispersion evolution in twin screw extruders remains difficult. Lertwimolnun and Vergnes [3, 13] characterized post-mortem samples collected from various locations along a co-rotating twin

Chapter 6. The effect of the processing conditions on the evolution of dispersion of different polymer-clay nanocomposites

screw machine, using oscillatory rheometry and X-ray diffraction. Considering previously proposed correlations between the rheological response and the dispersion of nanocomposites, the authors concluded that both intercalation and exfoliation can reach relatively high levels immediately after melting. More importantly, they concluded [3] that depending on the combination of screw speed, feed rate and the screw profile the initial structure could evolve, remain constant or apparently revert along the screw length. Reversion has been attributed to degradation of the matrix, although no experimental confirmation of that was provided.

In a previous unpublished work, the authors used on-line rheometry [25] and in-line Near-Infrared (NIR) spectroscopy [26] to monitor the evolution of dispersion of a polypropylene/polypropylene grafted with maleic anhydride/organoclay system along the extruder. Three screw profiles with distinct restrictive character were used, under constant processing conditions. The viscoelastic behaviour measured in oscillatory mode, and the chemometric analysis, provided evidences of reversion in the dispersion levels obtained beyond the first mixing zone of the screw. Further off-line characterization with electron microscopy (STEM), medium infrared spectroscopy (FT-IR) confirmed the reversibility of intercalation in the downstream region of the extruder having apparently been originated by the degradation of the organoclay surfactant which was confirmed by thermal gravimetric analysis (TGA). This work uses in-line NIR and appropriate chemometrics [26], to monitor the effects of screw speed (N) and throughput (Q) on the dispersion evolution along the extruder. For that two different systems are used: one based on polypropylene (PP/PP-g-MA/D67G) known for having less chemical affinity with the organoclay and proven to be affected by degradation; the other based on polyamide (PA6/D43B) that is highly compatible with the organoclay, which is reported to have stronger influence on the dispersion than the thermomechanical parameters. The materials were prepared under different conditions aiming at gather further information about the effect of the processing conditions (and chemical constraints) on the evolution of dispersion and the final levels attained. For this purpose, in-line NIR is performed in 5 locations along the extruder (die exit included) and using in-house developed sample collecting devices [27] the material was collected from the extruder (at the same locations) for further off-line characterization. The results show that under the same conditions higher levels of dispersion are obtained with the PA6 system, despite the lower thermal stability of the respective organoclay. Also both systems show a marked reversion of dispersion at the die exit, regardless of the processing

Chapter 6. The effect of the processing conditions on the evolution of dispersion of different polymer-clay nanocomposites

conditions use. It became clear that both systems are affected by the operating conditions. Seemingly, there is an optimum set of screw speed – throughput conditions for each system that can be used to maximize the dispersion.

6.2. Experimental

6.2.1. Materials and composites

Two different systems will be tested:

- the polypropylene matrix system (PPNC), includes an injection molding grade Polypropylene (PP), a Polypropylene grafted with Maleic Anhydride (PP-g-MA) with 1wt.% of maleic anhydride to function as compatibilizer, and Dellite 67G (D67G), a natural montmorillonite clay modified with dimethyltallow dihydrogenated quaternary ammonium salt (2M2HT);
- the nylon-6 matrix system (PANC), includes an injection molding grade nylon-6 (PA6) and Dellite 43B (D43B), also a natural montmorillonite clay modified with dimethyltallow benzylhydrogenated ammonium salt (2MBzHT).

The respective components are presented in Table 6. 1.

Table 6. 1. Materials used in the work.

Material	Acronym	Producer	Grade	MFI/lamellar distance
Polypropylene	PP	Lyondell Basell	Moplen HP500N	12 g/10 min (230 °C/2.16 kg)
Compatibilizer	PP-g-MA	Crompton	Polybond 3200	115 g/10 min (190 °C/2.16 kg)
Nylon-6	PA6	Rhodia Engineering Plastics SA	Technyl C206	-
Montmorillonite clay	D67G	Laviosa	Dellite 67G	$d_{001} = 3.70$ nm
			Dellite 43B	$d_{001} = 1.90$ nm

Chapter 6. The effect of the processing conditions on the evolution of dispersion of different polymer-clay nanocomposites

The organoclays (selected according to their affinities with the used matrices) and nylon-6 were dried overnight in a vacuum oven at 80 °C. In all cases the PP/PP-g-MA/D67G formulation was kept at 90/5/5 wt.% and the PA6/D43B was of 95/5 wt.%. All nanocomposites were prepared in a modular co-rotating intermeshing twin-screw extruder Leistritz LSM 30.34, the respective layout and screw profile are presented in Figure 6. 1. The barrel and die set temperature were kept constant at 200 °C and 240°C for all extrusion runs with PP matrix and PA6 matrix, respectively. In a first set of experiments, the feed rate (Q) was set at 3 kg/h by a Moretto Dosing System DVM18-L and the screw speed (N) was varied (50, 100, 200 and 300 rpm). In a second run of experiments, the screw speed was kept constant at 100 rpm and different feed rates (1.5, 3, 6 and 9 kg/h) were used.

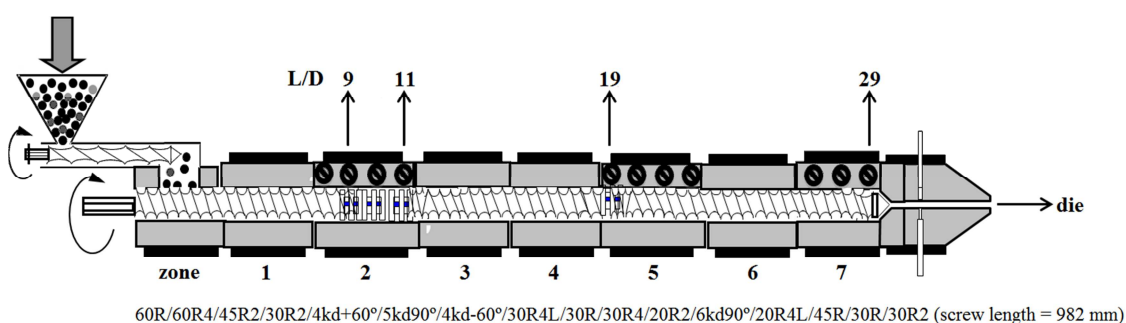


Figure 6. 1. Layout of the twin-screw extruder and screw profile.

6.2.2. Sample collection and process monitoring

A NIR Diffuse Reflectance (DR) probe for polymer extruders (from Hellma Analytics) was directly fixed to the extruder at L/D = 9, 11, 19, 29 and die (see Figure 1) by a Dynisco-type thread. The probe has a sapphire window (with a diameter of 5.7 mm, for an illuminated area with a diameter of 2 mm and a field depth of 3 mm) and contacts directly the melt stream, no modifications to the extruder or die being required. The connection between the probe and the NIR spectrometer (Matrix F, Bruker Optics) is made by fibre optic cable (the illumination cable has 7 fibres with 400 µm core diameter, whilst the detection cable has a single fibre with 600 µm core diameter). A more detailed description of the system and its validation can be found elsewhere [26]. The NIR spectra were measured from 12000 – 4500 cm⁻¹ with a resolution of 8 cm⁻¹ and accumulation of 4 scans, the

Chapter 6. The effect of the processing conditions on the evolution of dispersion of different polymer-clay nanocomposites

acquisition time for each spectrum being approximately 2 seconds. The background signal is acquired prior to installation, using a *Spectralon*[®] diffuse reflection standard target (Bruker Optics) with a reflectivity index of 99%. For each position, a total of 50 spectra were measured during regular intervals of continuous extrusion runs.

NIR enables also a quantitative assessment of the clay dispersion in real-time. This is done by means of a chemometric model, relating the spectral differences and reference parameters often used to describe the clay dispersion. The model encompasses 7 parameters derived from oscillatory rheometry (G' , G'' , σ_0 , b), FT-IR (wavenumber shift of the peaks at 1050 and 1080 cm^{-1}) and a process-related thermomechanical index, specifically the specific mechanical energy (SME) [26]. The model used here, was previously developed [26] to study the effect of throughput at the end of the first mixing zone (L/D 11), the calibration samples, having different levels of dispersion, were obtained by varying the clay loading, the compatibilizer content (only for the PP system) and the screw speed. The quality of the NIR predictions is assessed by the Root Mean Square Error of Prediction (RMSEP) and the bias. The statistical meaning, calculations and acceptance limits of these quality factors are explained in section 3.3.2 of this thesis. Although it is well-known that chemometric models should not be extended to conditions laying outside the calibration range, this model is applied here because the different constructions of the first mixing zone are expected to influence the hydrodynamic stresses, residence times and viscous dissipation effects, generating similar effects as screw speed and throughput variations. Figure 6. 2 shows the calibration models obtained for both systems.

Chapter 6. The effect of the processing conditions on the evolution of dispersion of different polymer-clay nanocomposites

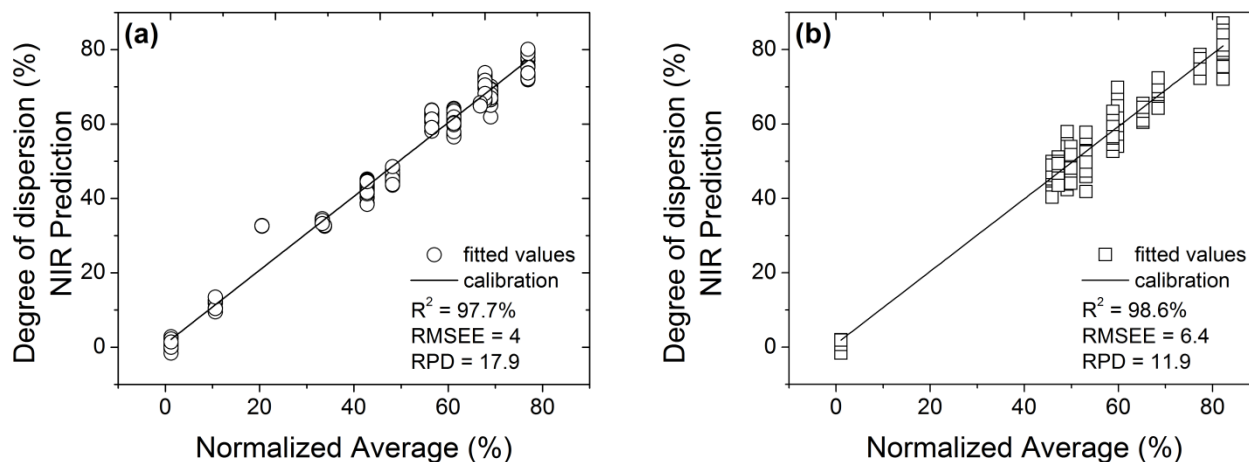


Figure 6. 2. NIR calibration curve developed at L/D 11 for the nanocomposites prepared under different processing conditions: (a) PP/PP-g-MA/D67G system; (b) PA6/D43B system.

In order to collect samples along the extruder, the barrel was fitted with modified segments (identified as zones 2, 5 and 7 in Figure 6. 1) [27]. At each sampling location – L/D 9, 11, 19 and 29 – the material is diverted from the plasticating chamber to an outer chamber by means of a rotating valve (more details in [27]). These valves also enable the local visual check of the presence of solid, the measurement of the average melt temperature (by sticking a fast response thermocouple in the freshly collected melt) and an estimation of the minimum residence time (by counting the time elapsed between feeding a pigment tracer into the screws and identifying a local colour change in the melt stream). The registered values of melt temperature, residence times and Specific Mechanical Energy (SME) are listed in Table 6. 2. For most of the conditions tested, the visual checking confirmed that at L/D 9 melting was not complete.

As expected, the melt temperature build up is delayed in both systems, when lower screw speeds or lower feed rates are being used, conversely local and global residence times are higher in these cases. Therefore, using different screw speed-throughput conditions should create distinct thermomechanical stresses, and thus influence the diffusion and shearing processes.

Chapter 6. The effect of the processing conditions on the evolution of dispersion of different polymer-clay nanocomposites

Table 6. 2. Process monitoring parameters registered during compounding with different conditions.

<i>Matrix</i>	<i>N</i> (rpm)	<i>Q</i> (kg/h)	<i>Melt Temperature (± error) (°C)</i>				<i>Residence time (± error) (s)</i>		<i>SME</i> (A.Kg.h ⁻¹)
			L/D 11	L/D 19	L/D 29	die	L/D 11	die	
PP	50	3	188.9 (±2.0)	197.5 (±0.3)	198.5 (±0.2)	207.7 (±0.4)	33.3 (±1.5)	142.3 (±2.5)	2.80
	100		198.2 (±1.4)	204.9 (±0.8)	198.9 (±0.5)	207.9 (±0.4)	27.0 (±2.0)	138.0 (±3.0)	3.00
	200		214.3 (±0.5)	216.5 (±2.0)	202.0 (±0.4)	215.6 (±0.8)	15.7 (±3.1)	129.0 (±3.6)	3.27
	300		217.4 (±1.6)	232.5 (±2.5)	207.4 (±1.3)	226.0 (±2.1)	10.0 (±1.0)	121.0 (±1.0)	3.33
		1,5	205.5 (±0.6)	208.9 (±0.5)	195.0 (±0.4)	209.7 (±0.4)	34.7 (±1.5)	240.3 (±1.5)	2.33
	100	6	193.1 (±1.0)	204.2 (±1.8)	198.1 (±0.4)	210.8 (±0.5)	17.3 (±0.6)	93.3 (±1.5)	3.80
	9	187.7 (±3.6)	203.4 (±0.3)	198.4 (±0.8)	213.6 (±0.8)	13.7 (±1.5)	74.7 (±2.5)	4.47	
PA6	50	3	239.4 (±0.5)	242.9 (±0.4)	240.0 (±0.2)	242.9 (±0.2)	37.3 (±2.1)	201.0 (±3.6)	2.67
	100		238.7 (±0.6)	248.5 (±0.5)	240.7 (±0.4)	247.1 (±0.6)	27.3 (±1.5)	188.3 (±3.1)	3.00
	200		238.7 (±1.0)	250.7 (±1.1)	245.9 (±0.6)	258.2 (±0.1)	13.3 (±1.5)	180.3 (±2.9)	3.53
	300		240.8 (±0.9)	251.8 (±0.5)	246.1 (±0.3)	259.5 (±0.5)	11.7 (±2.5)	171.7 (±1.5)	3.80
		1,5	239.4 (±0.6)	243.8 (±0.3)	240.9 (±0.6)	244.6 (±1.3)	34.0 (±1.0)	296.7 (±3.7)	2.80
	100	6	239.6 (±0.3)	248.4 (±0.4)	246.3 (±0.1)	250.4 (±0.4)	16.3 (±0.6)	107.3 (±5.7)	3.93
	9	234.8 (±0.9)	250.9 (±0.7)	246.5 (±0.2)	253.0 (±0.6)	11.0 (±1.0)	82.7 (±2.1)	4.80	

6.2.3. Off-line Characterization of the Composites

Rotational Rheometry (AR-G2, TA Instruments)

Isothermal frequency sweeps from 0.1 to 100 rad/s were performed, at 200 °C for the PP system and 240 °C for the PA6 system, using parallel plates with a diameter of 25 mm and a 1 mm gap, under a constant strain (1% for the PP matrix and 0.5% for the remaining materials). The disks had been previously compression molded at the same temperatures, applying a force of 20 Tons during 3 minutes. Several authors [3 – 5, 10, 13, 29 – 31] used the rheological response of polymer-clay nanocomposites (usually performed in SAOS mode) and established correlations with the state of dispersion of the organoclay. From a qualitative point of view, the increase of the storage (G') and loss (G'') moduli has been related to a finer dispersion [4 – 5, 13, 28, 30 – 31]. Also, the formation of a plateau at low frequencies has been attributed to the deformation and recovery of the dispersed particles [4 – 5, 13, 28 – 31]. Nevertheless, it is possible to the viscoelastic response of the nanocomposites for a quantitative analysis of the degree of exfoliation. Lertwimolnun and Vergnes [3, 7, 13] proposed the use a modified Carreau-Yasuda model with yield stress (σ_0 – equation 1) to describe the frequency (ω) dependence of the absolute complex viscosity (η^*) and successfully related this with the exfoliation level.

$$|\eta^*(\omega)| = \frac{\sigma_0}{\omega} + \eta_0 [1 + \lambda \omega^a]^{(b-1)/a} \quad (1)$$

Other studies used a power law expression to describe the complex viscosity behavior at low frequency and correlated the exponent (b – equation 2) with the state of clay dispersion [28 – 29].

$$|\eta^*(\omega)| = A\omega^b \quad (2)$$

Chapter 6. The effect of the processing conditions on the evolution of dispersion of different polymer-clay nanocomposites

Medium FT-IR (FTIR4100, Jasco)

The FT-IR analysis was done in transmission mode, in the 4000 – 500 cm^{-1} wavenumber range with a resolution of 4 cm^{-1} , using 32 scans. A polarizer lens was used to measure the spectra with different dipole moments, then calculation the Structural Factor (SF) spectra [32 – 34] thus eliminating the possible effects of clay orientation. The organoclays were analysed with a KBr mortar. The nanocomposite samples were compression moulded at 200 °C and 240 °C, for the PP and PA6 systems respectively, into $\pm 75 \mu\text{m}$ thick films. A total of 3 films per sample were analysed. The wavenumber accuracy and repeatability of the FT-IR equipment were checked prior to the measurement (the procedure is described elsewhere [26]).

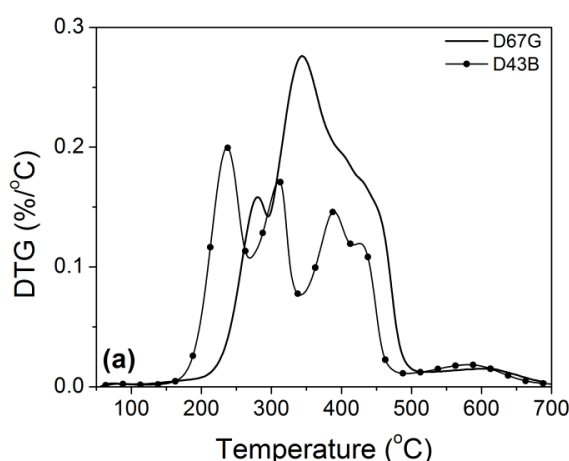
It has been demonstrated [32 – 34] that the Si-O clay band, appearing between 1300 and 750 cm^{-1} , can be decomposed in at least four peaks, three being related to the Si-O in-plane vibrations (1120, 1050 and 1020 cm^{-1}), and the fourth with the Si-O- out-of-plane (at about 1080 cm^{-1}). As the individual clay layers become more spaced, the peaks at 1050 cm^{-1} and 1080 cm^{-1} tend to shift. The negative shift of the peak at 1050 cm^{-1} is related to the penetration of the polymer chains inside the clay galleries, whilst the increase positive shift of the peak at 1080 cm^{-1} is attribute to delamination of the clay platelets (exfoliation) [32 – 33]. The region between 1300 and 750 cm^{-1} was fitted with the Pearson VII expression utilizing the Origin® Pro8 software, adjusting a 75% Gaussian shape ($\mu = 4$) for the determination of the wavenumber shift of the peaks [32 – 34]. Due to the different organic surfactants, the organoclays used in this work show distinct positions of the original Si-O peaks. The in-plane peak and the out-of-plane peaks are at 1050 cm^{-1} and 1080 cm^{-1} for the D67G, and at 1055 cm^{-1} and 1075 cm^{-1} for the D43B, respectively.

Thermal gravimetric analysis (Q500, TA Instruments)

Thermal gravimetric analysis (TGA) of the organoclays (D67G and D43B) and of the polymer matrices (95% PP/5% PP-g-MA and 100% PA6) was carried out under different conditions. Dynamic tests were applied to all samples, using a heating rate of 10 °C/min from 50 to 700 °C, and isothermal tests at different temperatures during 10 min, both under a constant flow of nitrogen (60 ml/min).

Chapter 6. The effect of the processing conditions on the evolution of dispersion of different polymer-clay nanocomposites

The low thermal stability of the clay surfactants is well known [35 – 39], and in a previous work (unpublished – Chapter 5) the authors concluded that the degradation is likely to occur, altering the dispersion process and causing great impact on the obtained levels of dispersion. The isothermal tests of D67G were conducted at 150 °C, at 200 °C (set processing temperature for the PPNCs) and 230 °C (maximum melt temperature – Table 6. 2). For D43B the isothermal tests were carried out at 150 °C, 200 °C (for direct comparison with D67G), 240 °C (set processing temperature for the PANCs) and 260 °C (maximum melt temperature – Table 6. 2). The TGA results are shown in Figure 6. 3. Using the methodology proposed by Bertini et al [36] the degradation temperatures are 213 °C for the D67G and 196 °C for D43B. The organoclay D43B is less thermally stable than D67G, but both clays suffer the effects of thermal degradation in a temperature range laying within the processing temperature intervals. Figure 6. 3(b) shows that D67G is practically unaffected at 150°C, but loses about 2.5 % of the initial weight at 200 °C and at 230°C the weight loss increases to 5.6%. Figure 6. 3(c) shows more severe effects, as D43B loses circa 2.5 wt.% at 150 °C and 5 wt.% at 200 °C, and more importantly within the processing temperature range the weight loss increases to 13% at 240 °C and 15% at 260 °C. In both cases, this weight loss includes some percentage of residual water bound to the silicate cations and low volatilization organic substances [34 – 36]. Similar results were reported by other authors [32 – 39].



Chapter 6. The effect of the processing conditions on the evolution of dispersion of different polymer-clay nanocomposites

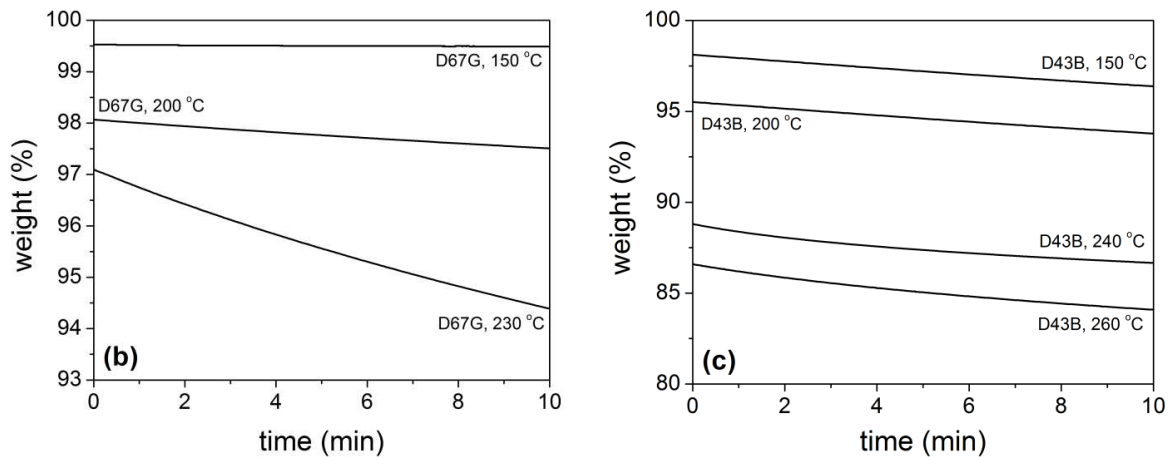


Figure 6. 3. Thermal stability of the organoclays by TGA: (a) derivative curve of the dynamic temperature sweeps of D67G and D43B, (b) isothermal at various temperatures of D67G and (c) isothermal at various temperatures of D43B.

6.3. Results and discussion

6.3.1. Global effects

Most studies comprising the effect of the processing conditions were performed on the final material, collected at the extruder die or at the end of a compounding cycle [1 – 3, 6 – 9, 10 – 17]. The majority of these studies show that a balance between shear and time is required to achieve proper dispersion. Lertwimolnun and Vergnes [3, 10, 13] showed that the processing conditions (screw speed, feed rate and temperature) have little impact on the extent of intercalation, but have great influence on the final exfoliation levels. The authors [3, 13] established that exfoliation is favoured by high screw speeds (N) and low feed rates (Q), showing the increase of melt yield stress (σ_0) with increasing screw speed and decreasing feed rates.

Using the relations previously established between the storage modulus and dispersion [4 – 5, 13, 28 – 31], Figure 6. 4 shows the effects of screw speed and throughput on the final dispersion levels, determined by the storage modulus and the NIR predictions [26], for both PP and PA6 nanocomposites collected at the die. Although not shown here, the remaining rheological parameters related to dispersion and exfoliation (G'' , σ_0 and b), shown the same outcome. Overall,

Chapter 6. The effect of the processing conditions on the evolution of dispersion of different polymer-clay nanocomposites

the results show that the PANCs yield higher dispersion levels, as can be seen from the G' values that are 1 order of magnitude higher those of the PPNCs. There are no obvious trends for the effect of the processing conditions on the final dispersion of both systems, although it appears to exist an optimum set of conditions for each material, since the PPNC prepared at 200 rpm (3 kg/h) and the PANC prepared with 6 kg/h (100 rpm) present higher G' values (the remaining rheological parameters, G'' , σ_0 and b show identical results) and better dispersion levels predicted by NIR.

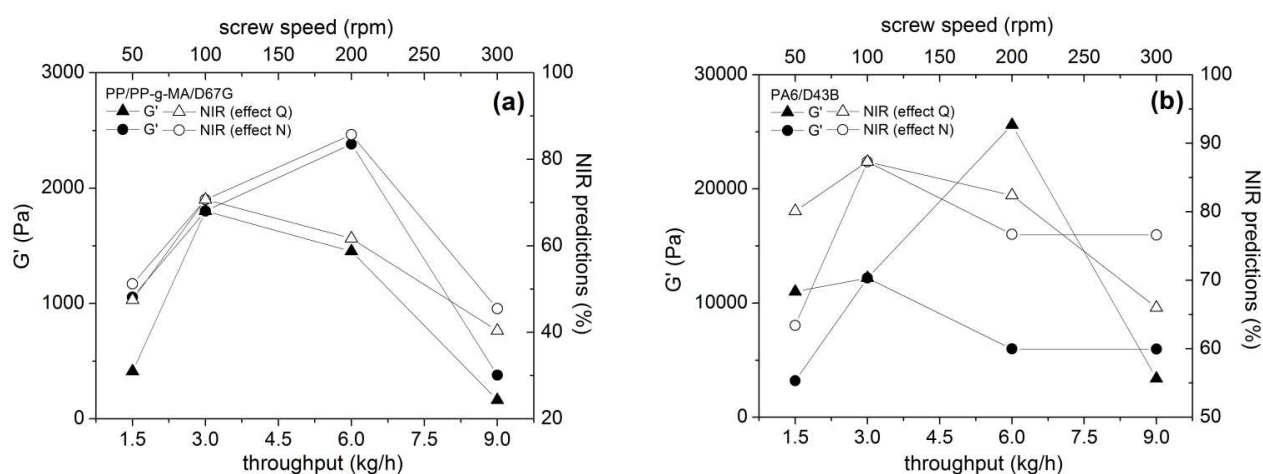


Figure 6. 4. Effect of the throughput and screw speed on the final dispersion levels: (a) PP nanocomposites, (b) PA6 nanocomposites.

Because the parameters in Figure 6. 4 do not allow discriminating between intercalation and exfoliation, Figure 6. 5 shows the FT-IR peak shift results. Figure 6. 5(a) shows that for the PPNC, the effect of the processing conditions on the intercalation levels (determined by the shift of the peak at 1050 cm^{-1}) has the same trend seen for G' and NIR predictions (Fig. 6. 4(a)). This suggests that the global dispersion levels of the PPNC are dominated by intercalated clay particles. There are no obvious trends for the effect of the processing conditions on the achieved intercalation/exfoliation levels; however the results confirm the previous observation that better dispersion (higher intercalation and higher exfoliation) is obtained with 200 rpm (3 kg/h). Also for both sets of conditions, the exfoliation (determined by the shift of the peak at 1080 cm^{-1}) increases, while intercalation decreases.

Chapter 6. The effect of the processing conditions on the evolution of dispersion of different polymer-clay nanocomposites

For the PANC (Fig. 6. 5(b)) the variation of the screw speed has little effect on both the intercalation and exfoliation levels. However, under the extreme conditions of higher screw speed (300 rpm) and higher feed rate (9 kg/h) significantly lower exfoliation levels are obtained. This is probably due to a combination of lower residence times and higher melt temperatures (Table 6. 2), which delays the dispersion mechanism and favours degradation.

Overall, the results suggest that for each system there is an optimum set of conditions (screw speed/throughput) that favour dispersion.

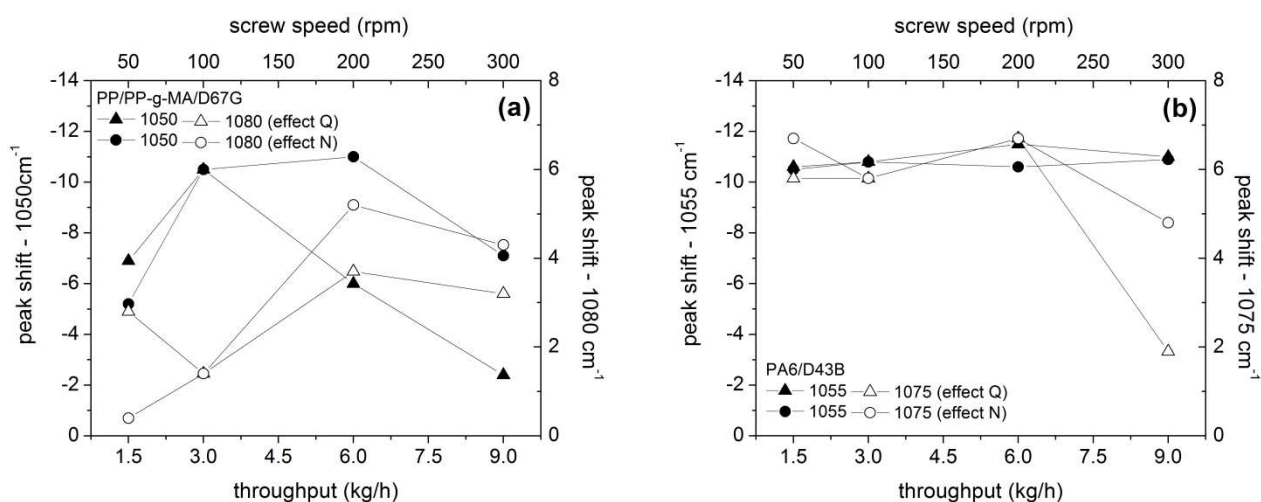


Figure 6. 5. Effect of the throughput and screw speed on the FT-IR peak shifts: (a) PP nanocomposites, (b) PA6 nanocomposites.

6.3.2. Effect of screw speed

Table 6. 3 lists the NIR real-time predictions of dispersion, for the nanocomposites prepared with different screw speeds and respective errors. As it was anticipated, some of the samples present higher degree of dispersion than the previously obtained for the calibration samples at L/D 11 [20]; therefore these extrapolated values have higher associated error, yielding higher global errors of prediction (RMSEP) and higher bias values.

For the majority of the PPNCs, the NIR predictions show a reversion of the clay dispersion along the second half of the extruder. Although, the material prepared with 50 rpm (3 kg/h) shows a steady

Chapter 6. The effect of the processing conditions on the evolution of dispersion of different polymer-clay nanocomposites

increase of dispersion along the extruder, decreasing only at the die exit. Actually, with these conditions the residence time between the feeding zone and the end of the first kneading block at L/D 11 is longer (Table 6. 2), which could explain the increasing dispersion along the screw length. Also, using 200 rpm results in the pronounced increase of dispersion between L/D 9 and L/D 11, followed by a minor decrease at L/D 19, after which is approximately constant until the die exit. At higher screw speed, the exerted shear rate is also higher which contributes to higher dispersion levels.

The PANCs exhibits an increase of dispersion until L/D 11 for all screw speeds, after which it keeps evolving or remains constant. Unlike the PPNCs, using the lower screw speed resulted in poorer dispersion. With this system, the moderate screw speed like 100 rpm or 200 rpm appears to yield better dispersion. Between L/D 9 and L/D 19 dispersion increases circa 30% and remains approximately constant until the die exit. Although, with the higher screw speeds (200 and 300 rpm) the dispersion levels at L/D 29 are higher, at the die exit dispersion decreases circa 16% in both cases. Also, beyond L/D 11, using 200 rpm or 300 rpm results in similar dispersion levels.

NIR predictions also show a pronounced decrease of the dispersion levels at the die exit, for both systems, regardless of the screw speed used. At the die the enhanced shear stresses and viscous dissipation effects, cause the increased of melt temperature to values high enough to cause degradation of the clays surfactant (Fig. 6. 2). Previous findings (unpublished work) confirm that degradation induces the collapse of the developed structure and/or re-agglomeration of the clay particles, regardless of the polymer matrix used [35 – 39]. Nevertheless, the PANCs yield higher dispersion levels than the PPNCs, prepared under the same conditions.

Chapter 6. The effect of the processing conditions on the evolution of dispersion of different polymer-clay nanocomposites

Table 6. 3. NIR real-time predictions of the degree of dispersion of the nanocomposites prepared using different screw speeds.

<i>N</i> (rpm)	<i>Q</i> (kg/h)	<i>Relative degree of dispersion (± error) –%</i>					<i>RMSEP</i> (%)	<i>bias</i>	
		L/D 9	L/D 11	L/D 19	L/D 29	die			
PPNC	3	50	39.5 (±4.9)	70.6 (±2.8)	78.6 (±3.2)	91.2 (±14.0)	51.2 (±4.0)	10.9	2.1
		100	76.1 (±3.5)	91.5 (±22.1)	98.9 (±17.7)	74.2 (±5.2)	70.7 (±4.1)	18.8	4.6
		200	54.6 (±2.9)	93.8 (±16.3)	89.3 (±9.9)	84.6 (±10.8)	85.7 (±7.5)	24.1	5.7
		300	38.4 (±3.1)	86.7 (±7.3)	67.3 (±3.1)	51.8 (±3.3)	45.5 (±2.2)	9.7	1.8
PANC	3	50	40.7 (±4.1)	71.9 (±3.4)	78.6 (±3.6)	76.1 (±3.9)	63.4 (±3.1)	4.8	0.98
		100	56.3 (±2.7)	75.9 (±2.7)	82.8 (±6.2)	86.2 (±5.7)	87.3 (±8.7)	8.1	1.1
		200	53.3 (±3.9)	68.2 (±3.2)	85.0 (±4.0)	92.8 (±12.6)	76.7 (±2.4)	10.5	2.2
		300	56.4 (±2.9)	72.6 (±2.9)	91.1 (±7.3)	92.4 (±10.6)	76.6 (±3.7)	9.9	2.1

Figure 5 presents the evolution along the extruder of the G' values at 0.1 rad/s, for both PP and PA6 nanocomposites prepared with different screw speeds. Increasing of the G' values at low frequencies, is attributed to finer levels of dispersion [4 – 5, 13, 28 – 31].

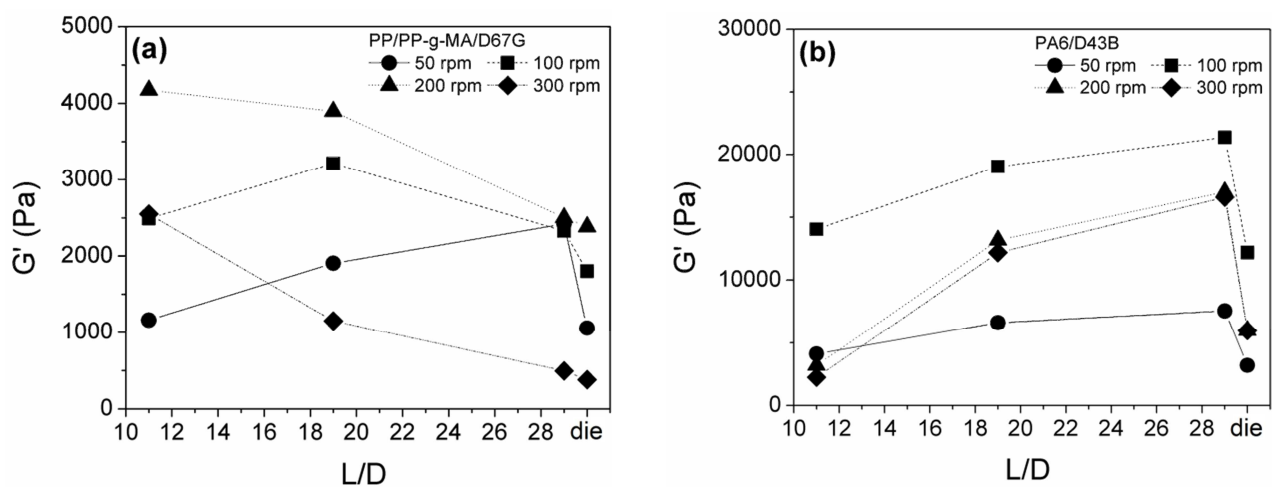


Figure 6. 6. Values of G' at 0.1 rad/s plotted against the extruder location for the effect of screw speed: (a) PP/PP-g-MA/D67G nanocomposites, (b) PA6/D43B nanocomposites.

Chapter 6. The effect of the processing conditions on the evolution of dispersion of different polymer-clay nanocomposites

The effect of screw speed is very different in both materials. The storage moduli values of the PA6 nanocomposites are almost five times higher than the values of the PP nanocomposites. Figure 6. 6(a) shows that for the PP based materials, the only set of conditions showing an increase of the viscoelastic response from L/D 11 to L/D 29 is 50 rpm, Using 200 rpm or 300 rpm results in the decrease of the viscoelastic response beyond L/D 11, which is more pronounced for the higher screw speed.

These findings are not entirely in agreement with the NIR predictions in Table 3, and surely do not conform to the associations between the screw speed and dispersion established by other authors [1 – 3, 6, 13 – 14].

For the PA6 nanocomposites, the results show a steady increase of G' along the extruder for all screw speeds (Fig. 6. 6(b)) used. However, the best rheological response is that of the PA6 nanocomposite is that of the material prepared with 100 rpm, which is in agreement with the NIR predictions.

Once more for both systems and all conditions tested, the values at the die exit show a pronounced decrease. Although not shown here, identical evolutions along the extruder are seen for the remaining rheological parameters (G'' , b and σ_0).

Since the chemometric model used for the real-time predictions is based on two different reference techniques (rheology and FT-IR) plus the SME [26], some contradicting information between rheology and the NIR predictions may exist. To obtain complementary information on the levels of intercalation/exfoliation attained, the collected samples were also analysed by FT-IR. Figure 6. 7 shows the FT-IR peak shifts [32 – 34] along the extruder for the samples prepared with different screw speeds.

Chapter 6. The effect of the processing conditions on the evolution of dispersion of different polymer-clay nanocomposites

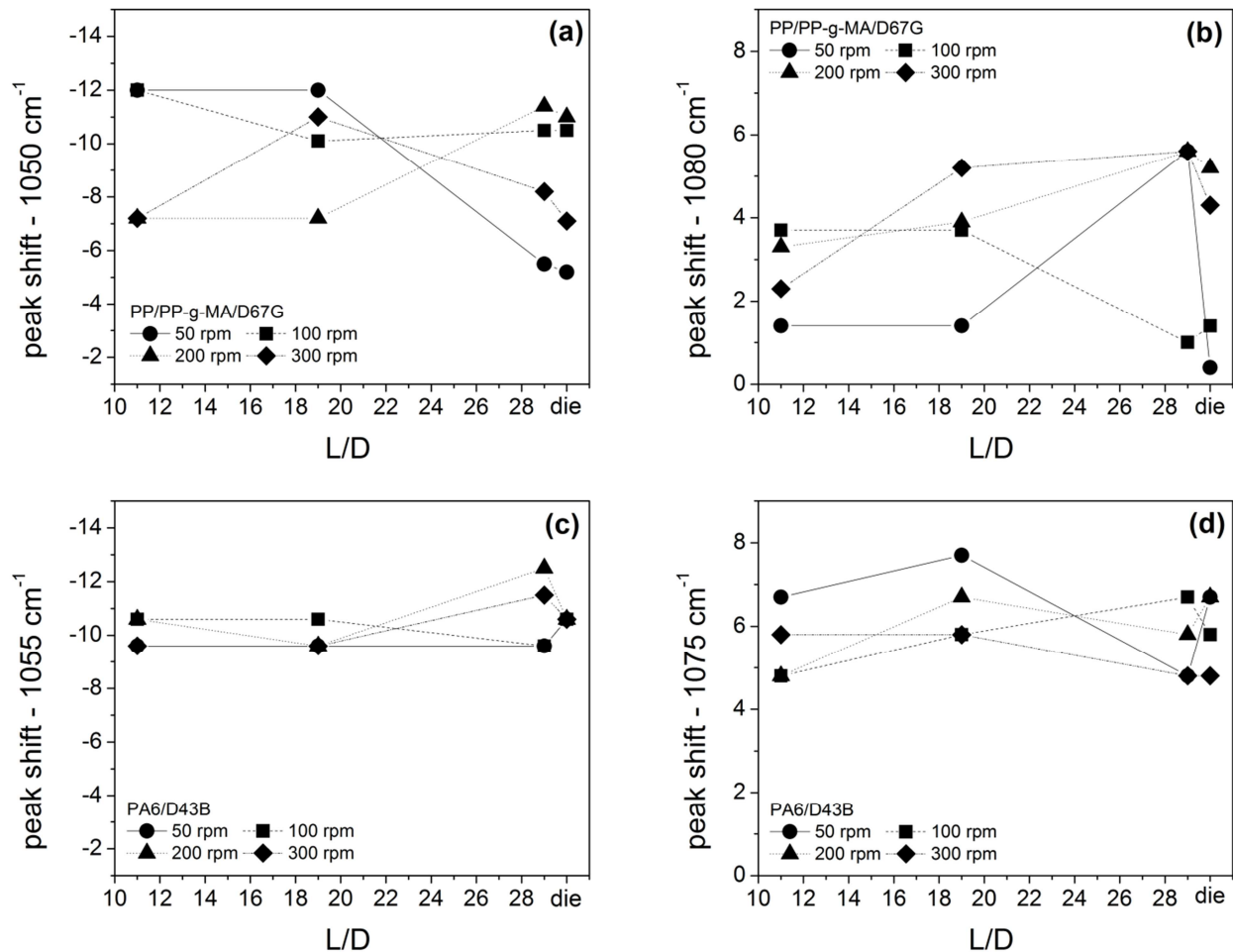


Figure 6. 7. FT-IR peak shifts along the extruder of the prepared with different screw speeds: PP based nanocomposites (a) 1050 cm^{-1} and (b) 1080 cm^{-1} ; PA6 based nanocomposites (c) 1055 cm^{-1} and (d) 1075 cm^{-1}

The screw speed has great impact on the intercalation (Fig. 6. 7(a)) and exfoliation (Fig. 6. 7(b)) of the PPNCs. Upstream, at L/D 11 (Fig. 6. 7(a)), the peak shift values of the samples prepared with the lower screw speeds are about 2 times higher those of the samples prepared with the higher screw speeds. However, while the materials prepared with 50 rpm and 100 rpm show a decrease of the intercalation along the extruder, the composites prepared with 200 rpm and 300 rpm show an increase, with 200 rpm yielding better results. With the exception of the nanocomposite prepared at 100 rpm (Fig. 6. 7(b)), all nanocomposites show an increase of the exfoliation along the extruder. Still, when using 50 rpm, the peak shift at the die exit reverts to almost zero.

Chapter 6. The effect of the processing conditions on the evolution of dispersion of different polymer-clay nanocomposites

Regardless of the screw speed used, the levels of intercalation of the PA6 system (Fig. 6. 7(c)) are high at L/D 11, and continue roughly constant along the extruder axis. In Figure 6. 7(d) the sample prepared with 50 rpm stands out, but beyond L/D 19 exfoliation decreases. For this PANC, the longer residence time at the initial mixing block (L/D 9 – L/D 11) may contribute to the degradation of the clay surfactant, explaining the lower rheological response and the decrease of dispersion.

FT-IR data presented complementary information, showing that for the PP nanocomposites better exfoliation is obtained with higher screw speeds (200 and 300 rpm), while for PA6 exfoliation is higher at moderate screw speeds (100 rpm). Ultimately, the FT-IR analysis clarifies the discrepancies between rheology and NIR predictions, showing that the higher levels of dispersion predicted by NIR for the PP nanocomposite prepared at 200 rpm (Table 6. 3) are a consequence of the increase of exfoliation, which may explain the lowering of the viscoelastic response (Fig. 6. 5(a)). Early studies by other authors [1, 5, 11, 40] showed that the particles on a nanometer scale can be easily aligned under flow (even in SAOS experiments), resulting in a negligible contribution of the solid particulates to the viscoelastic behaviour of polymer-clay nanocomposites. Kim et al [10] concluded that when exfoliation increases less intercalated stacks persist, justifying the decrease of the rheological properties. However, for the PP nanocomposite prepared with 50 rpm, the FT-IR peak shifts also show the increase of exfoliation until L/D 29, yet rheology (Fig. 6. 5(a)) and NIR also indicate higher levels of dispersion for this PPNC until L/D 29 (Table 6. 3). As such, for the prior case, the decrease of the rheological response may also be related to degradation of the clay surfactant.

To get further insight on the effects of the processing conditions, all G' and NIR predicted values were normalized, applying a simple ratio between the value at a specific location and the value at L/D 11, which is the most upstream location analysed with all techniques. The results were plotted against the extruder locations (L/D) and are depicted in Figure 6. 8. For simplicity reasons, the values at the die exit were neglected here. The results show that for PP matrix nanocomposites the increase of screw speed results in the reversion of the dispersion levels beyond L/D 11. It is confirmed that for this system working under mild shear results in a positive evolution of dispersion along the extruder, probably due to the higher residence time in the first mixing zone (Table 6. 2).

Chapter 6. The effect of the processing conditions on the evolution of dispersion of different polymer-clay nanocomposites

Conversely, for the PA6 matrix nanocomposites both dispersion development and the dispersion extent are favoured by increasing screw speeds.

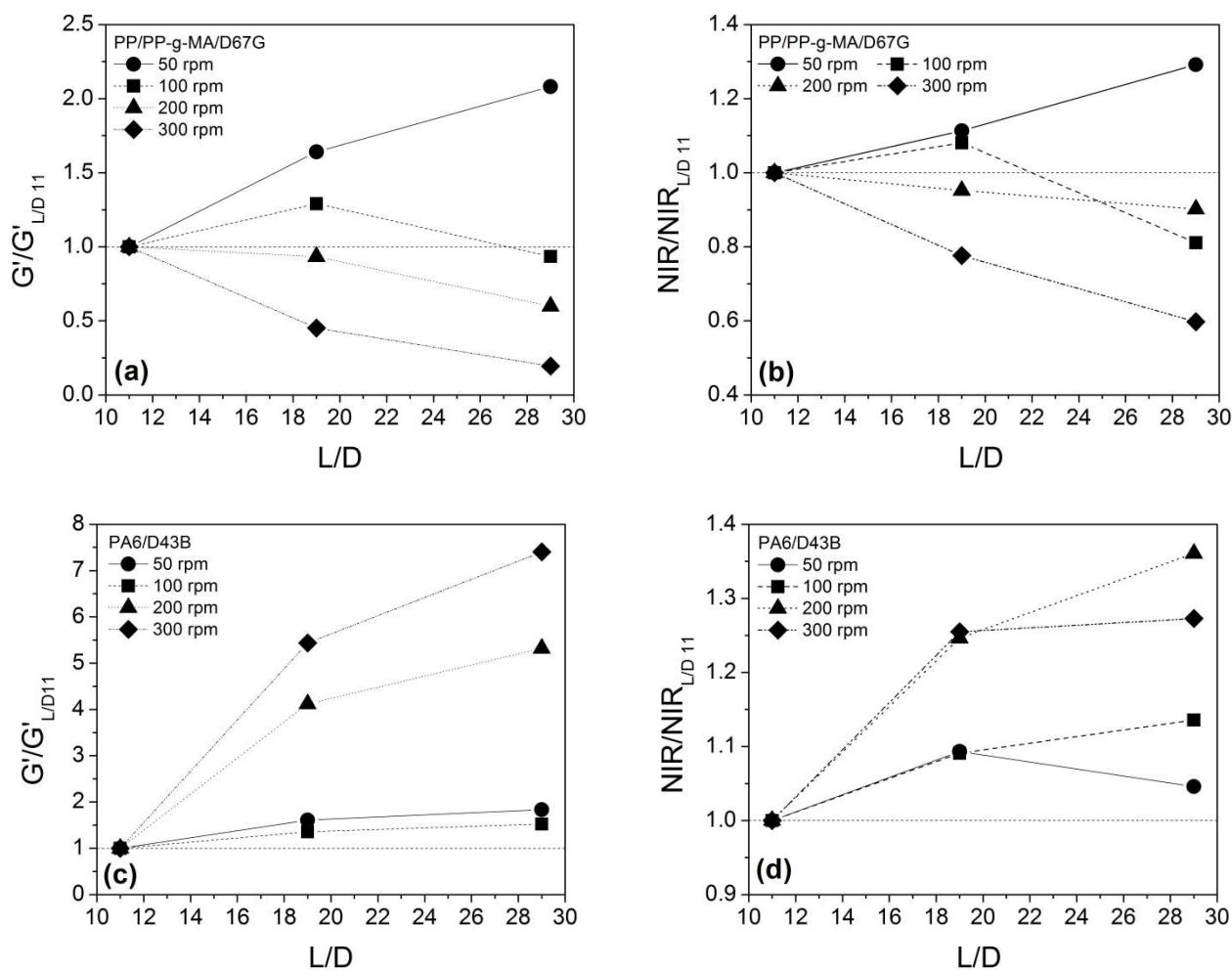


Figure 6. 8. Normalized values for the effect of screw speed: PP based nanocomposites (a) storage modulus and (b) NIR predictions; PA6 based nanocomposites (c) storage modulus and (d) NIR predictions.

6.3.3. Effect of the throughput

Table 6. 4 lists the NIR predictions of the degree of dispersion for the effect of throughput. The data shows that for PPNCs the preparation under mild conditions (3 kg/h) yields better results. In this case, the dispersion levels show a pronounced overshoot between L/D 9 and L/D 19, decreasing circa 20% at L/D 29, but at the die exit this feed rate yields higher dispersion levels.

Chapter 6. The effect of the processing conditions on the evolution of dispersion of different polymer-clay nanocomposites

For the PANCs the feed rate appears to have little impact on the dispersion levels attained, with the exception of the higher throughput tested (9 kg/h) the dispersion levels show marked increases along the first mixing zone and remains approximately constant until the die exit. However, similar to what was seen with the higher screw speed, for the higher throughput the dispersion at the die exit shows a pronounced decrease, becoming circa 30 % lower than that at L/D 29.

For both systems, the decrease in the residence time and the melt temperature boost (Table 6. 2) due to the effects of viscous dissipation in a higher filled channel may result in the collapse of the clay structure.

Table 6. 4. NIR real-time predictions of the degree of dispersion of the nanocomposites prepared using different throughputs.

Q (kg/h)	N (rom)	<i>Relative degree of dispersion (\pm error) – %</i>					<i>RMSEP</i> (%)	<i>bias</i>	
		L/D 9	L/D 11	L/D 19	L/D 29	die			
PPNC	100	1.5	49.1 (\pm 4.8)	87.1 (\pm 7.4)	97.4 (\pm 13.7)	72.9 (\pm 4.1)	47.5 (\pm 3.2)	11.2	1.9
		3	76.1 (\pm 3.5)	91.5 (\pm 22.1)	98.9 (\pm 17.7)	74.2 (\pm 5.2)	70.7 (\pm 4.1)	18.8	4.6
		6	52.7 (\pm 2.9)	96.0 (\pm 14.5)	87.5 (\pm 9.0)	70.8 (\pm 3.8)	61.7 (\pm 2.0)	12.1	1.7
		9	40.9 (\pm 4.3)	96.6 (\pm 23.9)	71.2 (\pm 4.8)	53.5 (\pm 3.1)	40.4 (\pm 2.4)	22.1	6.3
PANC	100	1.5	40.5 (\pm 4.8)	90.2 (\pm 12.7)	88.4 (\pm 6.7)	89.0 (\pm 13.3)	80.1 (\pm 2.7)	13.3	3.6
		3	56.3 (\pm 2.7)	75.9 (\pm 2.7)	82.8 (\pm 6.2)	86.2 (\pm 5.7)	87.3 (\pm 8.7)	8.1	1.1
		6	60.7 (\pm 3.9)	84.9 (\pm 6.3)	88.5 (\pm 8.3)	94.8 (\pm 11.3)	82.4 (\pm 3.6)	9.8	1.7
		9	51.7 (\pm 3.2)	76.1 (\pm 4.2)	96.3 (\pm 21.7)	95.4 (\pm 15.2)	66.0 (\pm 3.8)	19.2	5.1

Figure 6. 9 shows the evolution of the storage modulus along the extruder, for both systems. Clearly the G' values of the PA6 nanocomposites are over 10 times higher than those of the PP nanocomposites, prepared under the same conditions. Figure 6. 9(a) shows that for the PP based materials, G' increases between L/D 11 and L/D 19, but downstream it decreases to the initial values. The only exception is for 9 kg/h, causing the decrease of the viscoelastic response beyond L/D 11.

Chapter 6. The effect of the processing conditions on the evolution of dispersion of different polymer-clay nanocomposites

For the PA6 nanocomposites, the results show a steady increase of G' along the extruder for all throughputs (Fig. 6. 9(b)) used. However, the best rheological response is that of the PA6 nanocomposite prepared with 6 kg/h. Once more for both systems and all conditions tested, the values at the die exit show a pronounced decrease. Identical developments along the extruder are seen for the remaining rheological parameters (G'' , b and σ_0).

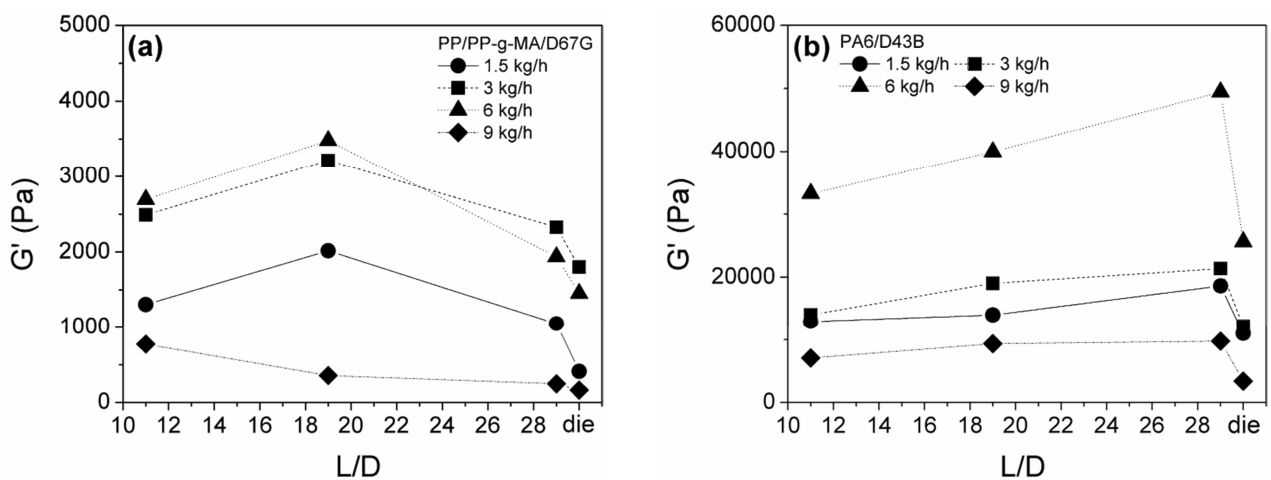


Figure 6. 9. Values of G' at 0.1 rad/s plotted against the extruder location for the effect of screw speed: (a) PP/PP-g-MA/D67G nanocomposites, (b) PA6/D43B nanocomposites.

Figure 6. 10, shows the FT-IR peak shifts along the extruder. The variation of the feed rate shows minor effects in the intercalation levels of the PPNCs at L/D 11 (Fig. 6. 10(a)) as all conditions tested yield identical results at this location. However, beyond this point the peak shift decreases along the extruder for all samples, being more pronounced for the higher throughputs. Figure 6. 10(b) shows that, with the exception of using 3 kg/h, the lower intercalation levels appear to be compensated by relatively high levels of exfoliation, which are approximately constant along the extruder.

Regardless of the feed rate used, the levels of intercalation of the PA6 system (Fig. 6. 10(c)) are high at L/D 11, and continue roughly constant along the extruder axis, though slightly lower levels of intercalation at L/D 11 are detected when using 9 kg/h, at L/D 19 the values level off and remain stable until the die exit. The throughput appears to have little influence on the exfoliation levels

Chapter 6. The effect of the processing conditions on the evolution of dispersion of different polymer-clay nanocomposites

attained with the PA6 system (Fig. 6. 10(d)), since all samples have identical peak shifts. Though, at the die exit the composite prepared at 9 kg/h exhibits a pronounced drop of the out-of-plane peak shift, suggesting a reversion of the developed structure. Overall, both systems show higher levels of exfoliation when prepared with 6 kg/h.

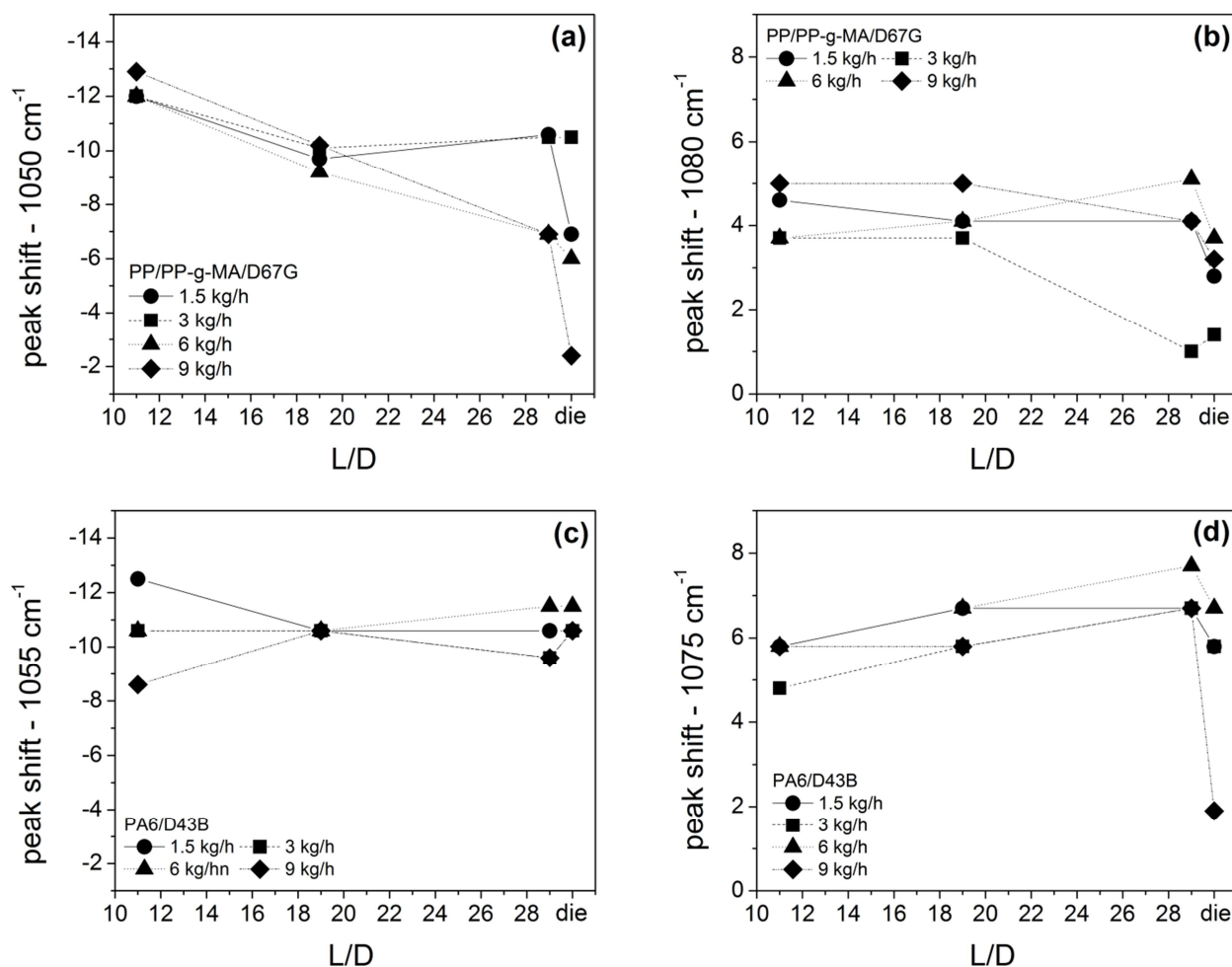


Figure 6. 10. FT-IR peak shifts along the extruder of the prepared with different throughputs: PP based nanocomposites (a) 1050 cm^{-1} and (b) 1080 cm^{-1} ; PA6 based nanocomposites (c) 1055 cm^{-1} and (d) 1075 cm^{-1}

Figure 6. 11 shows the normalized values of G' and NIR predictions. The results confirm that the effect of throughput less obvious than the screw speed. However for the PP system, moderate feed rates appear to favour dispersion. For the PA6, the rheological behaviour shows that better

Chapter 6. The effect of the processing conditions on the evolution of dispersion of different polymer-clay nanocomposites

dispersion is achieved at moderate throughputs, while NIR shows that higher throughputs favour the extent of dispersion and the dispersion development.

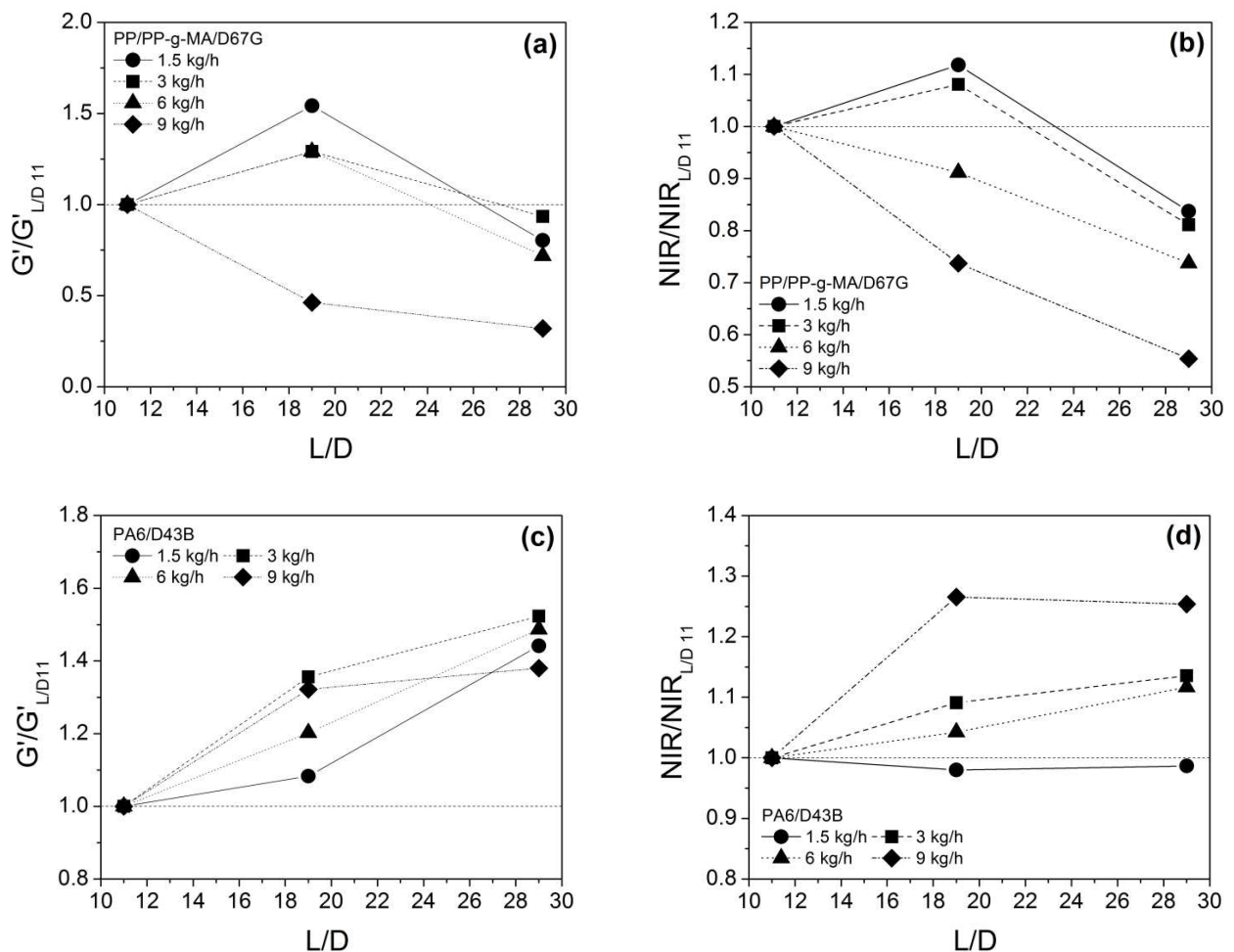


Figure 6. 11. Normalized values for the effect of throughput: PP based nanocomposites (a) storage modulus and (b) NIR predictions; PA6 based nanocomposites (c) storage modulus and (d) NIR predictions.

6.3.4. The relation between processing conditions – chemistry – dispersion

Looking back at the results in Table 6. 2, the possible explanations for the results obtained with the PP system are: (i) the excess melt temperature at higher screw speeds, promotes the degradation of the organoclay surfactant (Fig. 6. 2(b)); (ii) at lower feed rates residence time increases, favouring diffusion of the polymer within the clay galleries to occur [2, 18]. The dispersion evolution of PA6

Chapter 6. The effect of the processing conditions on the evolution of dispersion of different polymer-clay nanocomposites

nanocomposites appears to be less time dependent, but highly affected by shear/stress conditions. There is a noticeable trend showing that better dispersion is achieved at high shear (higher screw speed) or high stress (higher feed rates). Because the chemical interaction between the clay and the PA6 matrix is better (comparing to the PP system) intercalation and exfoliation occur faster, hence the irrelevance of the processing time in the overall dispersion levels. However, due to the higher thermal instability of the clay (Fig. 6. 9(c)), when using extreme conditions it is likely that degradation affects both clay surfactant and the PA6 matrix, resulting in contradicting information between NIR and rheology.

Shah and Paul [38] studied the degradation of different organoclays during melt processing of polyethylene based nanocomposites, and concluded that the nanocomposites show a greater mass loss of surfactant during melt compounding, than that determined by TGA analysis of the organoclay. Moreover, Xie *et al* [37] showed that the unsaturated olefinic degradation products of the surfactant may lead to unfavourable interfacial plasticization (or advantageous cross-linking depending on the matrix) reaction with the polymer, explaining the often unexpected rheological behaviour. Which explains the results obtained with the PP matrix at higher shear rates. It was also shown that the metallic cations of the original silicate structure have a catalytic effect on degradation of both the surfactant and the polymer matrix [37]. More importantly, Davis et al [39] showed that the degradation pathways of PA6 during processing may be altered due to the presence of the silicate, since the thermal degradation of MMT releases residual water bound to sodium ions and hydroxyl radicals leading to hydrolytic scission reaction with the PA6.

Overall, the results suggest that the evolution of dispersion is extremely influenced by the processing conditions. However, to explain the different evolution rates and dispersion extents between the two systems, the chemistry of polymer-clay interfaces must be taken into account [1 – 2, 5 – 6, 10, 18, 24].

Given our previous findings (Chapter 5 of the thesis) about the effect of the surfactant degradation on the evolution of dispersion and considering the mechanisms proposed by Dennis et al [2] as well as the effects of shear/stress/time addressed by Bousmina [18] a clear distinction should be made between the two nanocomposite systems studied.

Chapter 6. The effect of the processing conditions on the evolution of dispersion of different polymer-clay nanocomposites

The less favourable chemistry of the PP/PP-g-MA/D67G system is partially overcome by the use of the PP-g-MA compatibilizer, but dispersion is still process dependent [2, 18]. The dispersion evolution of this system depends on proper diffusion of the polymer chains within the clay galleries. This is a time dependent process, therefore it should be favoured by low screw speeds or low feed rates. Although in these conditions it is likely that degradation of the surfactant occurs, the highly intercalated/exfoliated particles may not be affected, but the remaining clay stacks will not evolve to a well dispersed structure, resulting in a partial dispersion [2], explaining the results obtained for the nanocomposite prepared with 50 rpm. In extreme conditions, degradation of the clay surfactant may trigger the degradation of the polymer matrix, thus the hydrodynamic stresses exerted by the polymer matrix are not enough to overcome the inherent attractive forces between the clay layers leading to the collapse of the developed structure [5, 18, 40], this appears a rational explanation for the results obtained with 1.5 kg/h.

The favourable chemistry of the PA6/D43B system yields faster and easier dispersion, regardless of the processing conditions used [2, 10 – 11, 16, 24]. All characterization results show that this system yields higher degree of exfoliation. Despite the lower thermal stability of the organoclay D43B, dispersion evolves fast and is likely that degradation would not affect the dispersion evolution. Though in high shear (300 rpm), high stress (9 kg/h) or even longer times (1.5 kg/h) conditions it is more likely that degradation of the PA6 matrix occurs, due to the chemical reactions between the clay surface and the polyamide [35, 37 – 39], explaining the reversion detected at the die exit, and the unexpected results for the samples prepared with higher screw speeds (300 rpm) and higher feed rate (9 kg/h).

6.4. Conclusions

The effect of the processing conditions (N and Q) on the morphology evolution along the extruder, of two different nanocomposite systems (PP/PP-g-MA/D67G and PA6/D43B), was followed by NIR spectroscopy. The NIR spectra and chemometric analysis showed unusual evolutionary trends that were confirmed by the results obtained with different off-line characterization techniques.

For the PP based nanocomposites, most of the conditions tested result in an increase of dispersion along the first mixing zone, followed by an apparent decrease in dispersion downstream. For the PA6 system, this apparent reversion is mostly detected at the die exit. The dispersion of the PP matrix nanocomposites depends on suitable processing. The results show that this system yields better dispersion when prepared under intermediate shear/stress and longer residence time conditions. In opposition, the PA6 system is favored by a more beneficial chemistry hence the dispersion evolution and the dispersion levels are more shear than time dependent.

The gathered in-line and off-line data suggest that degradation effects, of both the organoclay and polymer matrix, affect the nanocomposites dispersion. However, these effects seem to be minimized if a more thermodynamically stable structure is developed, which appears to be the reason why the PA6/D43B nanocomposites exhibit a steady dispersion evolution along the extruder, despite the lower thermal stability of the D43B organoclay. It is worth noting, that under extreme processing conditions, the overall dispersion of the PA6 system is still satisfactory, particularly when compared to the PP based materials, but degradation of the matrix may affect other fundamental characteristics of the nanocomposites.

Globally the results show that the right balance of shear/stress/time is needed in order to maximize the clay dispersion and to minimize degradation effects, regardless of the system used.

6.5. References

1. J.W. Cho, D.R. Paul. "Nylon 6 nanocomposites by melt compounding"; *Polymer* 42 p. 1083-1094 (2001)
2. H.R. Dennis, D.L. Hunter, D. Chang, S. Kim, J.L. White, J.W. Cho, D.R. Paul. "Effect of melt processing conditions on the extent of exfoliation in organoclay-based nanocomposites"; *Polymer* 42 p. 9513-9522 (2001)
3. W. Lertwimolnun, B. Vergnes. "Influence of screw profile and extrusion conditions on the microstructure of polypropylene/organoclay nanocomposites". *Polymer Engineering and Science*. 47 p. 2100-2109 (2007)
4. S. Tanoue, L.A. Utracki, A. Garcia-Rejon, J. Ttibouet, K.C. Cole, M. R. Kamal. "Melt compounding of different grades of Polystyrene with Organoclay. Part 1: Compounding and Characterization"; *Polymer Engineering and Science* 44 p. 1046-1060 (2004)
5. L. Xu, H. Nakajima, E. Manias, R. Krishnamoorti. "Tailored nanocomposites of Polypropylene with layered silicates"; *Macromolecules* 42 p. 3795-3803 (2009)
6. M. Modesti, A. Lorenzetti, D. Bon, S. Besco. "Effect of processing conditions on morphology and mechanical properties of compatibilized polypropylene nanocomposites". *Polymer*. 46 p. 10237-10245 (2005)
7. W. Lertwimolnun, B. Vergnes. "Influence of the compatibilizer and processing conditions on the dispersion of nanoclay in a polymer matrix" *Polymer*. 46 p. 3462-3471 (2005)
8. M.W. Spencer, L. Cui, Y. Yoo, D.R. Paul. "Morphology and properties of nanocomposites based on HDPE/HDPE-g-MA blends". *Polymer*. 51 p. 1056-1070 (2010)
9. K. Chrissopoulou, S.H. Anastasiadis. "Polyolefin/layered silicate nanocomposites with functional compatibilizers". *European Polymer Journal*. 47 p. 600-613 (2011)
10. S.W. Kim, W.H. Jo, M.S. Lee, M.B. Ko, J.Y. Jho. "Effects of shear on melt exfoliation of clay in preparation of Nylon 6/Organoclay nanocomposites", *Polymer Journal* 34 p.103-111 (2002)

Chapter 6. The effect of the processing conditions on the evolution of dispersion of different polymer-clay nanocomposites

11. T.D. Fornes, P.J. Yoon, H. Keskkula, D.R. Paul. "Nylon 6 nanocomposites: the effect of matrix molecular weight"; *Polymer* 42 p. 9929-9940 (2001)
12. L. Zhu, M. Xanthos. "Effects of process conditions and mixing protocols on structure of extruded polypropylene nanocomposites", *Journal of Applied Polymer Science* 93 p. 1891-1899 (2004)
13. W. Lertwimolnun, B. Vergnes. "Effect of processing conditions on the formation of polypropylene/organoclay nanocomposites in a twin-screw extruder". *Polymer Engineering and Science*. 46 p. 314-323 (2006)
14. P. Peltola, E. Valipakka, J. Vourinen, S. Syrjala; K. Hanhi. "Effect of rotational speed of twin screw extruder on the microstructure and rheological and mechanical properties of nanoclay-reinforced polypropylene nanocomposites"; *Polymer Engineering and Science* 46 p. 995-1000 (2006)
15. M.A. Treece, W. Zhang, R.D. Moffit, J.P. Oberhauser. "Twin-screw extrusion of Polypropylene-Clay nanocomposites: Influence of masterbatch processing, screw rotation mode and sequence"; *Polymer Engineering and Science* 47 p. 898-911 (2007)
16. P. Médéric, J. Ville, J. Huitric, M. Moan, T. Aubry. "Effect of processing procedures and conditions on structural, morphological and rheological properties of Polyethylene/Polyamide/Nanoclay blends"; *Polymer Engineering and Science* 51 p. 969-978 (2011)
17. S. Besco, M. Modesti, A. Lorenzetti. "Influence of processing parameters on the structure of melt blended polyethylene/organoclay nanocomposites produced by a masterbatch route"; *in press Polymer Engineering and Science* (2012) DOI: 10.1002/pen.23310
18. M. Bousmina. "Study of intercalation and exfoliation processes in polymer nanocomposites". *Macromolecules*. 39 p. 4259-4263 (2006)
19. D. Homminga, B. Goderis, S. Hoffman, H. Reynaers, G. Groeninckx. "Influence of shear flow on the properties of polymer layered silicate nanocomposites". *Polymer*, 46 p. 9941-9954 (2005)

Chapter 6. The effect of the processing conditions on the evolution of dispersion of different polymer-clay nanocomposites

20. S. Tanoue, A. Hasook, T. Itoh, M. Yanou, Y. Iemoto, T. Unryo. "Effect of screw rotation speed on the properties of polystyrene/organoclay nanocomposites prepared by a twin-screw extruder". *Journal of Applied Polymer Science*, 101 p. 1165-1173 (2006)
21. L. Scatteia, P. Scarfato, D. Acierno. "Processing, rheology and structure of melt compounded PBT-clay nanocomposites having different chemical composition". *e-Polymers* 23 (2006)
22. A.L.F. Giralardi, M.T.M. Bizarria, A.A. Silva, J.I. Velasco, M.A. d'Ávila, L.H.I. Mei. "Effects of extrusion conditions on the properties of recycled polyethylene terephthalate/nanoclay nanocomposites prepared by a twin screw extruder". *Journal of Applied Polymer Science*, 108 p. 2252-2259 (2008)
23. P.D. Fasulo, W.R. Rodgers, R.A. Ottaviani, D.L. Hunter. "Extrusion processing of TPO nanocomposites", *Polymer Engineering and Science* 44 p. 1036-1045 (2004)
24. M. Mehrabzadeh, M.R. Kamal, "Melt processing of PA-66/clay, HDPE/clay and HDPE/PA-66/clay nanocomposites". *Polymer Engineering and Science*. 44 p. 1152-1161 (2006)
25. S. Mould, J.M. Barbas, A.V. Machado, J.M. Nóbrega, J.A. Covas. "Measuring the rheological properties of polymer melts with on-line rotational rheometry". *Polymer Testing*. 30 p. 602-610 (2011)
26. J.M. Barbas, A.V. Machado, J.A. Covas. "In-line Near-Infrared spectroscopy: a tool to monitor the preparation of polymer-clay nanocomposites in extruders", *in press*, *Journal of Applied Polymer Science* (2012) DOI: 10.1002/app.38106
27. A.V. Machado, J.A. Covas, M. van Duin. "Evolution of morphology and of chemical conversion along the screw in a corotating twin-screw extruder"; *Journal of Applied Polymer Science*, 71 p. 135-141 (1999)
28. Durmus, A. Kasgoz, C.W. Macosko. "Linear low density polyethylene (LLDPE)/clay nanocomposites. Part I: Structural characterization and quantifying clay dispersion by melt rheology". *Polymer*. 48 p. 4492-4502 (2007)

Chapter 6. The effect of the processing conditions on the evolution of dispersion of different polymer-clay nanocomposites

29. Vermogen, K. Masenelli-Varlot, R. Séguéla, J. Duchet-Rumeau, S. Boucard, P. Prele. "Evaluation of the structure and dispersion in polymer-layered silicate nanocomposites". *Macromolecules*. 38 p. 9661-9669 (2005)
30. P. Cassagnau. "Melt-rheology of organoclay and fumed silica nanocomposites". *Polymer*. 49 p. 2183-2196 (2008)
31. R. Krishnamoorti, E.P. Giannelis. "Rheology of end-tethered polymer silicate nanocomposites"; *Macromolecules* 30 p. 4097-4102 (1997)
32. K.C. Cole. "Use of Infrared spectroscopy to characterize clay intercalation and exfoliation in polymer nanocomposites". *Macromolecules*. 41 p. 834-843 (2008)
33. L. Yan, C.B. Roth, P.F. Low. "Changes in the Si-O vibrations of smectite layers accompanying the sorption of interlayer water". *Langmuir*. 12 p. 4421-4429 (1996)
34. W.L. IJdo, S. Kemnetz, D. Benderly. "An Infrared method to assess organoclay delamination and orientation in organoclay polymer nanocomposites" *Polymer Engineering and Science* 46 p. 1031-1039 (2006)
35. L. Cui, D.M. Khramov, C.W. Bielawski, D.L. Hunter, P.J. Yoon, D.R. Paul. "Effect of organoclay purity and degradation on nanocomposite performance. Part 1: Surfactant degradation"; *Polymer* 49 p. 3751-3761 (2008)
36. F. Bertini, M. Canetti, G. Leone, I. Tritto. "Thermal behaviour and pyrolysis of modified organo-layered silicates as intermediates for in situ polymerization"; *Journal of Analytical and Applied Pyrolysis*, 86 p. 74-81 (2009)
37. W. Xie, Z. Gao, W. Pan, D. Hunter, A. Singh, R. Vaia. "Thermal degradation chemistry of alkyl quaternary ammonium montmorillonite"; *Chemistry of Materials* 13 p. 2979-2990 (2001)
38. R.K. Shah, D.R. Paul. "Organoclay degradation in melt processed polyethylene nanocomposites", *Polymer* 47 p. 4075-4084 (2006)
39. R.D. Davis, J.W. Gilman, D.L. VanderHart. "Processing degradation of polyamide-6/montmorillonite clay nanocomposites and clay organic modifier", *Polymer Degradation and Stability* 79 p. 111-121 (2003)

Chapter 6. The effect of the processing conditions on the evolution of dispersion of different polymer-clay nanocomposites

40. J. Ren, B.F. Casanueva, C.A. Mitchel, R. Krishnamoorti. "Disorientation kinetics of aligned polymer layered silicate nanocomposites"; *Macromolecules* 36 p. 4188-4194 (2003)

CONCLUSIONS AND FUTURE WORK

7

7.1. Conclusions

The research presented in this thesis aims at implementing on-line monitoring techniques for characterization of the clay dispersion, during the preparation of polymer-clay nanocomposites by melt intercalation. As such, using conventional mixing equipments, such as the batch mixer and, in a larger scale, a twin-screw extruder, it was possible to develop and establish a new methodology, based on Near-Infrared spectroscopy for assessing in real time the evolution of dispersion upon compounding. The ultimate goal is to gain knowledge on the evolution of dispersion and further understanding about the influence of the processing conditions on the mechanism of dispersion.

The work presented in Chapter 3 describes the implementation and validation of in-line Near-Infrared spectroscopy (NIR) for monitoring the preparation of polymer-clay nanocomposites in a batch mixer. This small scale compounding technique enables proper control over the main operating conditions known to influence the polymer-clay nanocomposites structure. It allowed the preparation of polypropylene matrix nanocomposites with different degrees of dispersion. Using different well established characterization techniques, such as XRD, rheology, medium FT-IR, tensile testing and two thermomechanical parameters of the processing equipment, it was possible to select the best set of parameters, for development of a chemometric model suitable for characterizing the dispersion. Proper statistical optimization of the sampling population was also achieved. The best outcome resulted from the use of a multi-parameter curve, that used 7 parameters derived from rheology (G' , G'' , σ_0 and b), FT-IR (wavenumber shift of the clay Si-O peaks at 1050 and 1080 cm^{-1}) and a thermomechanical index from the batch mixer (torque). The results also showed that NIR and adequate chemometrics can be applied for the real time prediction of the dispersion levels of the nanocomposites.

Regarding the use of in-line monitoring tools for the preparation of polymer-clay nanocomposites, Chapter 4 showed that NIR is a suitable technique to be applied in large scale production equipments such as twin screw extruders. Using a diffuse reflectance probe, NIR can be used in

Chapter 7. Conclusions and Future work

direct contact with the melt flow, without interfering with the process or requiring extreme modifications of the processing equipment. Following the methodology that was established for the batch mixer, the 7-parameter chemometric model was optimized accordingly. Different polypropylene matrix nanocomposites were prepared by varying the clay and compatibilizer contents and the screw speed. The calibration samples thus manufactured encompass a broad range of dispersion levels, allowing the development of a robust chemometric model. It was shown that NIR is capable of predicting in real time conditions the non-linear effect of feed rate on the dispersion.

In view of gaining better knowledge about the dispersion mechanism, and the effect of the operating conditions on the onset and extent of clay dispersion, Chapters 5 and 6 present the use of on-line/in-line techniques for monitoring the evolution of clay dispersion along the extruder axis. In Chapter 5, both on-line rheometry and in-line NIR were used to assess the evolution of dispersion along the twin-screw extruder. A good match was found between the results provided by the two techniques. Furthermore, the use of these techniques allowed perceiving the onset of degradation of the clay surfactant, and the subsequent effects on the development of the nanostructure. Overall the results show, that a highly dispersed structure is formed rapidly, but in order to be maintained (or to further evolve) a proper equilibrium between, shear, stress, time and temperature must exist.

Finally, Chapter 6 uses in-line NIR applied along the extruder axis, to monitor the effect of the processing conditions on the nanocomposites dispersion. The results obtained with different polymer matrices, specifically polypropylene and nylon-6, show that the impact of the polymer-clay affinity is greater than the effect of the operating conditions. Despite the lower thermal stability of the organoclay mixed with nylon-6, higher dispersion, and exfoliation, are achieved, regardless of the screw speed-throughput set applied. Nevertheless, the results also show that for each system it is possible to determine an optimum set of conditions in order to maximize the final dispersion levels.

Overall it was shown that NIR can be used as in-line monitoring technique for the characterization of dispersion during the preparation of polymer-clay nanocomposites. Moreover, the use of this in-line technique along the extruder enabled understanding the impact of the operating conditions on the mechanism of dispersion.

7.2. Future work

The results obtained with this research, particularly the ones presented in the last two Chapters, confirm that thermo-oxidative degradation greatly impacts the dispersion mechanism during melt mixing. It is worth mentioning that the results reported throughout this thesis were performed with polymer systems without thermal or process stabilizers. Understanding the onset of degradation and knowing the extent of the degradation mechanisms, is the main step in finding proper stabilization solutions for these materials.

Suggestions of prospective work include:

- Use the in-line methodologies developed in studying more complex systems, specifically those prepared with different process stabilizers
- Explore alternative solutions for the modification of the clay surface, granting higher thermal stability.